# CYP2E1 Activity in Cisplatin Resistant Cancer Cells

A thesis

Submitted by

Hussein Babsail

In partial fulfillment of the requirements for the degree of

Doctor of Philosophy

In

Pharmacology & Experimental Therapeutics program

Tufts University

Sackler School of Graduate Biomedical Sciences

Date

August-2015

Advisor:

Prof. David J. Greenblatt

Margery C. Beinfeld, Ph. D.

Martin Beinborn, M. D

Jeffrey Blumberg, Ph. D.

Michael H. Court, B.V.Sc., Ph. D.

## Abstract

Cisplatin (CP) is an anticancer drug that kills tumor cells by interfering with DNA replication. One of the main obstacles limiting its use is intrinsic or acquired resistance development. Reactive oxygen species (ROS) have a known role in cancer cell apoptosis upon CP treatment. An excessive increase in ROS generation leads to other modes of cell death such as necrosis. Microsomal Cytochrome P450 2E1(CYP2E1), known for its ROS generation upon CP treatment, might be a mechanistic link to hepatotoxicity and nephrotoxicity associated with CP exposure. The increase of metabolically active microsomal CYP2E1 enzyme could generate more ROS with CP that also might be exploited to sensitize resistant cancer cells to CP. Therefore, the aim of this study was to evaluate the role of microsomal CYP2E1 on cancer cells exhibiting resistance to CP. Thus, the main hypothesis was that microsomal CYP2E1 sensitizes CP-resistant extrahepatic and hepatic cancer cells by generating ROS upon treatment with CP. **Materials and Methods:** Two extrahepatic cancer cell lines, A2780/R and MOR/R, and the hepatic Hep G2 cell line, which are resistant to CP, were transfected with microsomal *CYP2E1* cDNA and treated with CP. High performance liquid chromatography (HPLC) was used to measure the metabolic activity of microsomal CYP2E1 using chlorzoxazone (CHZ) hydroxylation as an index reaction. Fluorescence activated cell sorting (FACS) measured ROS in transfected cells. The microculture tetrazolium viability assay (MTT assay) was used to evaluate the

effect of CP treatment with different concentrations on transfected cell death. **Results:** An increase in *CYP2E1* mRNA expression occurred in all transfected cells. However, no CYP2E1 metabolic activity was detected in extrahepatic cells when compared to microsomal *CYP2E1*-transfected Hep G2 cells. There were no significant changes in cell viability among Hep G2 cells transfected with microsomal *CYP2E1* when compared to controls. In conclusion, despite an increase in ROS with exposure to CP in Hep G2 cells transfected with *CYP2E1*, the cells tolerated the changes in ROS and did not demonstrate any change in CP sensitivity. Extrahepatic CP-resistant cancer cells lack some essential cellular biology to support active microsomal CYP2E1 overexpression.

.

## Acknowledgements

The experience and writing of this thesis has been a challenging procedure; this work would never have come to light without God willing it then the efforts and devotion of Professor Greenblatt, who contributed his valuable time and energy to my project. I appreciate how he handled my shortage of knowledge in some of the lab research of this project and his tolerance of my mistakes. This project would not have been completed without his kindness and his unlimited support. For these reasons, I dedicate this project to Professor Greenblatt, as well as to all my committee members: Dr. Beinfeld, Dr. Blumberg, Dr. Court and Dr. Beinborn.

I would also like to dedicate this work to my beloved mother, my lovely wife, and my sweethearts Yosra, Hasan, Solyman, Maryam, and Mohammed. Their support during the completion of this project has been immensely important to me. Along the way, they have inspired me and encouraged me to do my very best work.

# Table of Contents

# List of figures

# List of tables

# List of Abbreviations and Definitions

| Word list | Definition |
|---|---|
| Additive interaction | The effect of two drugs is equal to the sum of the effect of the two chemicals taken separately. |
| Adjuvant therapy | Additional cancer treatment given after the primary treatment to lower the risk that the cancer will recur. |
| Ala-Leucinal (PSI) | Proteasomes inhibitor |
| Amplification | Increase in the frequency of a gene or chromosomal region, as a result of replicating a DNA segment by in vivo or in vitro process. |
| Anaphase | The stage of mitosis or meiosis when chromosomes are split and the sister chromatids move to opposite poles of the cell. |
| Anode | The negative electrode of a primary cell, which is always associated with the oxidation or the release of electrons into the external circuit. |
| ANOVA | Analysis of variance |
| Apoptosis | Programmed cell death of living cells |
| BSA | Bovine serum albumin |
| CDR | Confluence dependent resistance |
| Chemotherapy | Treatment with drugs that kill cancer cells |
| Chromatid | One copy of a duplicated chromosome, which is generally joined to the other copy by a single centromere. |
| Chromosome | Thread-like structures located inside the nucleus of animal and plant cells. Each chromosome is made of protein and a single molecule of deoxyribonucleic acid (DNA) |
| CHZ | Chlorzoxazone is a skeletal muscle relaxant, and a CYP2E1 index substrate |
| Cirrhosis | A late stage of scarring (fibrosis) of the liver caused by many forms of liver diseases and conditions, such as hepatitis and chronic alcohol abuse |
| Cleavage furrow | The indentation of the cell's surface that begins the progression of cleavage, by which animal and some algal cells undergo cytokinesis |
| CP | Cisplatin, a cytotoxic drug, platinum based structure |
| Ct | Threshold cycle, used in qPCR, as the number of cycles required for the fluorescent signal to cross the threshold (ie exceeds background level). |
| CYP2E1 | P450, family 2, subfamily E, polypeptide 1 |
| Cys | Cysteine |
| Cyt b5 | Cytochrome b5 |
| Cytokinesis | The process in which the cytoplasm of a single eukaryotic cell is divided to form two daughter cells |
| Cytotoxic agent | A substance that kills cells, including cancer cells. These agents may stop cancer cells from dividing and growing, and may cause tumors to shrink in size |
| DCF | Fluorescent DCF (2',7'-dichlorofluorescein) |
| DCFH-DA | 2′-7′-Dichlorodihydrofluorescein diacetate |
| DDC | Diethyldithiocarbamate is an organosulfur compounds, used as an index inhibitor of CYP2E1 |
| Dysregulation | Impairment of a physiological regulatory mechanism |
| ED | Effective dose |
| Epigenetics | The study of cellular and physiological trait variations that are not caused by changes in the DNA sequence |
| FACS | Fluorescence activated cell sorting |
| FAD | Flavin adenine dinucleotide |
| FBS | Fetal bovine serum |
| FMN | Flavin mononucleotide |
| Fold change | A measure describing how much a quantity changes based on multiplicative increment going from |

| | |
|---|---|
| | an initial to a final value. |
| G418 | Selective antibiotic similar in structure to gentamicin B1, that blocks polypeptide synthesis in both prokaryotic and eukaryotic cells |
| GAPDH | Glyceraldehyde 3-phosphate dehydrogenase |
| Gene silencing | the ability of a cell to prevent the expression of a certain gene |
| GFP | Green fluorescent protein |
| Gpx | Glutathione peroxidase |
| GSH | Glutathione |
| Gsts | Glutathione S-transferases |
| H(2)DC | Dihydrodichlorofluorescein |
| HPLC | High pressure liquid chromatography |
| $IC_{50}$ | The concentration of a cytotoxic agent at which target cells are inhibited by 50% |
| Invasion | The movement of one cell type into a territory normally occupied by a different cell type, |
| Kbp | Kilo base pairs = 1,000 bp |
| Kinetochore | The protein structure on chromatids where the spindle fibers attach during cell division to pull sister chromatids apart. |
| Methylation | A chemical reaction in which a small molecule called a methyl group is added to other molecules. |
| Microsome | A small particle in the cytoplasm of a cell, typically consisting of fragmented endoplasmic reticulum to which ribosomes are attached. |
| Mitosis | The process by which a single parent cell divides to make two new daughter cells. Each daughter cell receives a complete set of chromosomes from the parent cell. |
| mM | millimolar |
| MONr | Monooxygenation reaction |
| MTT | Microculture tetrazolium viability |
| Mutation | A permanent change of the nucleotide sequence of the genome of an organism, virus, or extrachromosomal DNA or other genetic elements. |
| NADPH | Nicotinamide adenine dinucleotide phosphate |
| Necroptosis | Programmed form of necrosis, or inflammatory cell death |
| Necrosis | Cell injury that results in the premature death of cells in living tissue by autolysiso, not following the apoptotic signal transduction pathway |
| NSAIDS | Nonsteroidal anti-inflammatory drugs |
| PBS | Phosphate Buffered Saline |
| PCR | polymerase chain reaction |
| PKM2 | Pyruvate kinase M2 |
| POR | Oxidoreductase |
| PVDF | Polyvinylidene difluoride |
| Radiotherapy | The use of high-energy radiation from x-rays, gamma rays, neutrons, protons, and other sources to kill cancer cells and shrink tumors. |
| RNAi | RNA interference is a biological process in which RNA molecules inhibit gene expression, typically by causing the destruction of specific mRNA molecule |
| ROS | Reactive oxygen species |
| Scr. vector | Scrambled vector |
| Sensitize | Cells become more susceptible to a toxic agent effect |
| SOD | Superoxide dismutase |
| Synergistic | The interaction of two or more drugs when their combined effect is greater than the sum of the effects when each is given alone |
| Telophase | Telophase is the fifth and final phase of mitosis |
| TEMED | Tetramethylethylenediamine |

| | |
|---|---|
| Therapeutic window | The range of drug dosages which can treat disease effectively while staying within the safety range |
| TI | Therapeutic index |
| TNF | Tumor necrosis factors |
| Trx | Thioredoxin |
| Tubulin | One of a group of proteins found in high levels in the cell cytoplasm |
| Xenobiotic | A foreign chemical substance found within an organism that is not naturally produced by or expected to be present within that organism |

# Introduction

## 1.1 Cancer

### 1.1.1 Introduction

Cancer is a term for diseases in which abnormal cells divide without control and can invade nearby or distant tissues. According to the tissue of origin, cancers can be classified into several types. Carcinoma is a type of cancer that arises from epithelial cells. Sarcoma is a form that arises from connective tissues like bone, cartilage, fat, and muscle. Cancer cells can also develop from some vital organs like the brain, kidneys, ovaries, and liver.

Cancers cells resemble their cells of origin. The grading of cancer cells describes how far the cells have differentiated from their counterparts. Poorly differentiated cells are cells that are not like their cells of origin. While the cells that differentiate are similar to their origin cells, poorly differentiated cells, as a general rule, have more mutations and more genetic changes than their cells of origin; thus, cancer attributed to their type of cells have poorer prognoses when compared to well-differentiated cancer cells. The clinical behavior of cancer cells can be attributed to their cells of origin. For example, hepatic and extrahepatic tissue cancer cells have many differences that might direct how and what appropriate cancer therapy can be administered. In this way, the staging system of cancer tumors, related to the size and/or to the spread of cancer cells to other parts of the body, has, important clinical value for determining the most appropriate treatment plan.

Ovarian cancer develops from any part of the ovarian glands. The ovarian epithelial cancer that begins in the cells on the surface of the ovary is the most common form, followed by the malignant germ-cell tumors that begin in the ovary itself (1). According to the American Cancer Society, the incidence rate of ovarian cancer among women is near 3%; however, its mortality rate is higher than any other cancer of the female reproductive system.

Lung cancer is another extrahepatic cancer that has many types based on the cells of origin. Adenocarcinoma is a type of lung cancer that produces mucus. The incidence of adenocarcinoma is increasing among women (2). In developed countries, lung carcinoma accounts for the highest incidence of cancer (3).

Hepatocellular carcinoma (HCC) arises from aberrant hepatocytes, and is the most common type of liver cancer. HCC's most common form results from liver cirrhosis. Alcoholism, hepatitis B, and hepatitis C have a strong association with liver cirrhosis; specifically, cytochrome P450 has a role in causing alcoholic liver cirrhosis (4, 5).

The development of cancer in humans can occur through a complex sequence of slowly evolving events. Cancer cells obtain mutant alleles of proto-oncogenes, tumor-suppressor genes, and other genes that control cell division (6). Seemingly minor gene dysregulation via mutation, amplification, overexpression, or gene silencing may result in loss of local growth control, invasion, and metastasis (7).

Patients' survival is improved when cancer is diagnosed early. A more advanced stage at diagnosis is associated with increased treatment-related morbidities and a worse long-term prognosis.

### 1.1.2 Cancer statistics

The cancer incidence has increased for the last two decades. Several factors contribute to this, including the aging of the population and factors associated with an overall sedentary lifestyle, in addition to environmental toxins and tobacco use. In 2012, there were approximately 14.1 million new cancer cases, with a death rate > 55% worldwide (8). The principal cause of cancer-related death in males is lung cancer, while breast cancer is the leading cause of cancer-related death among females.

In the United States in 2009, the estimate new cancer cases in all body sites was 1,479,350 (in approximately 766,130 males and 713,220 females). The estimated number of related deaths was 562,340 (9).

The National Cancer Institute (Surveillance, Epidemiology, and End Results [SEER] Program), the Centers for Disease Control and Prevention (National Program of Cancer Registries), and the North American Association of Central Cancer Registries have reported a nearly 12% increase in the incidence of new cancer since 2009, with the projected incidence of new cancer cases in 2015 in the USA being 1,658,370, with a near 35% cancer-related death rate. However, the overall cancer death rate decreased from 215.1 per 100,000 in 1991 to 168.7 in 2011, a total relative decline of 22% (8).

### 1.1.3 Cancer chemotherapy overview

The term chemotherapy is generally usedd when cancer drugs are the chemotherapy agents. They are also termed antineoplastic agents. The term cytotoxic drugs is another accepted name for cancer agents, and will be frequently used in this paper.

Cancer chemotherapy has a wide range of distinct cytotoxic agents. These include hormonal, biological, alkylating and antimetabolite agents; plant alkaloids; antibiotics; topoisomerase inhibitors; and platinum compounds. The role of chemotherapy has increased due to several factors. First, there have been improvements in cancer chemotherapy discoveries accompanied by successful clinical trials when two or more distinct cancer chemotherapy agents have been combined (10). Another important factor is that when other cancer treatment modalities, such radiotherapy or surgery, are not feasible or are no longer effective, the need for chemotherapy emerges. Moreover, after a a course of chemotherapy is complete, patients may require maintenance or extended treatment to suppress undetectable residual disease.. With metastatic disease, chemotherapy may be a last resort.

The normal cell life cycle context helps to understand the concept of chemotherapy. Both normal and cancer cells undergo a succession of phases to form replicate cells. The three principal phases of the cell cycle are: interphase, mitosis, and cytokinesis. The interphase can be further divided into three main growth subphases: G1, S, and G2. In G1, the first gap in the cell cycle, in which cell function and centrosomes will double, is created. At the end of the

G1 subphase, DNA starts to duplicate, and the S subphase begins. After DNA synthesis, the cell then enters the G2 subphase, where it grows further and then starts to divide, proceeding first into the mitosis and then the cytokinesis phases. Mitosis involves five subphases: prophase, prometaphase, metaphase, anaphase, and telophase. In mitosis, DNA is packaged into chromosomes and forms the centromeres, which have kinetochores. The spindle fibers, which are made of tubulin comprised of microtubules, bind to the kinetochores and pull the chromosomes to split them into two chromatids in the metaphase. In the anaphase, the cells start to complete chromatid separation as the cells begin to elongate. In the telophase, a cleavage furrow emerges, where the cells start to separate. The cells then enter the G0 phase, where they rest for hours to years, depending on the type of cell.

Cytotoxic agents mainly work on actively dividing cells, and some of these agents work specifically on a particular cell cycle phase (11). Other types of cytotoxic agents do not work specifically on cell cycle phases, but can work on cycling or resting in the G0 phase. Examples of nonspecific cytotoxic drugs are alkylating and platinum based cytotoxic agents. Both groups are nonspecific drug that acts on cells in proliferating as well resting phases during cell cycling.

### 1.1.4 **Rationale for cancer chemotherapy treatment**

Chemotherapy is mainly used to cure cancer or palliate symptoms, in addition to shrinking tumor size to the level where surgical and/or radiological intervention will be much more feasible. While radiotherapy and surgery focus on localized caner tissue areas, cells may spread in clinically undetectable numbers (12). The average number of cancer cells detected by usual diagnostic methods is around $10^9$ cells (13). Undetectable cells have a high potential for proliferation, leading to failure of the treatment plan. Chemotherapy distributes throughout the body, spreading and reaching a wide area as do immunotherapy and biological-response modifiers (14). As such, cytotoxic agents can reach the cells where other treatments cannot. Patients who have received initial surgery or irradiation are often scheduled for maintenance chemotherapy, which is used to insure that undetected cells are killed or arrested.

In some advanced stages of cancer where metastasis has occurred, for which radiotherapy and surgery are not indicated, chemotherapy is usually the treatment of choice.

### 1.1.5 **Chemotherapy side effects**

Adverse effects of limit the use of chemotherapeutic agents. According to the National Cancer Institute (NCI), individuals who undergo chemotherapy treatment experience musculoskeletal symptoms in addition to vomiting, nausea, constipation, and/or diarrhea. Other serious negative effects on the

liver, kidneys, bone marrow, and immune system are considered a major drawback to these agents. The incidence of cytotoxic agents' side effects is linked to several factors, such as the dose, the mechanism of the drug's action, and the mode of administration. As a higher dose of cytotoxic agents kills cancer cells more efficiently, normal cells are also seriously affected. Platinum compounds are one of the agents that cause several side effects at higher doses. For instance, CP produces dose-dependent renal toxicity, which indicates a need to decrease or discontinue the medication.

### 1.1.6 **Limitations of using chemotherapy agents versus cost**

The side effects of chemotherapy limit the use of cytotoxic agents. The need to minimize and manage side effects is always priority for patients and their caregivers. Rapidly proliferating cells, such as those of the bone marrow, gastrointestinal mucosa, reticuloendethilial system, and gonads, are at higher risks for toxicity due to chemotherapeutic agents. Some of these adverse effects—such as nephrotoxicity, liver toxicity, and dermatitis—can be life threatening.(15).

Another limitation of cytotoxic agent use is drug resistance. When certain types of cancer develop resistance to a particular cytotoxic agent, an alternative agent should be considered (16). Resistance to treatment can be considered when cancer cells reappear within 6 months of effective initial treatment (17).

Chemotherapy resistance may require termination of the use of the cytotoxic agent. As a result, there is a continuing need for new treatments. With a nearly $1.3 billion cost for a chemotherapy drug to ultimately achieve approval, the high cost of newer drugs is ultimately passed on to the health care system (18). The average total drugs cost for one year for some particular type of cancer is near $120,000 (19). Thus, the cost of finding an approach to reverse drug resistance and allow continuing use of such drugs might be less than bringing a new drug entity to market.

CP is a chemotherapy drug that was discovered in the mid-fifties, and it was used in a number of forms of cancer, such as ovarian cancer, of which more than 70% of patients have CP-based treatment(20). However, ovarian cancers cells have developed resistance to CP, which limits its clinical use(21).

## 1.2 Cisplatin

### 1.2.1 Introduction

Cisplatin [cis-Pt $Cl_2(NH_3)_2$] (CP) is a water-soluble anticancer drug containing an inorganic platinum metal that binds to two amine groups and two chlorides, and is abbreviated as cDDP or CP (22). To allow CP to react within cellular biological systems, a chloride must be replaced with water (see Figure 1.2.1.1). The hydrolysis of cisplatin in aqueous solution has been investigated extensively.

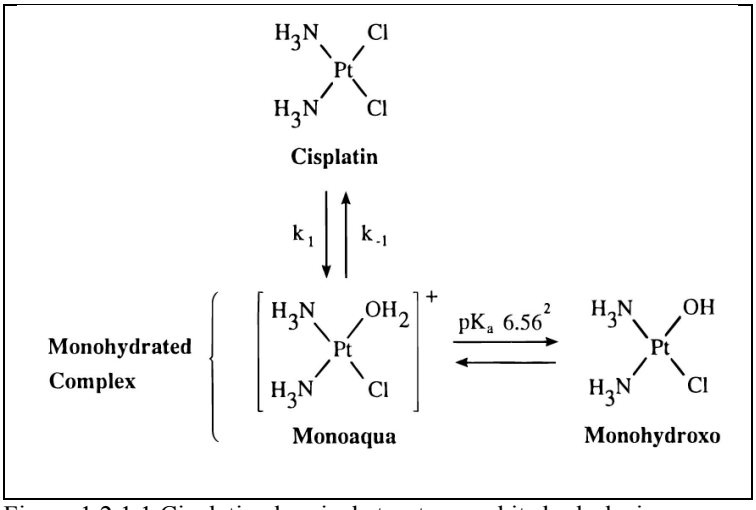


Figure 1.2.1.1 Cisplatin chemical structure and its hydrolysis
A platinum element is linked to two chloride atoms in the cis position and two ammonia molecules. The formation of a monoaqua results from a single Cl atom replacement with a single water molecule, the watered CP complex is essential for CP to perform its biological reactions. (23).

CP has been used to treat many kinds of cancers since FDA approval in 1978. Rosenberg discovered the platinum-based compound by chance in 1965 while trying to find the potential role of an electrical field on bacterial cell

growth(24). Despite the large debate that had been ongoing among oncologists regarding the use of large, heavy metals like platinum in treating cancer cells, the success of CP in treating disseminated testicular cancer with a 90% cure rate brought this compound to the attention of the medical community (25). CP started to be evaluated as an adjuvant for some other cancer types such as ovarian, head and neck cancers, and others. CP shares some similarities with alkylating agents in mechanism of action.

### 1.2.2 **Mechanism of CP cytotoxic effect**

The biological effect of CP is initiated when a water molecule replaces one Cl atom in CP and forming a hydrated CP which has been termed monoaqua CP. The fate of hydrated CP, as in Figure 1.2.2.1, varies according to the type of biological structures that it might interact with, such as GST or other proteins available in the circulation. In addition the hydrated form, CP can be carbonated or phosphated (23). The biological effects of the newly formed adducts with CP varies. When a CP nucleotide adduct is formed, destructive effects on the DNA structure of the living cells can occur due to the chemical interaction with cellular DNA. CP interacts with nucleotides to form irreversible DNA–DNA interstrand and intrastrand crosslinks structures that destroy cells(26). The chemical properties of platinum atoms make CP more balanced when reacting with the N7 of guanine in DNA (27). CP adducts to DNA deform the regular DNA structure, interfering with the DNA repair process. The high mobility group (HMG)-domain protein HMG1 later binds to

DNA adducts. The combination of the protein and a DNA adduct prevents the DNA from being repaired (28). Cells treated with CP show no further cell cycle progression. The DNA is damaged, forcing the cell to go through different biochemical cascades that trigger apoptosis. The necrosis process has also been reported when higher doses of CP are used (29). Other mechanisms of CP's destructive effect on cancer cells have been proposed. ROS have been widely investigated for their role in the growth of cancer cells (30, 31). CP can trigger cancer cell death by forming ROS (32). ROS showed a significant role in cancer initiation; however, excessive ROS showed triggering of apoptosis (31). Thus, the role of redox systems in ROS, the impact of ROS on CP resistance, and CP's side effects are timely research topics.

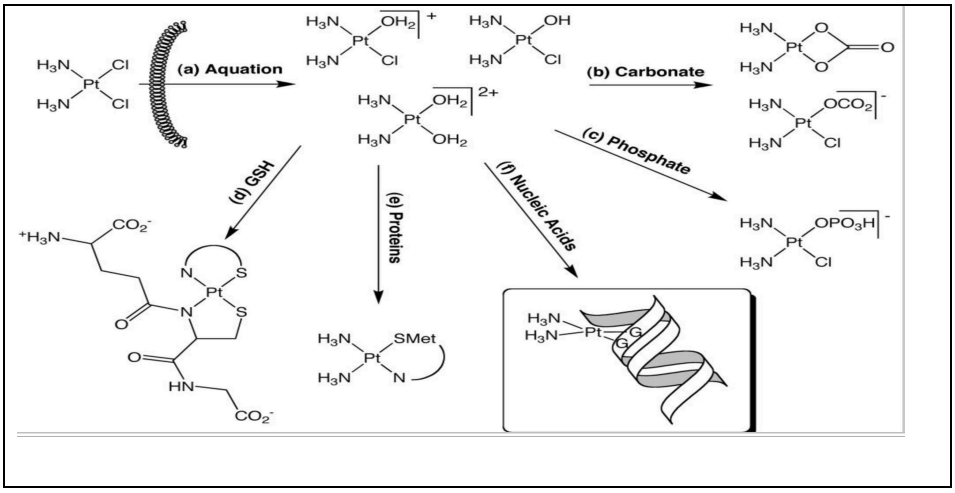


Figure 1.2.2.1 Cisplatin biological reactions
This figure was adopted from a previous study by Todd (33), and shows CP reactions in addition to aquation (hydration).

### 1.2.3 **CP therapeutic index**

The therapeutic window (TW) of a drug reflects the safety profile of chemotherapy drugs. TW is quantified as the therapeutic index (TI), which is the ratio of the dose that produces toxicity divided by the dose that achieves effective clinical results. The theraputic index $= \frac{TD50}{ED50}$, where $TD_{50}$ is the toxic dose for half of the population, and $ED_{50}$ is the effective dose for half of the population. A drug with a wider therapeutic window (see Figure 1.2.3.1a) reflects a more favorable safety profile than one that has a narrower TI (see Figure 1.2.3.1b). In general, the chemotherapeutic drug has a narrow TW and relatively small TI; therefore, the safety profile of these drugs is less than others.

Some pharmacokinetic properties of cytotoxic drugs unfavorably affect their safety profile. For CP, 90% of the circulating drug is protein bound, and is primarily excreted by the kidneys. During the first five days of treatment, between 27–45% of the drug is excreted. The concentration of CP is fivefold greater in the renal epithelium than in the plasma (34). Thus, when CP is considered in cancer patients, their renal function must be closely monitored. The use of smaller doses of CP, as in any cytotoxic drug, would favorably affect the TI. Decreasing the $IC_{50}$ of the cytotoxic drug by increasing drug sensitivity would be an effective way to improve safety while maintaining effectiveness.

CP infusion times in a clinical trial for ovarian cancer patients showed CP's therapeutic index improved when a lower dose of CP was used (35).

Different approaches can be used to widen the TI of cytotoxic drugs. For example, adjuvant therapy favors the TI by improving the positive clinical effects of the cytotoxic drugs either additively or synergistically (36-38).

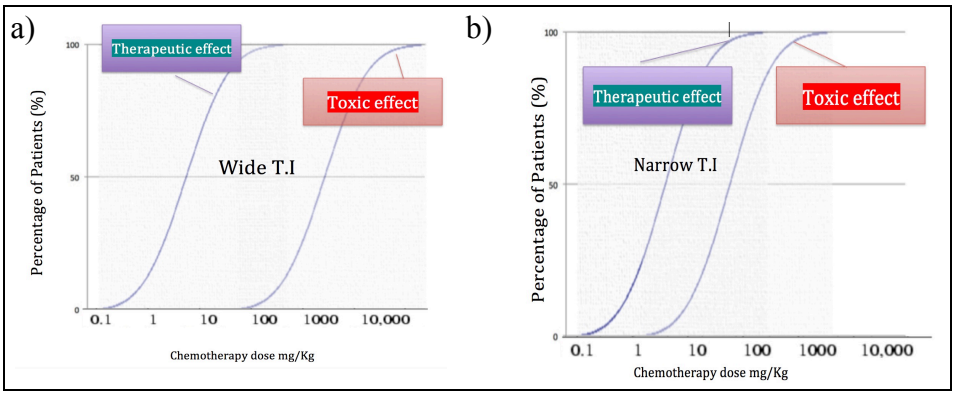


Figure 1.2.3.1 Wide and narrow therapeutic index
This is schematic graph to explain the therapeutic index: a) shows a wider therapeutic index than b).

### 1.2.4 **Cancer resistance to CP**

When cancer cells start to survive chemotherapy treatment, the term "chemotherapy resistance" is used. The resistance can be intrinsic, when there is no cytotoxicity response with the first exposure. When cancer cells that were initially sensitive later are not affected by the cytotoxic agent, "developed acquired resistance" leads to an increase in $IC_{50}$ of the toxic agents. When cancer cells are resistant to a particular cytotoxic agent, they may also have resistance to other related drugs; this is known as multidrug resistance (14). In clinical and laboratory studies, acquired resistance to CP often associated with resistance to other agents structurally and mechanistically discrete from CP (39).

Intrinsic and acquired resistances are both timely research topics, aimed at overcoming the downside of cytotoxic drugs. The underlying mechanism of chemotherapy resistance is not fully established. In the case of CP resistance, a kinetic resistance phenomenon has been observed, as in confluence-dependent resistance (CDR). This happens in certain types of cancer cells such as carcinoma, demonstrating resistance to forms of chemotherapy (40). CDR might occur due to accumulation of cancer cells protecting themselves against cytotoxic agents and preventing any cellular penetration (41). The Goldi-Coldman theory, addresses the genetic instability of cancer cells and dynamic changes in their structure the theory suggests the presence of subpopulations of resistant and sensitivity phenotypes, along with phenotypes sensitive to a particular cytotoxic agent (42).

Other factors in chemotherapy resistance are: decreased drug uptake; increased drug efflux; an increased level of GSH and increased activity of GSH-related enzymes; an increased level of metallothioneins; reduced bioavailability of platinum; alterations in nucleotide excision and mismatched repair in addition to increased DNA repair capacity and/or increased capacity to replicate through adducts; alterations in anti-apoptotic factors (e.g., BCL-2, IAPs); alterations in pro-apoptotic factors (e.g., p53, caspases, Fas, BAX, BAK); alterations in the MAPK cascade pathway; alterations in the PI3-K/Akt signaling pathway; alterations in transcription factors; failure to induce cell death; and alterations in cell cycle-related factors (43, 44).

Moreover, the upregulation of some antioxidant systems upon oxidative stress circumvents the disruption of antioxidant systems within cancer cells, resulting in resistance toward cytotoxic agents. For example, an increase in cellular glutathione is associated with CP-acquired resistance. The exposure of human ovarian tumor cell lines to CP led to the development of cell lines that exhibited increasing degrees of drug resistance, which were associated with an increase in the levels of cellular glutathione (45).

In the early-1920s, Warburg observed an increase in aerobic glycolysis in most cancer cells followed by lactic acid fermentation in the cytosol compared to normal cells that utilize low rate of glycolysis, followed by oxidation of pyruvate in mitochondria (46). The metabolic shift is apparently related to a disturbance in mitochondrial functionality; the increase in ROS production in mitochondria leads to alterations in oxidative phosphorylation

(OXPHOS). Stimulation of hexokinase II attachment to mitochondrial porin due to alterations in the Ras-PI3K-Akt signal transduction pathway can result in a metabolic shift (47). The importance of this shift is that the induction of the antioxidant NADPH within the cancer cells allows adaptation to oxidative stress. In lung cancer, the intracellular metabolic shift to the pentose phosphate pathway increases upon acute ROS generation, which reduces the activity of the glycolytic enzyme pyruvate kinase M2 (PKM2) by oxidation of Cys (358) in the enzyme. This ultimately leads to an increase in the antioxidant NADPH (48).

## 1.3 Reactive Oxygen Species (ROS)

### 1.3.1 Introduction

Oxidation refers to gaining oxygen or losing hydrogen or electrons, whereas reduction indicates the loss of oxygen or acceptance or gaining of hydrogen or electrons. Oxidizing agents accept electrons and cause other entities to be oxidized; however, the oxidizing agents themselves are reduced when they oxidize others. The reverse applies to reducing agents: They donate electrons to reduced entities, but they themselves are oxidized. Transferring electrons among species is called redox.

In cellular biology, redox systems have an important role in sustaining homeostasis and other biological reactions. The outcome of these reactions can create free radical species, an unpaired electron in its outermost orbital. When

an oxygen molecule is reduced, free radicals are formed. These species are prone to react with other molecules to reach equilibrium (49). The discovery of free radicals in the mid-fifties was followed by attempts to understand these species and how they form (50). Free radicals may participate in the stimulation and activation of guanylate cyclase and the formation of the "second messenger" cGMP (51).

Most free radicals are derivatives of oxygen, after which ROS were named. Agents that induce ROS or inhibit antioxidant systems are called prooxidants. In addition to oxygen, there are derivatives of nitrogen called reactive nitrogen species (RNS).

ROS are highly reactive particles by which $O_2$ undergoes reduction. ROS is a collective term representing a group of different free radicals or non-free radicals ($H_2O_2$), $O_3$, and HClO. When oxygen reduction takes place, one or up to three electrons will be lost; then, reactive intermediates are formed:

($O_2^-$), ($^{\cdot}OH$).

$O_2 + e^- \rightarrow O_2^- + e^- \rightarrow H_2O_2 + e^- \rightarrow {}^{\cdot}OH + e^- \rightarrow H_2O$

The principal source of exogenous ROS is ultraviolet light and radiation. Endogenous ROS are the byproducts of biochemical reactions within cells. The main source of endogenous ROS is the electron transport chain in the mitochondria; microsomal monooxygenation; oxidase flavoproteins in peroxisomes; and, in plasma membrane lipoxygenases, prostaglandin synthases and NADPH oxidase.

Hydroxyl radical formation can occur as a byproduct of the Haber–Weiss reaction and Fenton reaction, which is considered to be the principal mechanism by which the highly reactive hydroxyl radical is generated in biological systems (52).

$$Fe^{3+} + O_2^{\cdot-} \rightarrow Fe^{2+} + O_2 \qquad (1)$$

(Fenton reaction) $Fe^{2+} + H_2O_2 \rightarrow Fe^{3+} + OH^- + {}^{\cdot}OH$ (2)

The net reaction: $O_2^{\ -} + H_2O_2 \rightarrow O_2 + OH^- + {}^{\cdot}OH'$ (3)

ROS' half-life varies from milliseconds to minutes. Hydrogen peroxide has one of the longest half-lives (up to minutes), while the hydroxyl radical has the shortest (milliseconds) (53).

### 1.3.2 **Antioxidant system**

ROS originate mainly from the mitochondrial electron transport chain, thus the need to balance the quantity of free radicals to maintain cells' redox homeostasis within normal functional physiological levels.

An antioxidant can be defined as "any substance that when present at low concentrations compared with those of an oxidizable substrate significantly prevents or delays the oxidation of that substrate" (54). When an antioxidant becomes oxidized, the antioxidant resource must be replaced.

Antioxidants can be classified into two groups according to their action. Enzymatic antioxidants include SOD, catalase, Gpx, and glutathione reductase. Nonenzymatic antioxidants can be subclassed into 1) nutrient antioxidants such

as β-carotene, α-tocopherol, and ascorbic acid, and 2) metabolic antioxidants such as bilirubin, uric acid, ceruloplasmin, ferritin, transferrin, albumin, and glutathione.

Glutathione has protective roles against free radicals associated with xenobiotics, and potentially harmful electrophilic agents. Gluthine is a tripeptide consisting of cysteine, glutamic acid, and glycine, with sulfhydryl in the cysteine. It is synthesized in the liver and distributed ubiquitously. Glutathione exists in reduced (GSH) and oxidized forms (GSSH), with GSH more abundant than the GSSH form. The ratio of the two forms is a primary determinant of cell sustainability (55). Generated free radicals lead to the formation of $H_2O_2$, which is considered a GST inducer in plant and mammalian cells (56). ROS induction of GST is considered an adaptive response (56).

Glutathione reacts spontaneously with the help of glutathione transferase enzymes (GST) (57). Glutathione transferases (GST) are capable of catalyzing the basic reaction in which glutathione is added to an electrophilic canter of an acceptor molecule, resulting in a conjugate thioether compound (58).

GSH-associated enzymes involved in GSH metabolism are glutathione peroxidase (GSHPx), glutathione reductase (GR), glutathione S-transferase (GST), γ-Glutamyltransferase (GGT), γ-Glutamylcysteine synthetase (GCS), and glutathione synthetase (GSHS) (44). In mammalian cells, GST has six families that exist in dimers (alpha, Mu, Pi, Theta, Zeta, and Omega), having the principal function of detoxification of glutathione conjugated with

electrophilic structures (59). The GSH to GSSH ratio and the level of some of the relevant enzymes are modified in some types of cancer cells, and in some cancer cells resistant to anticancer drugs (60, 61). High levels of GSTpi attributed to anticancer drug resistance have been detected in some tumors. GSTpi enhances drug resistance by direct detoxification and by acting as an inhibitor of the MAP kinase pathway (62).

### 1.3.3 **Oxidative stress**

When ROS production (prooxidants) and the counteracting antioxidant system are imbalanced, the excess ROS leads to oxidative stress (63). This imbalance, favoring the prooxidant, will produce cellular damage potentially affecting the apoptotic system.

Oxidative stress can contribute to any of the three known forms of cell death: apoptosis, necrosis, and necroptosis. Apoptosis, also known as programmed cell death, is characterized by a series of morphological and biochemical alterations which involve early nuclear collapse, condensation of chromatin, generation of nucleosomal ladders, and cell fragmentation, with little or no early alteration of lysosomes (64, 65). The earliest hallmark of appoptosis is caspase-activated DNase (CAD), an enzyme responsible for cleaving DNA into fragments (66). Necrosis is an uncontrolled process associated with sudden loss of cellular integrity and extracellular release of content, with a possible humoral immune response (67). The third form of cellular death is necroptosis, which is a form of necrosis associated with

inhibition of the apoptotic pathway. Necroptosis induces TNF superfamily members of the “ death receptor” (67).

All three forms have been described as a direct consequence of ROS increase, and are associated with oxidative stress. In addition to its necrotic effect on cells, oxidative stress may be associated with TNFα-induced necroptosis (68-71). In addition, oxidative stress induces downstream serine-threonine kinase (RIPK)1 activation (68).

### 1.3.4 **ROS and cancer**

Intracellular ROS concentrations must be regulated for beneficial biological effects to occur. When ROS is increased, the cell will undergo oxidative stress unless antioxidant systems overcome the increase. Free radicals are prone to interact with molecules to achieve stability. Therefore, when ROS species exceed the limit of biological value, damage to DNA might occur, followed by cascades of cellular signaling and ultimately activation of the apoptotic pathway. DNA mutations might also be produced which could modify proliferative capacity. As such, ROS may act as cancer initiators.

On the other hand, an increase in ROS can be advantageous when cancer cells undergo death either by the apoptotic or necrotic pathways.

### 1.3.5 **ROS and CP**

Increased ROS formation due to CP has been described, but the exact mechanism for such an increase is still unknown. When an interaction between

CP and DNA was evaluated for oxygen free radical formation, an increase in free radicals was observed upon CP interaction with DNA (72). The ROS increase upon CP treatment might be related to adverse effects such as nephrotoxicity and hepatotoxicity.

#### 1.3.5.1 Nephrotoxicity

One of the principal dose-dependent side effects of CP treatment is nephrotoxicity (73-79), occurring in about one-third of patients who receive CP treatment (80). Nephrotoxicity is more likely when CP is used in higher doses and over a longer time (81). Several mechanisms have been proposed to explain CP nephrotoxicity (82). The cause is not straight forwardly linked to the heavy-metal loading, since chelating agents do not prevent CP- related nephrotoxicity. Delivering the platinum-containing drug in its trans-iso form does not cause nephrotoxicity as CP does (34). A Role of hemodynamics in initiating CP-induced nephrotoxicity has also been ruled out (78). Some observations suggest a direct role of proximal tubular impairment in initiating CP nephrotoxicity (78). Lipid peroxidation is increased by CP, which might be directly linked to the development of nephrotoxicity (83). Some data show that glutathione S-transferase Pi (GSTP) may have a role in CP-induced nephrotoxicity, in that it processes CP-glutathione adducts into nephrotoxic compounds (84). Moreover, the CP-Glutathiol adduct showed evidence of a direct contribution to nephrotoxicity when the adduct was processed by gamma glutamyl transpeptidase (GGT) in the renal tubules (85).

CYP2E1 may have a role in CP nephrotoxicity upon ROS formation (86). The nephroprotective effect of some substances was evident when CYP2E1 monooxygenases' reaction-induced oxidative stress was mitigated (87).

#### 1.3.5.2 Hepatotoxicity

Hepatotoxicity is another important dose-limiting side effect of CP-based chemotherapy. The possible association of CP associated hepatotoxicity with ROS increases may be related to CYP2E1 expression and activity (88), as well as depletion of reduced glutathione (GSH) associated with an increase in ROS (88). Administration of riboflavin (vitamin B(2)) as an antioxidant mitigated hepatotoxicity in cancer host animals who received CP, consistent with a role of hepatocyte damage related to ROS (89).

CP can cause acute apoptosis by disrupting the antioxidant systems within the biological cell environment (90). CP-induced hepatotoxicity was augmented when *CYP2E1* expression increased in situations in which ROS production was involved in oxidative stress (88).

.

## 1.4 Cytochrome P450

### 1.4.1 Introduction

Cytochrome P450 (P450s) is an superfamily of heme-thiolate proteins (91). The origin of the word came from the protein's natural existence within the cell; therefore, 'cyto' means cell, while and 'chrome' and 'P' come from the heme pigmentation in which these enzymes have heme . The pigmentation in P450s, when exposed to CO, is reduced; the reduced P450s absorbs light at a wavelength of 450 nm (Soret peak) (92, 93). Nearly 75% of drugs are metabolized by the P450 group. There are approximately 57 human P450s; five of these are involved in nearly 95% of all metabolic activities (94). A systematic nomenclature is used to designate CYPs, The number that comes after CYP is an Arabic number that denotes the family (for example, CYP2); next comes a letter that represents a subfamily, such as CYP2E, then the last Arabic number denotes specific protein isoforms; i.e., CYP2E1 (95, 96). When CYP is written in italics, it denotes a gene (96). P450 enzymes are primarily expressed in the liver (94).

P450s do not work alone; they require an electron transport system (redox) to assist in oxygen activation and the subsequent substrate hydroxylation and electron transfer cycle (Figure 1.4.1.1.). In general, when a substrate binds to ferric cytochrome, a P450 monooxygenation reaction cycle is initiated (97). By breaking the $O_2$ bond of the activated oxygen molecule, oxygenation of the substrate occurs. The process requires two external electron

donors; the first electron is transferred to substrate-bound cytochrome P450, which reduces the ferric ($Fe^{+3}$) heme to a ferrous ($Fe^{+2}$) form to yield an oxygen molecule. Meanwhile, the second electron is given to an oxygenated heme, leading to activation of the bound oxygen molecule, and an oxygen atom attaches to the substrate (97).

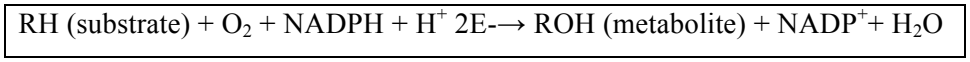


Figure 1.4.1.1 Stoichiometry of the monooxygenation reaction (MonR) of P450s
The role that P450s plays in catalyzing the incorporation of only one atom of molecular $O_2$ into its substrate while reducing the second into $H_2O$

## 1.4.2 **Structural characteristics of membrane-bond P450s**

In eukaryotic cells, P450s's membrane-bound proteins incorporate into the endoplasmic reticulum by the N-terminal polypeptide chain. The catalytic domain followed by the N-terminal polypeptide chain anchors microsomal P450 into the endoplasmic reticulum. The process of anchoring stops at the hydrophobic amino acid residues (98-101) (see Figure 1.4.2.1).

In mitochondrial P450s, the precursor of P450 is imported into the mitochondria, where the mitochondrial P450s is truncated. The proteolytic processing of newly synthesized P450 is exclusive to mitochondrial microsomes (99).

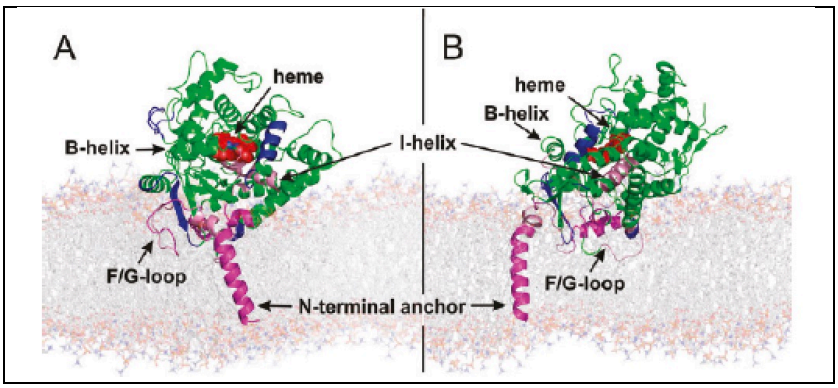

Figure 1.4.2.1 N-terminal of P450s
This image depicts N-terminal anchoring in similar endoplasmic reticulum membrane structures. The role of the N-terminal is to immobilize P450s from being displaced to other sites in the cell (102).

### 1.4.3 **P450s electron transport systems**

The electron transport systems that yield the two necessary electrons for cytochrome P450 can be divided into two main classes based on their cellular location and the redox system that is used: the mitochondrial P450 system, and the liver microsomal P450 system. However, approximately nine other classes can also be identified, each of which provides a unique electron system (103).

Class I includes mitochondrial and bacterial P450s, which use two separate redox partners consisting of an iron–sulfur protein, ferredoxin and adrenodoxin, a flavin-containing reductase, and adrenodoxin reductase (104-106). Meanwhile, class II P450s includes microsomal P450, which receives electrons from a single NADPH-cytochrome P450 oxidoreductase (POR) containing FAD and FMN.

In microsomal systems, the transfer of electrons from NADPH is catalyzed by oxidoreductase, which is part of the diflavin oxidoreductase family; it has multi-domain enzymes containing distinct FAD and FMN domains that are connected by a flexible hinge with flavin cofactors (107, 108). NADH dehydrogenase contains flavin mononucleotide, which can be used to reconstitute recombinant P450s as a cofactor (109). In Figure 1.4.3.1, R-H is one of a wide ranges of substrates that can interact with P450s heme; as mentioned previously, the reaction requires two electrons that can be given by two main donors, POR and Cytochrome b5 (Cyt-b5). POR can give both

electrons for many P450s monooxygenases reactions. However, in some P450s, the second electron can come from another donor.

Cyt-b5 is an ER-anchored protein with ~134 amino acids. It is considered a membrane-bound electron transfer heme, which has an opposite effect on P450s. For some P450s, like CYP2B4, Cyt-b5 as a second electron donor is much faster than POR (110, 111). Four possible mechanisms have been proposed to explain Cyt-b5 activity. The first is direct input of an electron into the monooxygenase cycle, which is necessary to activate molecular oxygen and is considered a rate-limiting step. The second mechanism could be the rate of electron donation by Cyt-b5 when compared to others; this speed is needed to prevent an uncoupling reaction during which a superoxide anion can be formed instead of the formation of two-electron reduced oxygen. The third possible mechanism is the formation of a hemoprotein complex that is comprised of P450s and Cyt-b5; this complex will accept the second electron for POR. The last possible mechanism is Cyt-b5 enhancing the flow of the electrons through the cycle without a direct role in the redox system (111).

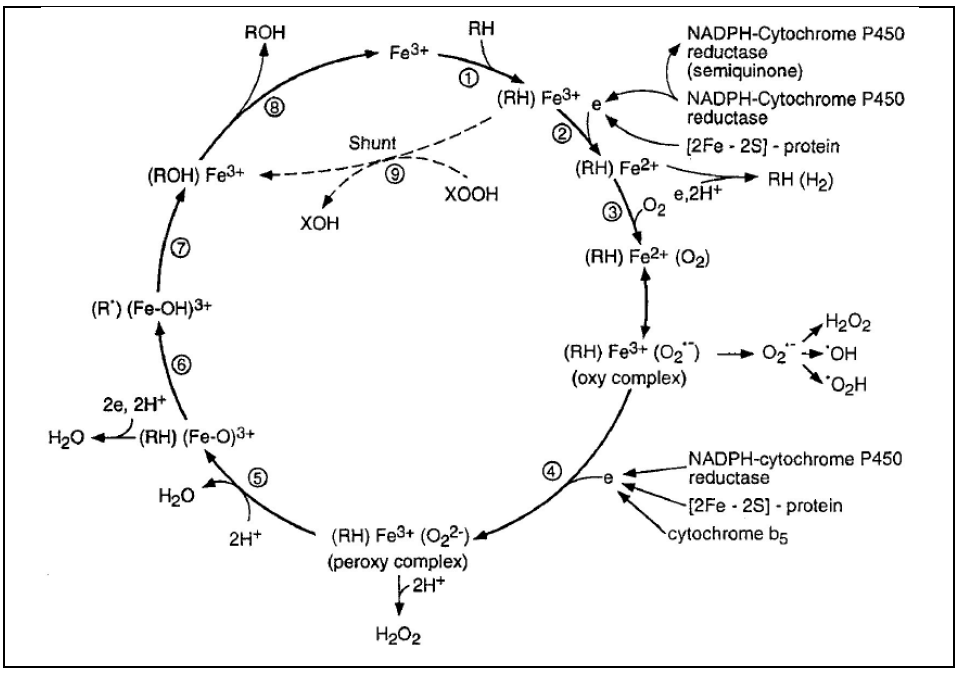


Figure 1.4.3.1 Cytochrome P450s monooxygenase reaction cycle
The P450 cycle starts when RH (Substrate) reacts with $Fe^{3+}$ and two electron donors in step 2 and step 4.

## 1.4.4 **CYP2E1**

### 1.4.4.1 Introduction

CYP2E1(112) is involved in the metabolism of xenobiotics in the body and features high catalytic activity with ethanol (113). Substrates for biotransformation by CYP2E1include: ethanol, isopropanol, capsaicin 1,3-butadiene, methanol, chlorzoxazone, and chloroform, in addition to a number of other xenobiotics, (114).

CYP2E1 is present in the liver, and in extrahepatic tissues (115, 116). The liver expresses most of the CYP2E1, which is induced by ethanol, and which is localized primarily in the endoplasmic reticulum (117).

Besides ethanol, some compounds like nicotine may induce CYP2E1 (118). The possible effect of reducing the degradation of CYP2E1 (protein stabilization) has been reported (119).

An inhibitor for CYP2E1 metabolic activity is N,N-diethyldithiocarbamate (DDC), a metabolite of disulfiram. In some studies, DDC and some of its derivatives may also have a direct cytotoxic effect on some cancer cell lines (120, 121).

### 1.4.4.2 CYP2E1 and proteasome complex

Some investigators have addressed the role of the proteasome complex as non-transcriptional regulators of human *CYP2E1* in HepG2 cells transfected with *CYP2E1* cDNA. Human CYP2E1 appears to have a short half-life, and its turnover rate can be regulated by substrates in living cells (122). Apparently,

intracellular proteolytic systems have a role in the regulation of CYP2E1 (122). Ala-Leucinal (PSI) inhibits chymotrypsin-like activity of proteasomes, the only inhibitor to influence CYP2E1 degradation. PSI had no direct effect on CYP2E1 as a ligand or substrate (123). Ethanol inhibits the proteolytic system, such that its apparent CYP2E1 induction effects could be explained by a reduced turnover rate of CYP2E1. Ethanol inhibits proteolytic enzyme activity upon ROS generation by CYP2E1 (124). Inhibition of the CYPE2E1 degradation process without a change in *CYP2E1* mRNA has also been reported (125).

### 1.4.5 **Platinum based compounds' effect on CYP450 activity**

Since 1969, platinum-based compounds have been known to act against cancer cells (126, 127). However, the pharmaceutical industry's development of platinum-based drugs requires balancing of efficacy and safety. This includes evaluation of drug interactions. The potential inhibitory effects of some platinum-based drugs on P450s have been explored. JM216 is a platinum-based drug that can be given orally to inhibit the catalytic activities of CYP isozymes (128). Another platinum-based drug is oxaliplatin, whose derivatives have inhibitory effects on human liver microsomal CYP3A4 activity (129). The possible inhibitory effect of platinum-based compounds on human drug-metabolizing activity needs more extensive evaluation (130).

### 1.4.6 **CYP2E1, ROS, and CP**

Cytochrome P450s may provide a source of catalytic iron (catalyzing free radical reactions) related to CP-induced nephrotoxicity (131). ROS play a significant role in CP-induced nephrotoxicity; however, the site and mechanism of formation are not established (132, 133). CYP2E1 is localized to the kidney proximal tubule, and is related to ROS generation (134). Increased levels of ROS were linked to the overexpression of CYP2E1 when triggered by CP in a hepatocellular carcinoma cell line (134, 135). The results confirm that CYP2E1 overexpression potentiates CP cytotoxicity, which in turn might involve enhanced production of oxidative stress.

### 1.4.7 **In vitro studies of CYP2E1**

Microsomal and mitochondrial *CYP2E1* genes have been used to produce transfected hepatocellular cell lines that overexpress CYP2E1 (136, 137). Hep G2 cell models are used for this purpose, since they lose their ability to express active CYP2E1 (138, 139). In addition, induction of CYP2E1 has been observed with long-term exposure to Ethanol for one year.

CYP2E1 overexpression has been achieved with human *CYP2E1* plasmid-transfected Hep G2 cells (140). These cells show metabolic enzyme activity based on the capacity to metabolize chlorzoxazone. This indicates that the biological environment within these cells is suitable to allow CYP2E1 synthesis.

For extrahepatic cells, transfection of *CYP2E1* has been reported for cell lines such as L6 (myoblast), primary rat adipose (PRA) cells, and Chinese hamster ovary cells. (141, 142). Moreover, heart tissue-specific CYP2E1 transgenic mice were produced to study the effects of CYP2E1 overexpression in the heart (143).

The effect of generating ROS via mitochondrial CYP2E1 upon CP treatment has also been explored. A new cell line from Hep G2 can overexpress mitochondrial CYP2E1; this cell line is different from previously established cell lines in that it is an $NH_2$-terminally truncated form of *CYP2E1* that is exclusive to mitochondrial CYP2E1(144). Therefore, the electron transfer system used within the cells differs from the microsomal CYP2E1. Subsequently an increase in CP toxicity in HEP G2 cells was observed in relation to expression of mitochondrial CYP2E1. Glutathione and thioredoxin regulate the mode of CP toxicity in mitochondrial CYP2E1 overexpressed Hep G2 cells via the redox regulation of caspase (135).

## 1.5 Aims and Objectives

The cost of bringing new anticancer agents to market may exceed the cost of finding new approaches to improve the efficacy and safety of existing clinically-approved cytotoxic agents. Through the wide use of CP as primary or adjuvant chemotherapy, the emergence of resistance has worked against the applicability of CP in clinical oncology. If CP resistance could be reversed and antineoplastic sensitivity increased, the existing value of CP could be enhanced and the therapeutic index widened.

Therefore, the principal objective of this study is to sensitize cancer cells that show resistance to CP, thereby maximizing CP's clinical value by widening its therapeutic index.

The specific aims are:

1) To identify cancer cell lines that exhibit resistance to CP treatment using cell viability assays.
2) To overexpress microsomal CYP2E1 enzymes in hepatic and extrahepatic cancer cell lines.
3) To evaluate the ability of CYP2E1 to be overexpressed in cancer cells that are resistant to CP.
4) To assess the inhibitory effect of CP on CYP2E1 activity.
5) To assess the effect of a CYP2E1 inhibitory agent (DDC) on cell viability.
6) To evaluate ROS generation upon CP treatment in CYP2E1 overexpressed cells.

7) To evaluate the effects of generated ROS on CP treatment in CYP2E1 overexpressed cells.
8) To reverse the effect of CYP2E1 on cell viability by inhibiting its metabolic activity.

## 1.6 Hypotheses

Our principal hypothesis states that increasing active microsomal CYP2E1 expression and metabolic functions will sensitize CP-resistant cancer cells when treated with CP.

Hepatic cells have the appropriate cellular environment for CYP2E1 to actively process its substrates. However, it is not established whether human extrahepatic cancer cells, with or without CP, possess the necessary functional capacity to produce active microsomal CYP2E1 upon external transfection with *CYP2E1*. Our study hypothesizes that extrinsically CP-resistant extrahepatic cancer cells will produce active microsomal CYP2E1 upon non-truncated *CYP2E1* transfection, and that this will enhance CP sensitivity.

Our study will rule out any potentially confounding inhibitory effect of CP on microsomal CYP2E1 activity. We also will investigate the cytotoxic effect of DDC itself on cancer cells. If such effects are excluded, DDC could be used as a CYP2E1 inhibitory agent to reverse oxidative stress that might be caused by ROS, which is generated when CP interacts with CYP2E1. To determine the appropriate mode of exposure of the CYP2E1 inhibitor DDC to the index substrate CHZ, the study will examine whether CYP2E1 inhibiters act reversible or irreversible mechanisms.

# 2 Materials, Methods, Results

## 2.1 Cell lines, culture and maintenance

### 2.1.1 Cell lines

Six cell lines were used in the experiments. For the **Hep G2 human hepatocyte carcinoma** cell line, 85011430 SIGMA (the growth mode adherent with epithelial morphology), the recommended culture media were used according to the supplier: Minimum Essential Medium Eagle MEM (EBSS) M2279 SIGMA, plus 2mM L-glutamine, G7513 SIGMA, plus 1% MEM non-essential amino acid solution M7145 SIGMA, plus 10% fetal bovine serum (FBS) F2442 SIGMA. According to the supplier, the following subculture routine was followed when the cells reached confluence of 70-80%, splitting 1:3 to 1:8 (i.e., seeding at 2-3x$10^3$ cells/$cm^2$); however, the number of cells seeded increased when transfection with the DNA plasmids were planned to reach a confluence of 75-85%, depending on the size of the plates used. According to the size of the tissue culture plate, 100µl-1ml of 0.1% trypsin or 0.25% trypsin/EDTA was used for 2-5 minutes in 5% $CO_2$ at 37°C, and then neutralized with 1:9 culture medium. The media were changed every 2 days. Most of the experiments were conducted after 3-6 passages, which is an acceptable range for this cell line to retain biological properties.

**A2780 ovarian cancer** cell line, 93112519 SIGMA, the growth mode adherent with epithelial morphology, was the parent line for the CP-resistant cell line, A2780CPR. The following culture media were used, according to the supplier: RPMI-1640 with sodium bicarbonate, R0883 SIGMA, 2mM

glutamine and 10% FBS. The supplier recommended subculture routine was followed by splitting sub-confluent cultures (70-80%) 1:3 to 1:6, which means seeding at 3-6x$10^3$ cells/$cm^2$ using 0.25% trypsin for one minute at 5% $CO_2$ and 37°C.

For **A2780/CPR ovarian cancer resistant to CP cell line**, 93112517 SIGMA, derived from A2780 when treated with increasing CP concentrations for more than 6 month, the culture medium used was the same as that for the A2780 cell line.

In the **human lung adenocarcinoma cell line MOR**, 84112312 SIGMA, growth mode adherent with epithelial-like morphology, these cells grow as colonies. The supplier-recommended culture medium was used (RPMI 1640, 2mM glutamine and 10% FBS). The following subculture protocol was used with MOR: splitting sub-confluent cultures (70-80%) 1:2 to 1:4 (i.e., seeding at 2-4x10,000 cells/$cm^2$) using 0.25% trypsin for 2 minutes, at 5% $CO_2$ and 37°C.

The MOR cell line is the parent for the **CP-resistant MOR/CPR** cell line, 96042333 SIGMA, which has the same growth pattern and morphology as MOR. The culture medium used is the same as that used for MOR, but with addition of 1μg/ml CP. Cultivating the parent MOR cell line with increasing concentrations of CP for more than 6 months has yielded MOR/CPR.

For the HEK 293 embryonic kidney human (HEK 293 cells) cell line, 85120602 SIGMA, with adherent growth pattern and epithelia morphology,

RPMI-1640 was used as the culture medium with sodium bicarbonate, R0883 SIGMA, 2mM glutamine and 10% FBS.

### 2.1.2 **Thawing and cultivating the cells**

The cell lines were received from Sigma in cryogenic vials containing $100X10^4$ cells per vial in dry ice at -20°C; they were stored in vapor liquid nitrogen. The thawing and cultivating procedures were as follows: using a 37°C water bath, the frozen cells in cryogenic vials containing 1ml FBS with 10% DMSO were put into circular motion for less than one minute. Before complete melting, the outsides of the vials were wiped with 70% ethanol, then the contents were transferred slowly into 9ml pre-warmed culture medium in sterile Corning® 15 mL centrifuge tubes. The tubes were then centrifuged for 5 minutes at 200 × g, after which the clear supernatant was decanted aseptically without disrupting the cell pellet. The cell pellet was resuspended by slowly adding 1 ml of the recommended culture medium. The contents were transferred into 10 cm culture dishes, 92 x 17 mm, 56.7 $cm^2$/well, in the recommended culture medium, Z688819 SIGMA. Then the plates were incubated at 5% $CO_2$ and 37°C. Each cell line then grew until it reached 70-80% confluence. Sub-splitting and cultivating were done for 2-5 passages.

### 2.1.3 **Cryogenic cells storage**

The cells growing in 10 cm plates were trypsinized with 0.25% trypsin for one minute at 5% $CO_2$ at 37°C. The contents were moved into 15 ml centrifuge tube and normalized with 9 ml of the medium. After centrifuging the tubes at 200 × g for five minutes, the supernatant was decanted and the cell pellet was resuspended in FBS. Nalgene™ General Long-Term Storage Cryogenic Tubes, catalog number 5000-1020, were used to store the cells by addition of a cryoprotectant 10% dimethyl sulphoxide (DMSO) into the FBS suspension. The cryogenic tubes were then placed in a pre-chilled Mr. Frosty™ Freezing Container, catalog number 5100-0001, which was filled with alcohol to the line indicated by the manufacturer, then stored in a freezer at -80°C. After 24 hours, the cryogenic tubes were moved into liquid nitrogen ($N_2$) in a cryogenic container, immersing the vials in vapor-phase nitrogen at -195.8°C.

### 2.1.4 **Cell maintenance and passages**

When the cells were needed for specific procedures, they were thawed as previously described and grown in full growth medium in 5% $CO_2$ at 37°C. When the cells reached 70-80% confluence, they were detached using 0.25% trypsin with EDTA for 1-5 minutes. For the HEK 293 cells only, we used PBS without trypsin to detach the cells. The contents were transferred and centrifuged; the cell pellet was then resuspended in full-growth medium and seeded in T75 flasks. The cells were passed several times, up to 10 passages,

based on the experiment's needs. However, when cells exceeded 10 passages, some changes in CP sensitivity were noted. Following detachment of the 1 mL of cells, the suspension was added to 11 mL of complete medium and transferred into T75 flasks, which were left in the incubator overnight to let the cells adhere to the surface of the flask.

### 2.1.5 **Cell counting and percentage viability**

To ensure accurate and consistent counting, the following steps were used: after harvesting the cells and resuspending the cell pellet with full-growth medium, 100 µL was taken from the tube and added to an Eppendorf tube with 100 µL trypan blue, pipetting 10 µL into the cell hemocytometer. The following protocol was followed, using the 10X objective of the microscope and counting the cells within the grid lines of the hemocytometer, as shown in Figure 2.1.5.1. The cells were counted in the 4 square corners indicated in orange. The four 1 $mm^2$ squares contained 16 corner squares. The cells on the upper or right lines of each corner set were counted, while cells that settled on the lower or left lines of each corner set were excluded. The healthy cells unstained by trypan blue were counted, while the cells that showed trypan blue discoloration were counted separately, using a handheld tally counter. The total number of cells counted in the 4 corner sets was multiplied by $1x10^4$; this number was equivalent to the number in cells of each corner square set per mL. Therefore, the total cell count from 4 sets of 16 squares from one hemocytometer grid was multiplied by $10^4$ (cells/mL $x10^4$). Then, taking the

average (dividing by 4 then multiplying by 2 to adjust for the trypan blue dilution factor) we calculated the cell density representing the number of cells in each mL of the suspended cell pellets. For cell viability, the dead cells that appeared dark or faint blue within the grid were counted, and then the total live cell count was divided by the total cell count (including the dead cells), yielding the percentage viability.

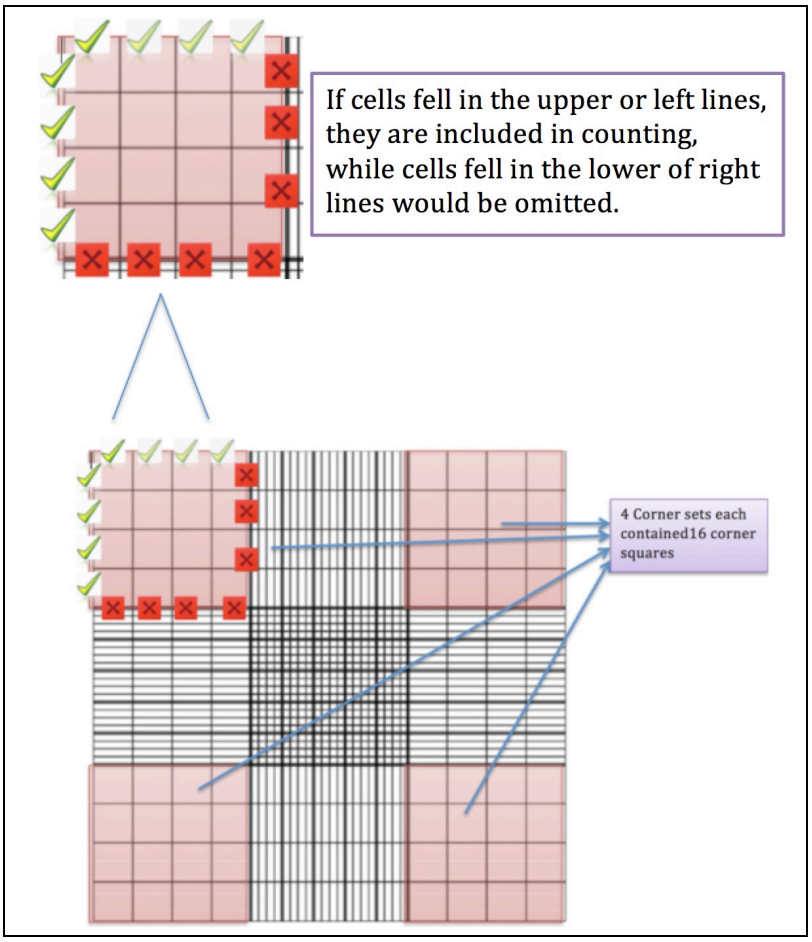


Figure 2.1.5.1 Hemocytometer cell counting system
The light orange squares were included in counting; any cells falling on the upper and left lines of each orange square were included in the count, while the lower and right lines were excluded.

## 2.2 Plasmids and *CYP2E1* cDNA

### 2.2.1 Introduction

Plasmid was earlier used to describe any extrachromosomal genetic particle of DNA (145). Plasmid more recently is used a vector or vehicle for a particular gene. *Plasmid* and *vector* are often used interchangeably, though vector is a more specific term that retains the meaning of engineered plasmid (146). The backbone vector possesses three basics features: multiple cloning sites, origin of replication, and selectable marker. The multiple cloning site is the location in the plasmid where *CYP2E1* and/or *GFP* or *nonsense CYP2E1 (scrambled)* is inserted. The origin of replication is the site where the DNA replication begins, which ensures that the exact replication of the plasmid takes place during the replication process.

### 2.2.2 Plasmid construction

Four cloned plasmids used from Origene®: *DDK-CYP2E1*, (Cat. Numb. RC213502); *CYP2E1*, (Cat. Numb. CW102031); Green fluorescent protein (*GFP*), displayed when exposed to ultraviolet light, (Cat Numb. PS100010); and nonsense *CYP2E1* cDNA (Scrambled (*Scr*) cDNA.), (Cat Numb. PS100001).

The cDNA genes of interest were inserted into a pCMV6-Entry vector (C-terminal Myc and DDK Tagged) (Cat. No. RC213502) containing two resistant genes; Kanamycin resistant gene (Kan r) for the subcloning process

during selection of transformed bacteria, and the Neomycin resistant gene (Neo r) giving the transfected cells resistance toward G148 antibiotic.

Figure 2.2.2.1 mv6 Vector with *CYP2E1* illustrates the full vector customized and supplied by Origene®. This used PCR subcloning to pCMV6-entry where SgfI-MluI, site of restriction enzymes used as indicated in data sequence of the vector which is highlighted in red color (see Figure 2.2.2.2). The restriction enzymes used Sgf I/ASIS I and Mlu I from Fermentas®. The Figure 2.2.2.2 pCMV6 sequence ligation reaction used T4 DNA ligase, 0.5 µL from Promega®. The full data sequence for the CYP2E1 nucleotide is shown in Figure 2.2.2.3.

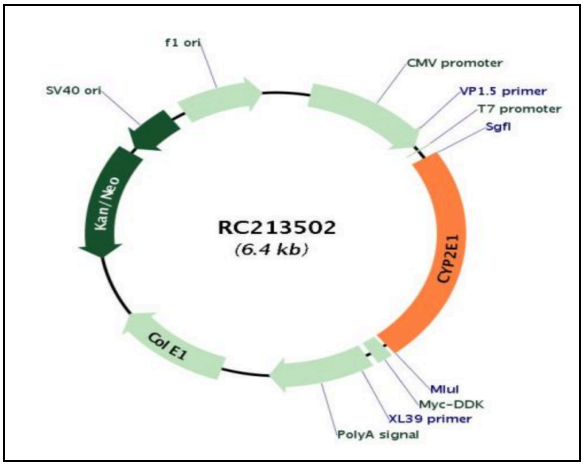


Figure 2.2.2.1 mv6 Vector with *CYP2E1*
The pCMV6 vector used by Origene®, to carry on the *CYP2E1* gene; the total size of the plasmid is 4.9 kb (= kbp), and SgfI MluI is the restriction site used to insert the *CYP2E1 gene*, The vector used by Origene® to carry the *CYP2E1* gene; the total size of the plasmid is 4.9 kb (= kbp), and two resistant genes are included in the vector backbone: a kanamycin-resistant gene (Kan r) and a neomycin-resistant gene (Neo r).

Figure 2.2.2.2 pCMV6 sequence
Full sequence of the pCMV6 vector indicating the restriction sites, in red, where the SgfI-MluI enzymes were used to make sticky ends where the gene of interest was inserted.

TTTTGTAATACGACTCACTATAGGGCGGCCGGGAATTCGTCGACTGGATCCGGTACCGAGGAGATCTGCGCCG
CGATCGCC
ATGTCTGCCCTCGGAGTCACCGTGGCCCTGCTGGTGTGGGCGGCCTTCCTCCTGCTGGTGTCCATGTGGA
GGCAGGTGCACAGCAGCTGGAATCTGCCCCCAGGCCCTTTCCCGCTTCCCATCATCGGGAACCTCTTCCA
GTTGGAATTGAAGAATATTCCCAAGTCCTTCACCCGGTTGGCCCAGCGCTTCGGGCCGGTGTTCACGCTG
TACGTGGGCTCGCAGCGCATGGTGGTGATGCACGGCTACAAGGCGGTGAAGGAAGCGCTGCTGGACTACA
AGGACGAGTTCTCGGGCAGAGGCGACCTCCCCGCGTTCCATGCGCACAGGGACAGGGGAATCATTTTTAA
TAATGGACCTACCTGGAAGGACATCCGGCGGTTTTCCCTGACCACCCTCCGGAACTATGGGATGGGGAAA
CAGGGCAATGAGAGCCGGATCCAGAGGGAGGCCCACTTCCTGCTGGAAGCACTCAGGAAGACCCAAGGCC
AGCCTTTCGACCCCACCTTCCTCATCGGCTGCGCGCCCTGCAACGTCATAGCCGACATCCTCTTCCGCAA
GCATTTTGACTACAATGATGAGAAGTTTCTAAGGCTGATGTATTTGTTTAATGAGAACTTCCACCTACTC
AGCACTCCCTGGCTCCAGCTTTACAATAATTTTCCCAGCTTTCTACACTACTTGCCTGGAAGCCACAGAA
AAGTCATAAAAAATGTGGCTGAAGTAAAAGAGTATGTGTCTGAAAGGGTGAAGGAGCACCATCAATCTCT
GGACCCCAACTGTCCCCGGGACCTCACCGACTGCCTGCTCGTGGAAATGGAGAAGGAAAAGCACAGTGCA
GAGCGCTTGTACACAATGGACGGTATCACCGTGACTGTGGCCGACCTGTTCTTTGCGGGGACAGAGACCA
CCAGCACAACTCTGAGATATGGGCTCCTGATTCTCATGAAATACCCTGAGATCGAAGAGAAGCTCCATGA
AGAAATTGACAGGGTGATTGGGCCAAGCCGAATCCCTGCCATCAAGGATAGGCAAGAGATGCCCTACATG
GATGCTGTGGTGCATGAGATTCAGCGGTTCATCACCCTCGTGCCCTCCAACCTGCCCCATGAAGCAACCC
GAGACACCATTTTCAGAGGATACCTCATCCCCAAGGGCACAGTCGTAGTGCCAACTCTGGACTCTGTTTT
GTATGACAACCAAGAATTTCCTGATCCAGAAAAGTTTAAGCCAGAACACTTCCTGAATGAAAATGGAAAG
TTCAAGTACAGTGACTATTTCAAGCCATTTTCCACAGGAAAACGAGTGTGTGCTGGAGAAGGCCTGGCTC
GCATGGAGTTGTTTCTTTTGTTGTGTGCCATTTTGCAGCATTTTAATTTGAAGCCTCTCGTTGACCCAAA
GGATATCGACCTCAGCCCTATACATATTGGGTTTGGCTGTATCCCACCACGTTACAAACTCTGTGTCATT
CCCCGCTCA
ACGCGTACGCGGCCGCTCGAGCAGAAACTCATCTCAGAAGAGGATCTGGCAGCAAATGATATCCTGGATT
ACAAGGATGACGACGATAAGGTTTAA

Figure 2.2.2.3 DNA sequencing for the *CYP2E1* vector
This figure is depicted from the Origene® manufacturer to indicate the full sequence for *CYP2E1*, DDK tagged, where red is the cloning site, blue is the open frame reading (ORF), and green indicates tags.

### 2.2.3 **cDNA subcloning**

To generate enough volume of the previously mentioned vectors, subcloning vectors were produced using competent bacteria, Alpha-Gold competent cells (20 x 50 µL), (Cat. Numb. CC100001) as follows:

Selected marker genes were inserted into the vector backbones. For *CYP2E1* and *GFP* cDNA, ampicillin-resistant genes were used; for *DDK-CYP2E1* and nonsense *CYP2E1* (scrambled), kanamycin-resistance genes were used. The selectable marker genes yielded the transformed organisms, which were resistant to ampicillin and kanamycin, respectively. Ampicillin and kanamycin were prepared in petri dishes using LB Broth (Miller), L3522 SIGMA by suspending 25g LB powder in 1L distilled water in two separate jars. One jar was used to prepare an agar plate for bacterial cell colonization by adding agar, A1296 Sigma®; the other jar had no agar and was used to grow the selected colony from the agar plate. The two jars were autoclaved for 15 minutes at 121$^{o}$ C, and allowed to cool prior to adding of antibiotics. Ampicillin (100 µg/ml) and kanamycin (25 µg/ml) were prepared and added separately. The mixture was poured into TPP tissue culture dishes, Z707686 SIGMA, then each dish was passed over a Bunsen burner to make sure no bubbles were left behind. The plates were left at room temperature. The following day they were stored at 4$^{o}$C.

The Alpha-Gold competent bacterial cells (50 µL), were thawed by placing the cells in ice for 5-10 minutes. The working concentration of each

plasmid was 20 ng/μL added to 50 μL competent cells and incubated on ice for 30 minutes. Heat shock of the component cells took place by moving them to a water bath at 42$^{o}$C for 30-40 seconds without shaking. The component bacterial cells were immediately moved to ice for 2 minutes, then diluted by adding 900-950 μL of SOC medium. The competent cells were then moved to a water bath shaker at 37$^{o}$C and shaken for 60 minutes at a speed of 200 RPM. Then, 20 μL of the component cells were spread over the antibiotic constructed agar plate using sterile, glass rounded beads; 20 μL of the non-transformed competent cells were spread over an antibiotic control plate as a control. The agar plates were then placed in a hot room and left inverted for 24h. Colonies of transformed component cells formed over the agar plate, while the control showed no cell growth. A sterile pipette tip was used to transfer one of the colonies into a bottle with 500 μL sterile liquid. LB Broth (Lennox) contained the appropriate antibiotic, and was left in a shaker in the hot room at 37$^{o}$C. After 24h the LB bottle turned turbid, which indicated the growth of the bacteria. Then by centrifuging at high speed, the bacterial cells could be collected and stored under -80$^{o}$C.

To isolate nucleic acids from the collected cells, QIAGEN Plasmid Purification Kits, Cat Numb. 12162 were used. The kit contains several bottles are numbered as P1, P2, P3, QC, QBT and QN; these bottles contain different buffers and solutions important for the nucleic acid isolation process. The first step was to suspend the bacterial pellets using 10 μL of P1, then 10 μL of P2 was added; the mixture was vigorously inverted 4-5 times and incubated at 15

°C. During this step, a QIAfilter was prepared and the screw was inserted; 10 µL of P3 (chilled) was added and mixed by vigorously inverting the tube 4-5 times. The lysate was poured into the QIAfilter and incubated at room temperature for 10 minutes. During the incubation, took place equilibrate a QIAGEN-tip by using 10 µL Buffer QBT. After filtering the contents from the QIAfilter into a 50 mL Corning® centrifuge tube, the contents were poured into QIAGEN-tip and left under gravity. The QIAGEN-tip containing the nucleic acids was washed using 15 mL of Buffer QC. Then, using 15 µL of QN, the nucleic acids were eluted. DNA was precipitated using 10.5 mL isopropanol, the immediately mixed and centrifuged at high speed for 30 minutes; then the endotoxin was washed with 5 mL of 70% ethanol. The tube was then centrifuged for 10 minutes and the suspension was removed. The DNA had to be carefully observed in the tube as a thin white line; otherwise it could have been lost during aspiration. The tube was left open in the hood for 5 minutes to make sure the ethanol contents were volatized. The DNA was then dissolved in 1mL sterilized DNA-RNA free water and measured using nano-drop DNA concentration.

## 2.3 Cells transfection and validation

Several transfection reagents such as Turbofectin, (Cat.Numb. TF81001z), had been used with low transfection efficiency (see Figure 2.2.3.1). HEK 293 cells were used to validate and optimize the methods of transfection using Turbofectin. Viral transfection had been considered, but the improvement of transfection efficiency using X-tremeGENE HP DNA Transfection Reagent (Cat. Numb. 06366236001) in A2780 cells delayed the viral transfection process.

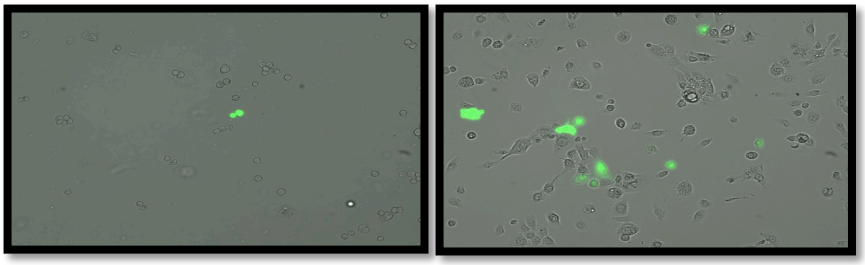

Figure 2.2.3.1 Low Transfection efficiency of A2780 and MOR with GFP Using fluorescence microscopy, in the right side, the A2780 cells GFP view is shown in an overlay view. In the left, MOR cells show GFP transfected cells in an overlay view. The transfection reagent used was Turbofectin.

### 2.3.1 Optimizing transfection conditions for HEK 293 cells

HEK 293 cells were split 1-4 times before use in transfection experiment studies, with 70-80% confluence reached after one day. The cells were seeded in 6-well plates having 70-80% confluence. The next day the full growth medium was aspirated and replaced with fresh medium. In a 15-ml conical tube, a Turbofectin/DNA complex was prepared by mixing specific ratios of the transfection reagent with the DNA. The Turbofectin was added

(1:2, 1:3, 1:4, and 2:1) first and incubated for 5 minutes, followed by the DNA. The optimum ratio was 2:1, consisting of 6 μL of Turbofectin and 3 μg of DNA in the optimum medium.

### 2.3.2 **Standardizing the transfection technique for cell lines**

A2780 cells showed low transfection efficiency, using turbofectin and Lipofectamine®. The use of X-tremeGENE HP DNA Transfection Reagent allowed reasonable transfection efficiency with all cell lines, (see Figure 2.3.2.1). The optimal DNA to reagent ratio for A2780 was 1:2. The 1:1 ratio was best for MOR cells. For Hep G2 cells, transfection using 1:2 and 1:1 were equivalent. The procedure for cell transfection using X-tremeGENE requires initial adding of DNA to Opti-MEM® (Reduced Serum Medium), followed by adding of the reagent. The mixture was incubated at room temperature for 25-30 minutes, with longer incubation durations giving inconsistent results. The cell plates were prepared as described above, and the DNA complex was added in dropwise fashion. The cells were incubated for 24 hours in 37$^{o}$C and 5% $CO_2$; under fluorescence microscopy, the cells were examined. The GFP transfected cells exhibited bright green fluorescence when exposed to light (see Figure 2.3.2.1).

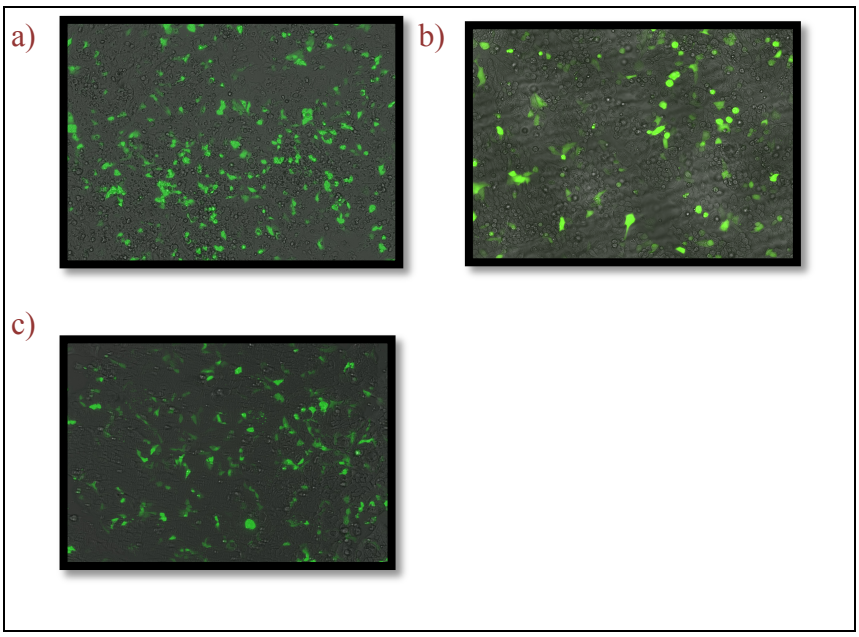


Figure 2.3.2.1 GFP transfection of: a) Hep G2, b) MOR/R, and c) A2780/R, The transfection efficiency for each cell lines was calculated as from GFP fluorescence stain. The transfection reagent used was X-tremeGENE HP

### 2.3.3 **Transfection efficiency**

We used the GFP stain method to calculate the transfection efficiency for the transiently transfected cells, using fluorescent microscopy. The number of the cells that exhibited GFP fluorescence was divided by the cells without fluorescence in the same field of cell view, multiplied by 100. For Hep G2 cells, we obtained ~57% transfection efficiency while in MOR/R A2780/R cells we obtained ~28%, ~40% respectively.

### 2.3.4 **Establishing stable cell lines overexpressing CYP2E1**

Sustained expression of the *CYP2E1* gene can be achieved by integrating the transfected plasmid, which contained a neomycine gene, into the target cell genome. The neomycin gene conferred resistance to geneticin (G418), an aminoglycoside antibiotic that can be inactivated by a neomycin resistance (*neo*$^{r}$) gene. Cells that contained the *neo*$^{r}$ gene had covalent modification of G418 by 3'-aminoglycoside phosphotransferase(147). The extrahepatic A2780, A2780-R, MOR and MOR-R cells were seeded into 6 well plates as explained previously. After 24 h., the cells were treated with different concentrations of G418 in the range of 200-800 μM. The master stock solution of G418 was prepared at a concentration of 10 mM by dissolving 200 mg in 28.87 mL sterile PBS, then filtering it through 0.45 micron Titan3™ PTFE (Hydrophilic) Syringe Filters. The cells were maintained in G418 antibiotic for 7-10 days, and every two days fresh growth medium was replaced with the same G418 concentration.. The optimum concentration of G418 killed all non-transfected cells, while the transfected cells with *Neo*$^{r}$ gene survived. The concentration was determined for each cell line after observing the growth of the cells within 7-10 days, (Table 2.3.4-1).

Figure 2.3.4.1 shows one of the trials to establish a sustained line that expressed GFP. The living cells showed fluorescence under an epifluorescence-inverted microscopy compared to the dying cells, which were sensitive to G418.

| Cell line | Number of cells seeded | Days left in medium | Amount of full growth medium | Optimum [G418] |
|---|---|---|---|---|
| A2780 | $900*10^3$ | 7-10 | 2ml | 500µM |
| A2780-R | $900*10^3$ | 7-10 | 2ml | 400 µM |
| MOR | $900*10^3$ | 7-10 | 2ml | 450µM |
| MOR-R | $900*10^3$ | 7-10 | 2ml | 400 µM |

Table 2.3.4-1 G4180 optimum concentrations for each cell line

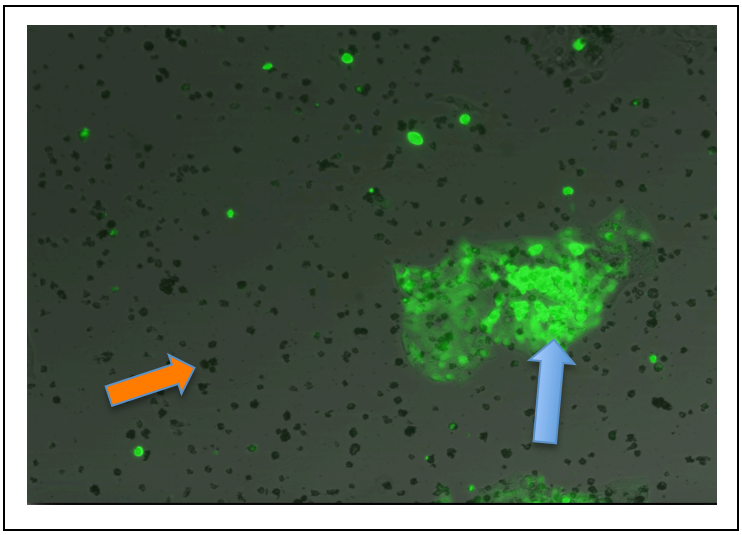

Figure 2.3.4.1 A2780/R GFP selection
In this fluorescence image, A2780/R were transfected with GFP and treated with G418 for 6 days. The red arrow indicates dying cells, while the blue colored arrow shows GFP survived cells. The survived cells were then maintained under G418.

## 2.4 Real time qPCR

The concept of qPCR followed other earlier methods used in gene identification and amplification. Southern blot analysis using electrophoresis opened a variety of methodological options to quantify specific genes (148). Alwin and his group developed Northern blot to identify RNA (149). Mullis used the polymerase chain reaction (PCR) to amplify genes, and introduced real-time PCR to quantify a specific gene in vitro (150). The basic principle of PCR is the amplification of specific genes by denaturing a double stranded DNA through overheating to 95$^{o}$C, and applying a primer that attaches to the DNA strand. Then, the polymerase enzymes start to attach to the first nucleotide 3'-OH group in the DNA strand from 5′-end to 3′ end. After the cooling process, annealing of the two strands will take place (151). The qPCR process allows visualization of the PCR reaction with a special fluorescence nucleotide dye, SYBR® Green, which binds only with double stranded DNA. During the PCR extension process, the dye binds to minor grooves of dsDNA and gives a strong fluorescent signal, which is detected via a specialized detector.

Each DNA cycle of is counted until it reaches the highest level of fluorescence is reached. *CYP2E1* overexpression is based on comparison with control. Giving two samples, one transfected with *CYP2E1* and the other transfected with nonsense *CYP2E1* cDNA (Scrambled. vector) as control, the transfected samples with the *CYP2E1* cDNA will require fewer cycles than the non-transfected ones because the targeted *CYP2E1* genes will be abundant,

thus reaching the maximum detectable fluorescence in fewer cycles than the control. The maximum detectable fluorescence is identified as the threshold cycle or Ct. The resulting Ct values are used to calculate changes in mRNA levels relative to nonsense-*CYP2E1*-transfected controls. GAPDH was used as a housekeeping control to normalize *CYP2E1* mRNA levels.

### 2.4.1 **Sample preparation and RNA extraction**

To examine the *CYP2E1* mRNA expression in the cell lines, the cells transfected with *CYP2E1*, GFP or Scr. vectors were harvested as previously explained. The cell pellets were disrupted according to the number of cells harvested using, 400-600 μL of a specific buffer supplied from RNeasy Mini Kit (Cat. Numb. 74104). To homogenize the mix, sonication for 10 seconds took place 3 times, and one volume of 400-600 μL of 70% ethanol was added. 700 μL of the mix was pipetted into an RNeasy spin column placed in a 2 ml collection tube. The tubes were then centrifuged for 15 seconds at high speed. The liquid that passed through the column to the collecting tube was discarded, then 700 μL of Buffer RW1 was added to the tube and centrifuged for 15 sec. The flow liquid was also discarded, and 500 μL of RPE (mild washing buffer) was added, followed by centrifugation for 15 sec. The same volume of RPE was added and centrifuged for 2 min. All flow liquids were discarded and the RNeasy spin column transferred into a new 2ml collecting tube. To elute the RNA, 30-40 μL of $H_2O$ free of RNA-DNA was used and then centrifuged for 2 min. The last step in this process was to measure the [RNA] using a nanodrop instrument supplied by Thermo®.

### 2.4.2 ***CYP2E1*** **qPCR**

cDNA synthesis was performed for A2780, A2780-R, MOR, MOR-R and Hep G2 cells that were transfected with *DDK-CYP2E1, CYP2E1, GFP* and

*Scr.* vectors. To quantify the relative overexpression of CYP2E1 cells, they were compared to scrambled transfected cells with the use of SYBR® Green as a nucleotide fluorescent dye, and a specific primer for *CYP2E1* from Origene® and qSTAR qPCR primer pairs against human gene *CYP2E1* (Cat. Numb.. HP200715). The forward sequence was GAGCACCATCAATCTCTGGACC and the reverse sequence was CACGGTGATACCGTCCATTGTG. The internal control GABDH housekeeping gene, qSTAR qPCR primer pairs against human genetic GAPDH (Cat. Numb. HP205798) has been used in cancer research, and applied for use in human cells (152, 153). The forward and reverse sequence of GABDH housekeeping gene used are: GTCTCCTCTGACTTCAACAGCG and ACCACCCTGTTGCTGTAGCCAA, respectively.

### 2.4.3 **qPCR Data analysis**

In *CYP2E1* qPCR studies, relative quantification of *CYP2E1* mRNA was used by relating Ct *CYP2E1* of cells transfected with *CYP2E1* to Ct in the control scrambled transfected group. To compare the fold *CYP2E1* expression change accurately, the $2^{-\Delta\Delta C}{}_T$ method was used (154), in which the Ct ratio for *CYP2E1* transfection is normalized for the corresponding Ct ratio in GAPDH.

### 2.4.3.1 Results of qPCR for cell lines transfected with *CYP2E1*

A2780 and A2780R (stable) were transfected with *CYP2E1*, *scrambled*, and *GFP* plasmids as described previously. The results showed nearly a 3500-fold increase in *CYP2E1* mRNA for both A2780 *CYP2E1* (stable) and A2780/R *CYP2E1* (stable) when compared to the corresponding cells that are untransfected or transfected with GFP or with the scrambled message. (see Figure 2.4.3.1).

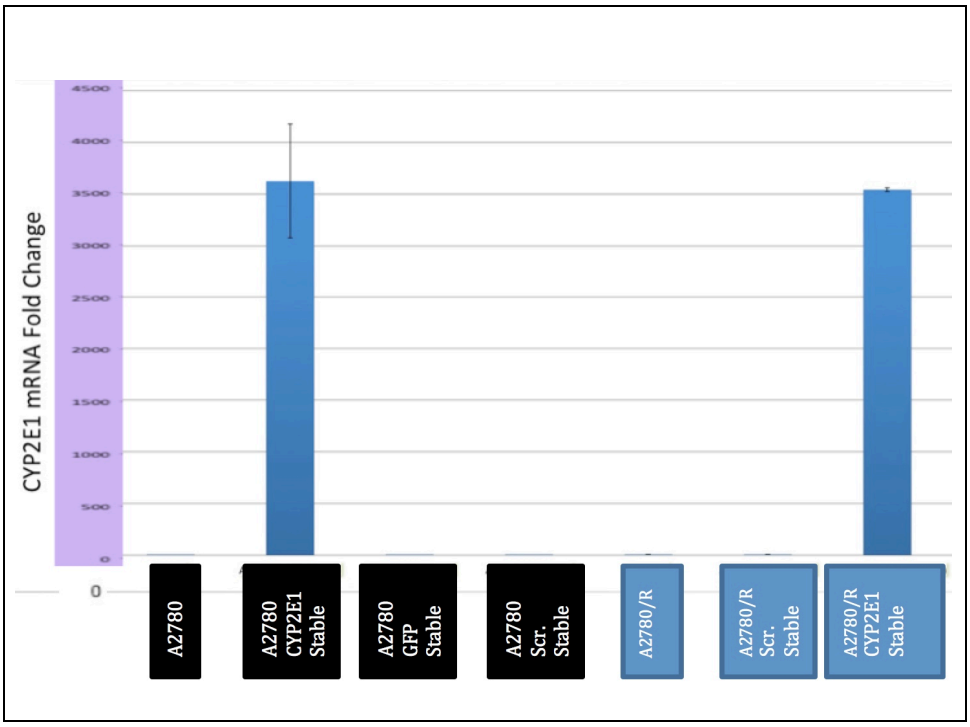


Figure 2.4.3.1 qPCR for A2780, A2780/R and Hep G2
When A2780 and A2780/R were all stably transfected with *CYP2E1*, mean (± SD) cDNA showed significant increases in *CYP2E1* mRNA expression compared to their corresponding controls.

To examine the effect of cell passages on *CYP2E1* mRNA expression, cells were stably transfected with *CYP2E1* and scrambled plasmids. After 8- 10 passages for both stable cell lines that express CYP2E1 with their corresponding GFP and scrambled transfected cells, the cells transfected with

*CYP2E1* maintained a significant high *CYP2E1* mRNA expression when compared to the corresponding controls (see Figure 2.4.3.2).

.

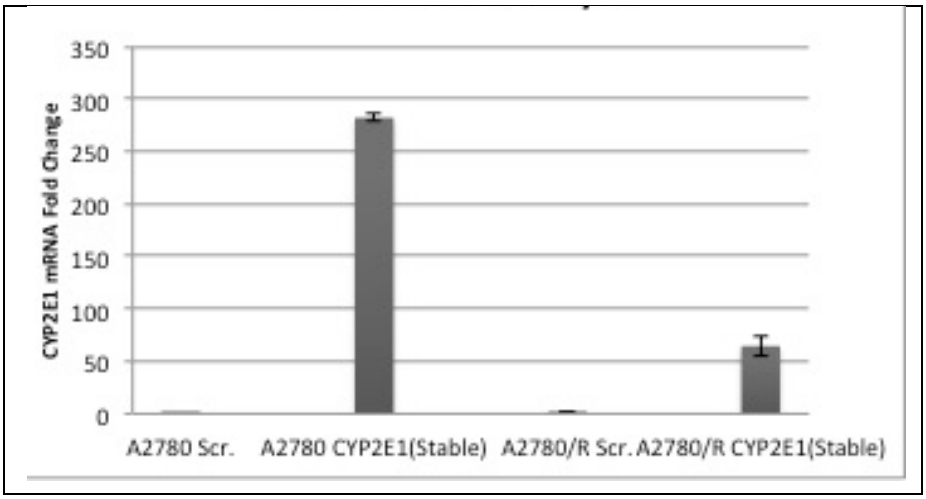


Figure 2.4.3.2 qPCR for A2780 and A2780/R and their stable transfected cells Both A2780 *CYP2E1* (stable) and A2780/R *CYP2E1* (stable) transfected cells showed a mean (± SD) (270 and 65 fold change in *CYP2E1* mRNA, respectively.

Figure 2.4.3.3, shows that Hep G2 CYP2E1 transiently transfected cells have large increases (greater than 150000-fold) in *CYP2E1* mRNA expression when compared to Hep G2 Scr. transfection cells as the control group. Hep G2 cells with GFP transfection cells did not show any significant change.

In Figure 2.4.3.4, MOR/R (T) cells were transiently transfected with *CYP2E1* or scrambled gene. *CYP2E1* mRNA increased more than 10 fold in the *CYP2E1* transfected cells when compared to scrambled control.

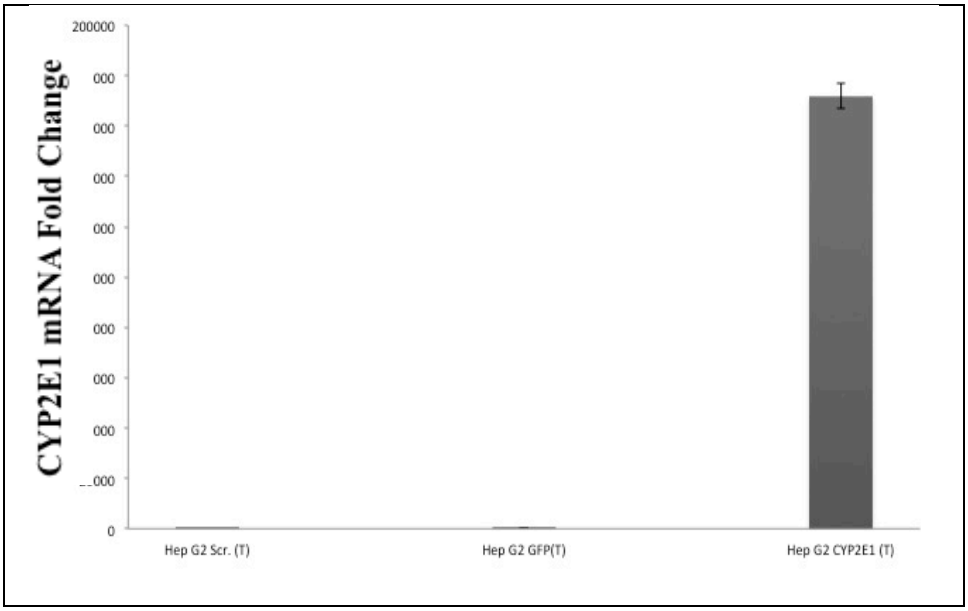


Figure 2.4.3.3: qPCR for Hep G2 cells transiently transfected with *CYP2E1*
More than a 150000-fold increase in mean (± SD) *CYP2E1* mRNA was observed for Hep G2 *CYP2E1* when compared to Hep G2 GFP and scrambled controls.

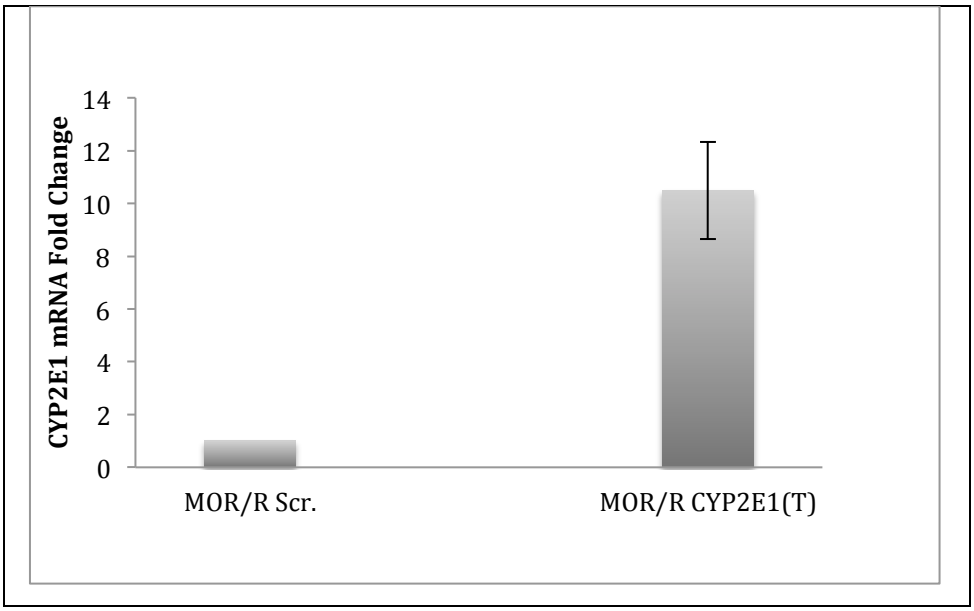


Figure 2.4.3.4 qPCR for MOR/R transiently transfected with *CYP2E1*
Nearly an 11-fold increase in mean (± SD) *CYP2E1* mRNA for MOR/R when compared to MOR/R Scr. Control.

## 2.5 Western blot

### 2.5.1 Introduction

Western blot analysis is based on separation of denatured proteins according to their molecular weight, followed by immunoquantification. An electrical current is passed from a negative anode to a positive cathode through polyacrylamide gel (see Figure 2.5.1.1). Sample homogenates are treated with sodium dodecyl sulfate (SDS) that covers the polypeptide with a negative charge, allowing the migration of the polypeptides toward the positively charge anode (155). According to the molecular weight of each polypeptide, the smaller proteins migrate faster.

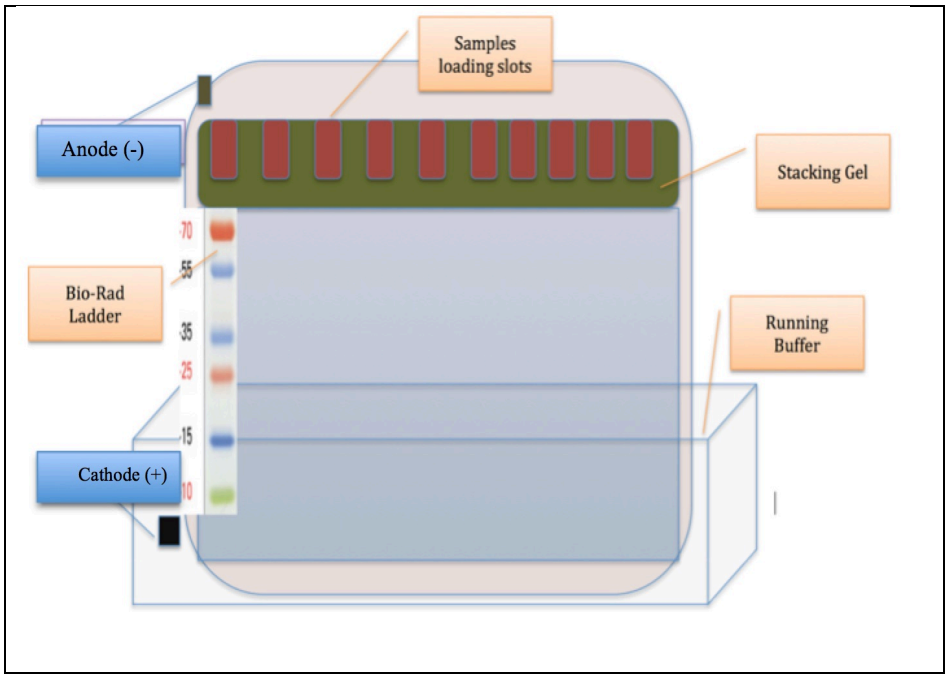


Figure 2.5.1.1 Western blot protein separation
On the polyacrylamide gel, the loaded homogenates migrate according to their molecular weight.

### 2.5.2 **Sample preparation**

After aspiration of all growth medium from tissue culture plates, the adherent cells remain on the plate. The plate was placed on ice to maintain a cold environment and to avoid protein denaturing and degradation. Addition of 80 μL of RIPA Buffer from Thermo Scientific (Cat. Numb. 89900), which was originally developed for radio-immunoprecipitation assay, was followed by addition of 20 μL of SIGMAFAST™ Protease Inhibitor Tablets (Cat. Numb. S8820 SIGMA), which enables efficient cell lysis and protein solubilization. The lysed cells were collected using sterile white spatulas in Eppendorf tubes and kept on ice. The collected lysate was sonicated and centrifuged for 10 minutes at high speeds in the cold room. The supernatant was transferred into labeled Eppendorf tubes. Samples were either used immediately, or stored at -80°C.

### 2.5.3 **Protein concentration determination**

For determination of total protein concentrations, a standard curve was made using bovine serum albumin (BSA) protein at 2mg/mL, with serial dilutions in 6 Eppendorf tubes, (see Table 2.5.3-1). The total volume in each tube was 50 μL. Using the Pierce™ BCA Protein Assay Kit (Cat. Numb. 23225). 18 mL of Reagent A Reagent A(1 gm sodium bicinchoninate (BCA), 2 gm sodium carbonate, 0.16 gm sodium tartrate, 0.4 gm NaOH, and 0.95 gm sodium bicarbonate, brought to 100 mL with distilled water; adjust the pH to

11.25 with 10 M NaOH) was mixed with 300 µL of Reagent B (0.4 gm cupric sulfate (5 x hydrated) in 10 ml distilled water), then 1 mL of the mix was added into each Eppendorf tube and vortex mixed. Total protein concentrations in unknown samples were determined by diluting the samples in distilled water at a ratio of 1 to 5, after which 1 mL of BSA mix was added and vortexed. Both serially diluted and unknown samples were incubated in a water bath for 20 minutes. Then, 2 µL of the serial dilution was applied into a nanodrop spectrophotometer at a wavelength of 562 nm where the absorbance wavelength was recorded, as in Figure 2.5.3.1. A standard curve is then automatically generated from the recorded wave absorbance as shown in Figure 2.5.3.2.

| Eppendorf Tube Number | Doubling dilution | [Serum bovine] mg/mL |
|---|---|---|
| 1 | 1 | 2 |
| 2 | 1/2 | 1 |
| 3 | 1/4 | 0.5 |
| 4 | 1/8 | 0.25 |
| 5 | 1/16 | 0.125 |
| 6 | 1/32 | 0.0625 |
| 7 | 1/64 | 0.03125 |

Table 2.5.3-1 Serum bovine serial dilutions for standard curve

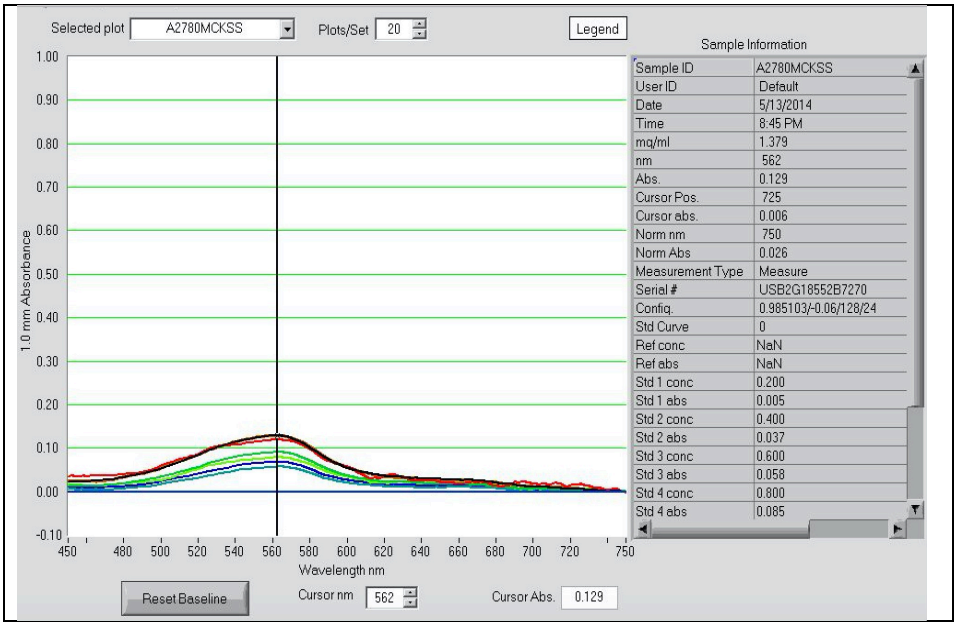


Figure 2.5.3.1 Nanodrop spectrophotometer used to measure unknown protein concentrations

The curves formed here represent serial dilutions of BSA. The unknown samples can then be measured by their absorbance at a wavelength of 562 nm

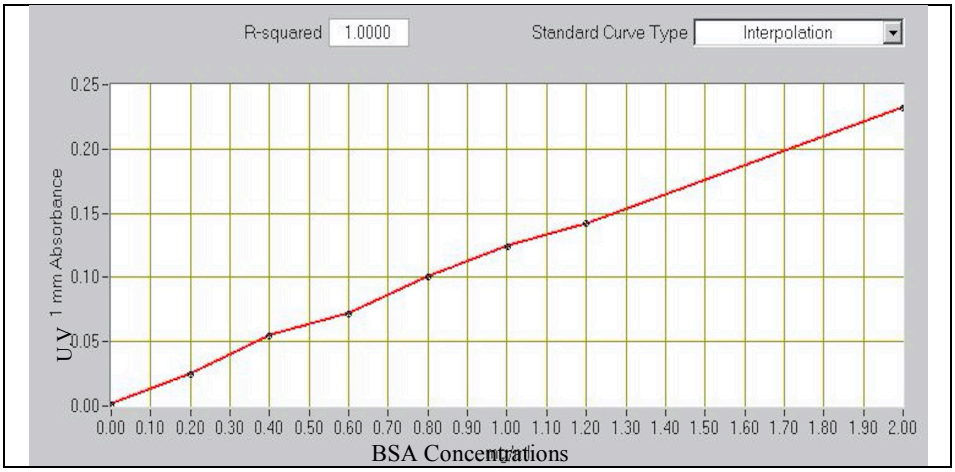


Figure 2.5.3.2 Bovine serum albumin standard curve

To determine the protein concentration for unknown samples, the NanoDrop spectrophotometer was used for direct measurement of protein concentration at 560 nm. The x- axis is BSA concentrations, while the y-axis is U.V absorbance.

### 2.5.4 **Polyacrylamide gel construction**

Using Biorad® casting apparatus gel, the following gel recipe was used to prepare 8% gel in a total volume of 10 mL of the separating section. The mixture contained 2.7 ml 30% Acrylamide/Bis, 2.5 mL 1.5 M TRIS pH 8.8, 50 μL of 20% SDS and 4.64 mL $H_2O$, 100 μL 10%APS and 10 μL TEMED. For the stacker part, the same 4 mL was prepared by mixing up 670 μL of 30%Acrylamidr/Bis, 500 μL of 1.0.M TRIS PH 6.8, 20 μL of 20%SDS, 2.76 mL $H_2O$, 40 μL 10% APS, and 4 μL TEMED.

### 2.5.5 **Western blot procedure**

By loading 8 μL of Western Blot Protein ladder, Precision Plus Protein™ Kaleidoscope™ Standards (#161-0375 BioRad®), and loading the positive control recombinant Cytochrome P450 human Sigma (Cat. Numb. C5740 SIGMA), the prepared samples were resolved with the immune blot gel. The loading volume of the positive control was adjusted to 18 μL after several trials to determine appropriate bandwidth when using 2 minutes of exposure to a Kodak ISM 2000MM. This is a fluorescence-based molecular imaging station equipped with a 415/100 nm excitation filter from Omega Optical (Brattleboro, VT, USA) and the 570-, 600-, 670-, and 700-nm wide-angle emission filters for the 565, 605, 655, and 705 nm Qdot Conjugates and Kodak 1 D Image Analysis Software. The appropriate concentration of the positive control recombinant CYP2E1 was 0.6 μM. The sample loading volumes

ranged from 15 μL to 22 μL. The optimized 18 μL loading volume was obtained after several trials based on clarity of the bands and the presence and absence of multiple bands. Figure 2.5.5.1 shows the electrophoresis scheme, with electrical potential usually at 100 volts for 45 minutes. In a running buffer, the protein separates in the gel according to size. The band formed in the gel is transferred onto an Immune-Blot® PVDF Membrane.

The first step in PVDF membrane preparation is to wet the appropriate size in methanol for 2 seconds, then to immerse it in transfer buffer with two absorbance pads and sponges for five minutes. The gel is then removed from the glass and immersed in a transfer buffer for five minutes. The gel is then placed over the PVDF membrane as in Figure 2.5.5.1, which shows the order of the transfer process components.

The proper time for transfer was optimized based on voltage and number of gels transferred. In the PVDF membrane, the appearance of the ladder was indicative of successful transfer. Then, the PVDF membrane was immersed for one hour in 10% milk and left for purpose of blocking. The membrane was then incubated overnight at 4°C. with a primary CYP2E1 antibody. Several trials were conducted to optimize the concentration of CYP2E1 primary antibodies used, which was 1:50000 dilution (1 μL primary antibody in 5 mL 5% milk). The optimal incubation time was overnight at 4°C, with trials at room temperature for one hour. The membrane was then washed for three 5-minutes cycles, and then incubated with a secondary antibody in dilution of 2:5000 (2 μL of secondary antibody in 5 mL 5%milk) for one hour,

then washed for four 5-minutes cycles. The membrane was then incubated in a Chemiluminescent reagent from Thermoe® for 2-3 minutes, followed by 2-5 minutes of exposure with Kodak ISM 2000 MM.

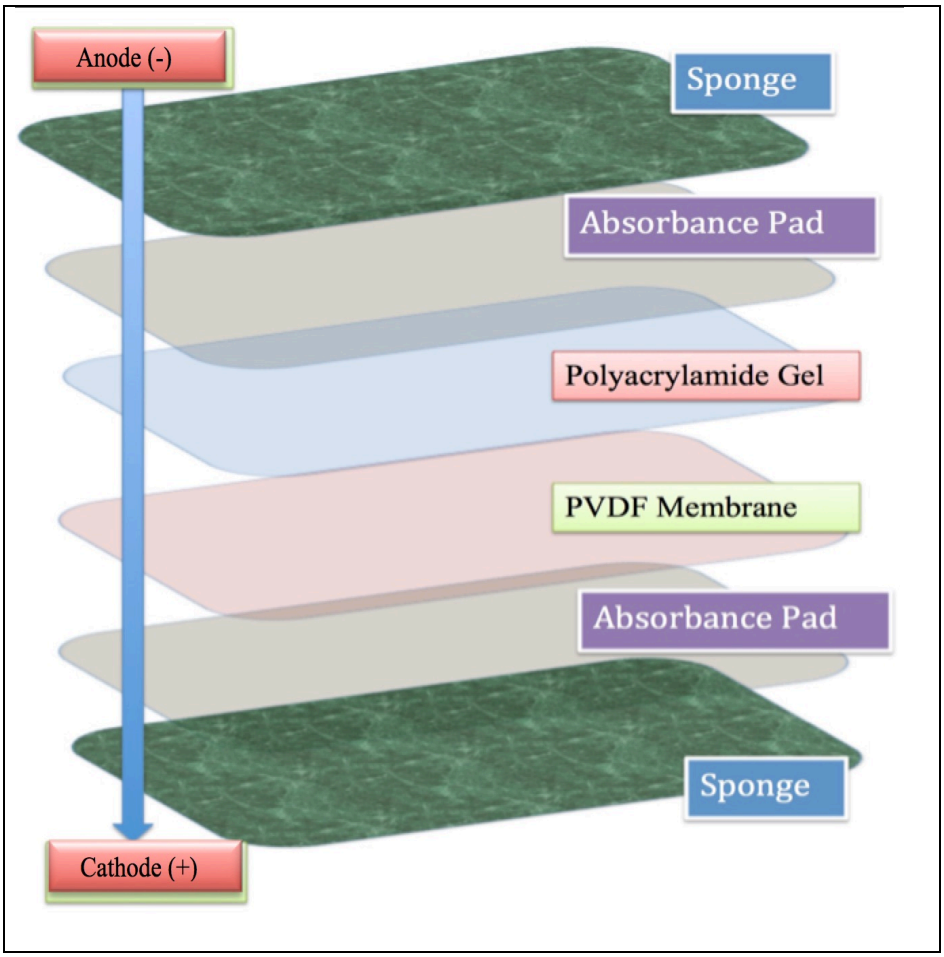


Figure 2.5.5.1 Protein transfer in Western blot
The order must be as in the figure, with the polyacrylamide gel above the PVDF membrane. The direction of protein transfer is as indicated by the arrow, from anode (-) to cathode (+).

### 2.5.6 **Western blot quantification and standardization process**

To quantify CYP2E1 protein in cell lysates, a recombinant Cytochrome P450 human (C5740 SIGMA) was used to construct a calibration curve through serial dilutions (Table 2.5.6 1). Concentration of the recombinant cytochrome P450 was 87.7 μM. Serial dilutions for 10 times of the recombinant CYP2E1 was prepared. The equivalent CYP2E1 concentration for each dilution is indicated in (Table 2.5.6-1 CYP2E1 serial dilution).

CYP2E1 serial dilutions allowed optimization of the positive control band concentration. The best concentration used for the positive control was 0.68 μM of recombinant CYP2E1 (Figure 2.5.6.1). This concentration minimized the appearance of non-specific bands, and reduced the extent of band superimposition.

Figure 2.5.6.2 shows a typical Western blot done for unknown concentration of CYP2E1. The figure shows three immunoblots in one film exposure. The upper part shows the unknown CYP2E1 samples, while the middle one shows the serial diluted recombinant CYP2E1, and the last one shows the GAPDH control which represented the same protein concentration in all lysates. GAPDH protein ensures the exact loading volume for all samples.

Figure 2.5.6.3 shows, CYP2E1 standard curve within an exposure time of 2 minutes, based on Table 2.5.6-2. Each band was measured using the Kodak band software.

| Tube number | Doubling dilution | [CYP2E1] μM |
|---|---|---|
| 1 | 1 | 87.7 |
| 2 | 1/2 | 43.85 |
| 3 | 1/4 | 21.92 |
| 4 | 1/8 | 10.96 |
| 5 | 1/16 | 5.48 |
| 6 | 1/32 | 2.74 |
| 7 | 1/64 | 1.37 |
| 8 | 1/128 | 0.68 |
| 9 | 1/256 | 0.34 |
| 10 | 1/512 | 0.17 |

Table 2.5.6-1 CYP2E1 serial dilutions
The table shows the corresponding concentration for each dilution.

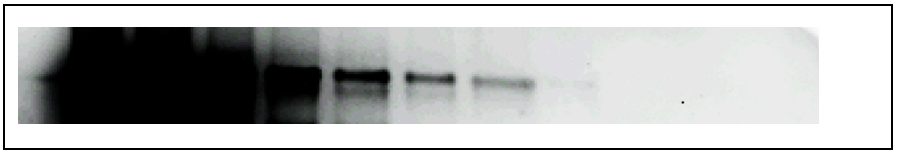

Figure 2.5.6.1 Recombinant CYP2E1 Serial dilution for positive control band. In this figure, the first band from the left has a concentration of 10.9 μM of CYP2E1; the fifth band from the left has 0.68 μM. the fifth band has clean edges with minimum non-specific bands.

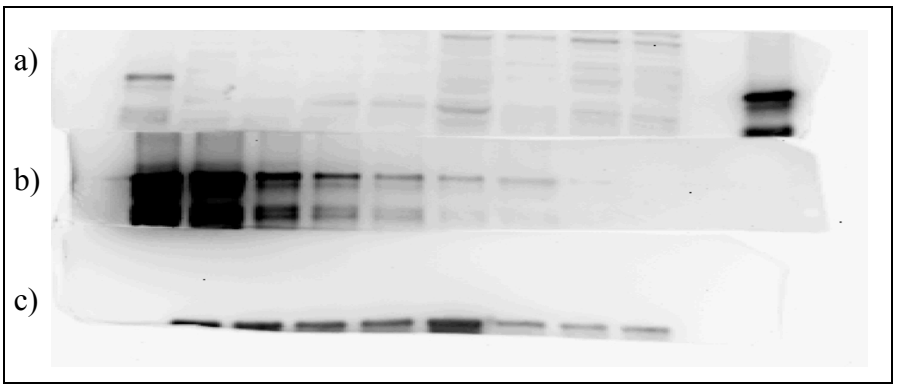


Figure 2.5.6.2 Western blot typical model for unknown [CYP2E1]
The blot consists of three parts: a) the upper for unknown [CYP2E1], b) the middle for serial dilution of recombinant CYP2E1, and c) the lower part for GABDH.

.

| Tube Number | [CYP2E1] μM | Relative resolution in Pixel |
|---|---|---|
| 4 | 10.96 | 1600 |
| 5 | 5.48 | 1088 |
| 6 | 2.74 | 578 |
| 7 | 1.37 | 340 |
| 8 | 0.68 | 272 |
| 9 | 0.34 | 136 |
| 10 | 0.17 | 34 |

Table 2.5.6-2 CYP2E1 Standard curve
Recombinant CYP2E1 protein was used for serial dilutions; corresponding immunochemistry blot bands were measured using Kodak software

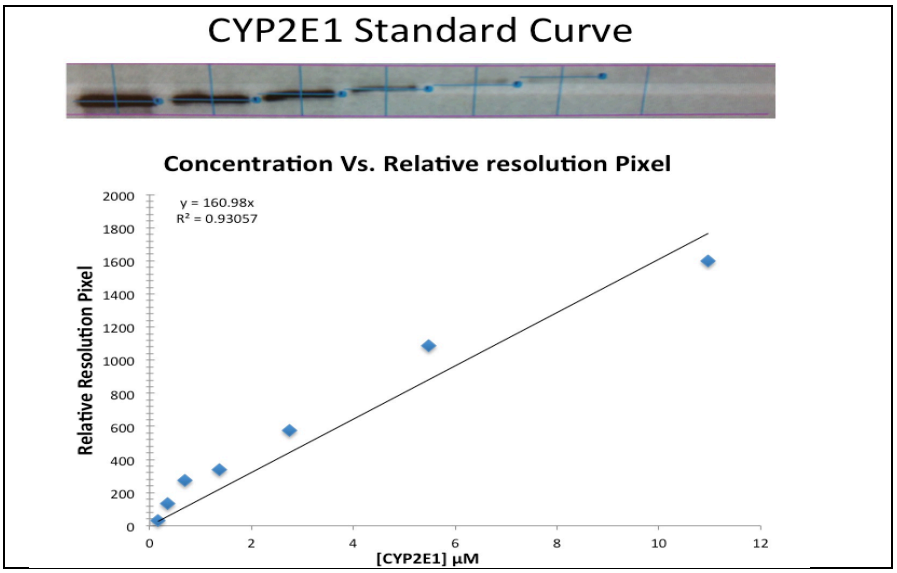


Figure 2.5.6.3 CYP2E1 standard curve

The CYP2E1 concentration is an X-axis; the y-axis is pixel density. Using the calibration line, CYP2E1 protein concentrations in unknown samples can be determined.

### 2.5.7 **Issues with CYP2E1 Western blot**

Some issues were encountered with western blot analysis.

1) No bands formed:

Several possible causes were considered, including: incompatibility or inaccurate ratio of primary and secondary antibodies; cross-reaction of the blocking agent and the primary antibody; excessive washing leading to inactive substrate. These potential causes were investigated and excluded. Ultimately the cause of lack of bands was attributed to a shipment of defective Kodak film.

2) Multiple bands:

As evident in Figure 2.5.7.1 a), Western blot showed multiple bands that were thought to be related to antibody ratios. Optimization of the ratios through titration decreased the multiple band problem. However, the loading volume of the samples also influenced the appearance of multiple bands. In addition, when homogenates were prepared from cell populations that went through several passages, the appearance of multiple bands was noticed. Ultimately the multiple band problem was not fully resolved.

3) Positive control issues:

The use of recombinant CYP2E1 from Abanova® (Cat. Numb.H00001571-Q01) showed higher band location in the Western blot when compared to recombinant CYP2E1 supplied by Sigma®. CYP2E1 Abanova® includes a GST-tag that might explain the higher molecular weight observed in its Western blot. Recombinant CYP2E1 from Sigma® had the

standard molecular weight for CYP2E1 in the literature, which is 57 (kDa). This was tested along with human liver microsomal lysate. The use of Abanova® CYP2E1 recombinant protein showed inconsistent results related to CYP2E1 transfected A2780 cells lysate compared to GFP or scrambled plasmid lysate samples as in Figure 2.5.7.1 b).

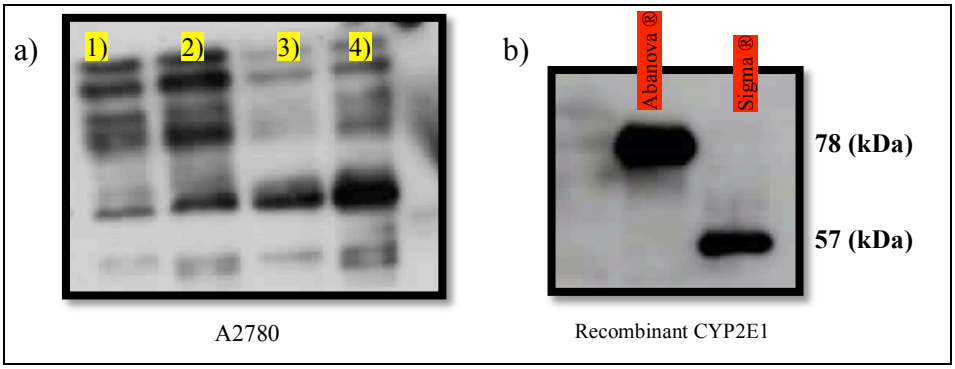


Figure 2.5.7.1 Western blot issues
Multiple bands were an issue that obscured the correct blot reading. In a) A2780 cells under different conditions: 1) and 2) the cells had 10 passages, while in 3) and 4) 3 passages. In addition, sample volume effect can be noticed in 2) and 4); when the volume increased, the multiple bands became more noticeable compared to 1) and 3). In b), different band locations for recombinant CYP2E1 were obtained from Abanova and Sigma. The Abanova CYP2E1 was tagged with a GST-tag at the N-terminal that might explain the different band location due to higher molecular weight.

### 2.5.8 **A2780 and A2780/R transfected with *CYP2E1***

The lysate for A2780 Scr. (stable) and A2780 CYP2E1 (stable) cell lines were prepared as explained previously. The Western blot in Figure 2.5.8.1 showed an increase in CYP2E1 protein when compared to its corresponding control. This outcome could not be replicated in subsequent trials. One of these trials is shown in b), where the positive control used was from Sigma. The transfected sample showed no significant change in bandwidth compared to control, indicating no change in CYP2E1 protein expression. The CYP2E1 band that appeared could be from constitutive CYP2E1.

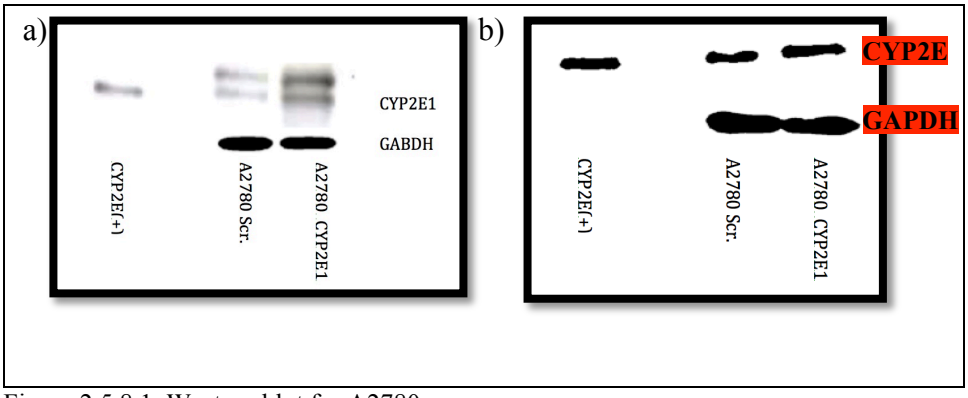


Figure 2.5.8.1 Western blot for A2780
In a), the positive control used was Abanova® CYP2E1, the A2780 CYP2E1 cell lysate compared to A2780 Scr. cell lysate showed more CYP2E1 formation. In b), inconsistent findings when the positive control used was from Sigma®, but there was no change in the CYP2E1 band width at 57 (kDa)

## 2.5.9 **Hep G2 cells and MOR/R transfected with *CYP2E1***

The lysate for Hep G2 Scr. (Transient) and Hep G2 CYP2E1 (Transient) cell lines was prepared as explained previously. The Western blot in Figure 2.5.9.1 showed a slight increase in CYP2E1 protein in Hep G2 cells when compared to its corresponding control.

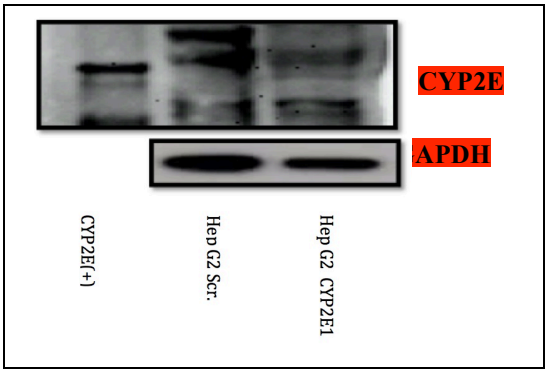


Figure 2.5.9.1 Western blot for Hep G2 CYP2E1 transfected cells have a faint band at 56 KD confirmed by using positive control recombined CYP2E1 from Sigma®. This can be noticed when compared to Scr. CYP2E1 Hep G2.

.

## 2.5.10 **Conclusion**

Due to the methodological and operational obstacles and inconsistent results, the Western blot analysis did not impact the study hypothesis one way or another.

## 2.6 CYP2E1 Metabolic activity

### 2.6.1 General concept

In vitro metabolism of drugs by preparations such as human liver microsome is widely applied research approach to the study of human drug biotransformation (156, 157). Under appropriate conditions the enzyme preparation will biotransform chemical in much the same way as happens in vivo. To focus specifically on the activity of CYP2E1 chlorzoxazone (CHZ) is used as probe or index compound (158). The procedure is based on hydroxylation of CHZ by CYP2E1 into 6-hydroxy-CHZ (6-OH-CHZ) (see Figure 2.6.1.1).

The cellular preparation is incubated, along with suitable cofactors, with CHZ. After a specific incubation duration, the reaction is stopped by addition of acetonitrile containing phenacetin as internal standard.

Separation of the substrate, its metabolite, and the internal standard was done by HPLC. The sample was delivered through a C18 µ-Bondapak column, 300 mm x 3.9 mm i.d. (Waters Assoc., Inc., Milford, Mass.) as the stationary phase, with a mobile phase of potassium phosphate buffer ($KH_2PO_4$)/ Acetonitrile, 75:25 v/v, pH 7.0.

The mobile phase was prepared by dissolving 13.60 g of $KH_2PO_4$ in 2L of distilled water to yield a 50 mM concentration. The mix was filtered and degassed for 10 min using a sonicator bath. Acetonitrile was added with a ratio of 75:25 v/v, therefore preparing 1L total volume of mobile phase—750 mL of

$KH_2PO_4$ mixed with 250ml acetonitrile. The HPLC pump and autosambler delivered the solvent containing the biological samples through the C18 column at a rate of 1.8 mL/min, and the effluent was detected by ultraviolet absorbance at 295 nm wavelength for quantitation of 6-OH-CLZ (Waters Lambda Max Model 481 LC, Milford, MA, USA). The sequence of compounds was: 6-OH-CHZ, phenacetin, and CHZ in that order (see Figure 2.6.1.2).

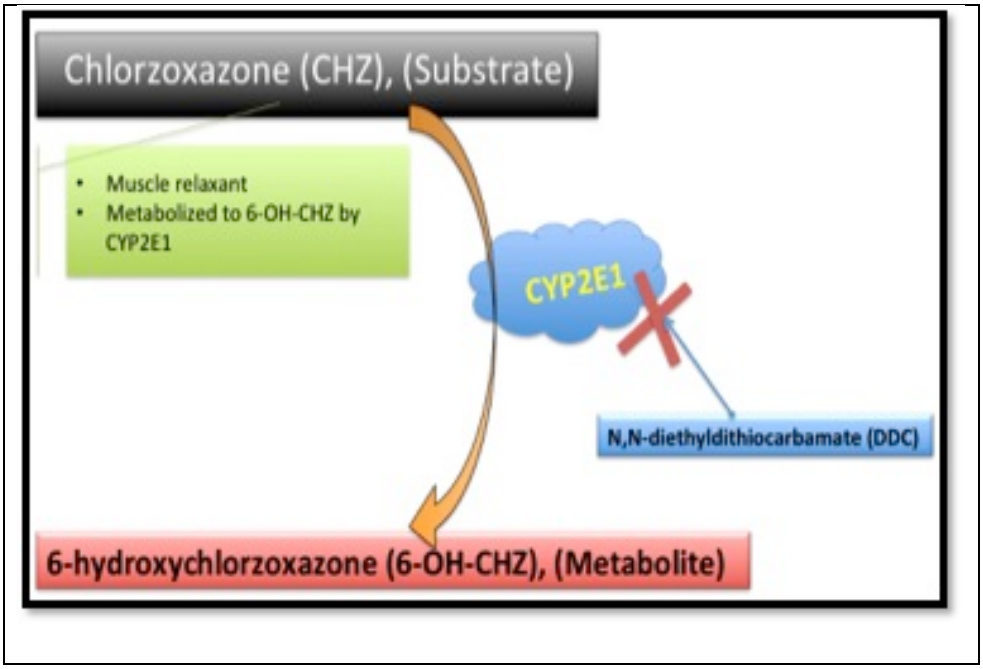


Figure 2.6.1.1 CHZ as index substrate for CYP2E1
Transformation of CHZ to 6-OH-chlorzoxazone (6-OH-CHZ) is the index reaction used to profile activity of CYP2E1. The reaction is inhibited by N,N-diethyldithiocarbamate (DDC).

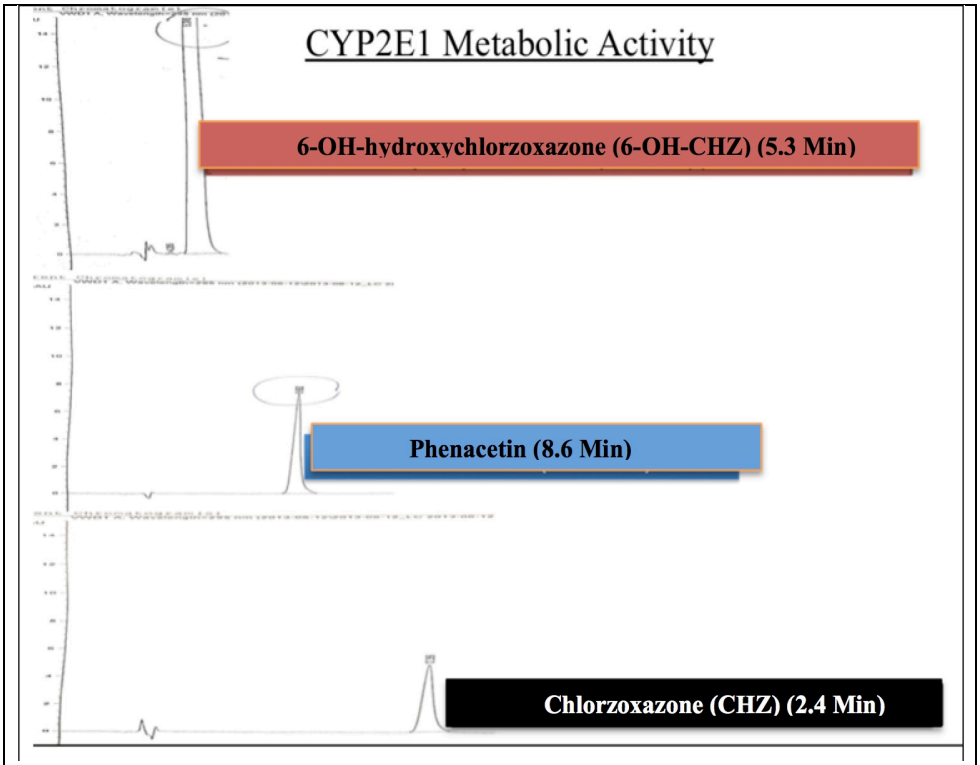


Figure 2.6.1.2: HPLC tracing showing retention times of 6-OH CHZ, phenacetin, and CHZ

## 2.6.2 **Sample preparation**

Two sample preparation methods were used to study CYP2E1 metabolic activity. For intact cells, as described previously (142), the living cells were incubated with 2-5 mL growth medium contained 500 µM CHZ for 24 hours at 37$^{o}$C and 5% $CO_2$, the volume determined based on the plate size. The growth medium was then collected and internal standard 250 µM phenacetin added. The pH was adjusted using 30 µL of 43% phosphoric acid/1mL of collected growth medium. Ethyl acetate and chloroform (159, 160) were used to extract the three components in the medium as follows: one volume of ethyl acetate or chloroform was added to the collected growth

medium, then vortexed for five min. The mixing was done with circular motion, and the tube centrifuged for 30 minutes. The organic phase is separated into another tube, and the same process repeated three times. With chloroform extraction, the organic phase was on the bottom; with the ethyl acetate extraction, the organic phase was in the top. If the organic phase was turbid (not translucent) due to formation of emulsions, the tubes were frozen in -20$^{o}$C for 1 hour, then thawed and centrifuged for 30 min. This caused the organic phase to become translucent and clear enough for separation.

For analysis of cell homogenates, the harvested cells were centrifuged, and the supernatant discarded. The tubes containing the remaining cell pellet were frozen at -80$^{o}$C for 24hours, then thawed in ice and refrozen for 24 hours at -80$^{o}$C. The samples were then thawed in ice for 20 minutes and homogenized at 4 $^{o}$C by sonication, with three 10-second cycles.

Protein concentrations were determined using BCA and NanoDrop Spectrophotometers (see Figure 2.5.3.2).

Both human liver microsomal samples as positive control and cell lysate samples were prepared at final concentrations of 0.25 mg/ml in 200 μL as the final volume in the incubation mixtures.

### 2.6.3 **HPLC Issues**

To optimize the pH of the extraction method, we conducted several experiments using pure 6-OH-CHZ, CHZ, and phenacetin in the full growth medium simulating the cells growth medium. Close to 50-70% extraction recovery was obtained compared to unextracted controls. Improved results were obtained when the vortex time was adjusted to 10 minutes, and the collection tubes changed to glass to minimize the possible plastic polymer effect. We used 30 μL of 43% phosphoric acid/1mL to adjust the pH.

Another issue was contamination by 6-OH-CHZ in the negative control samples. To solve this issue, 100% methanol was used for 24 hours to wash the column. Further, after injection of each sample into the HPLC, two samples of pure methanol followed by $H_2O$ tubes were injected to eliminate cross-contamination. Theses maneuvers successfully removed contamination.

### 2.6.4 **Irreversible CYP2E1 Enzyme Inhibition**

Diethyldithiocarbamate (DDC) is a potent though not fully specific inhibitor of CYP2E1 (161, 162). DDC has been previously described as a time – dependent (mechanism-based) inhibitor of CYP2E1. This means that inhibiting potency is increased if the inhibitor is exposed to metabolic enzymes prior to addition of substrates (163). We verified this property of DDC by conducting a preincubation study of CYP2E1 inhibition by DDC. Human liver microsomes were incubated with different concentrations of DDC (10, 50, and

100 μM) in Eppendorf tubes for 10 min, then transferred into lyophilized Eppendorf tubes containing CHZ 25μM (see Figure 2.6.4.1). Tubes were then incubated in a water bath for 30 min at 37$^{o}$C, after which the stop solution (100 μL) was added. The tubes were then left for 10 minutes in ice, and then centrifuged for 10 minutes at 3000 rpm. The content was then moved into HPLC vials, for analysis as described above.

### 2.6.4.1 The results

As depicted in Figure 2.6.4.2, there was significant inhibition of 6-OH-CHZ formation when DDC used in 50 and 100 μM, respectively, when compared with negative control sample which did not contain DDC. When the preincubation method was used, there was enhanced inhibition of 6-OH-CHZ formation compared to inhibition without preincubation. This verifies the time-dependent mechanism of CYP2E1 inhibition by DDC.

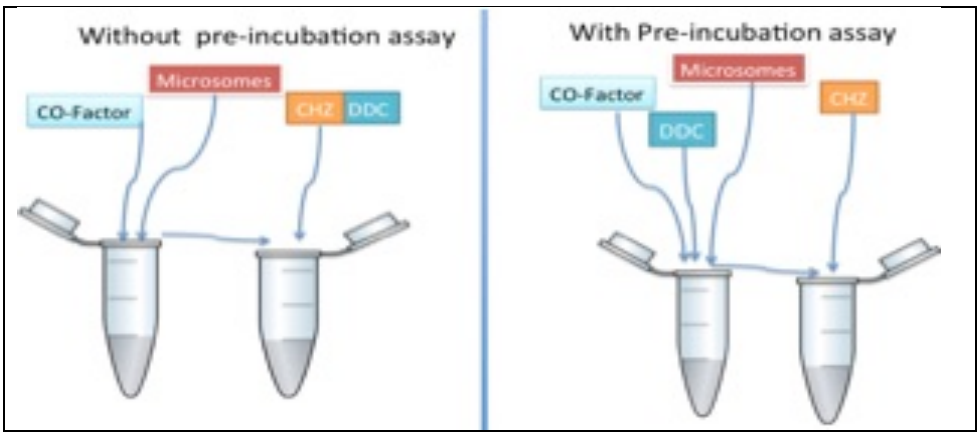


Figure 2.6.4.1 Preincubation method
These schematic diagrams depict the preincubation method, showing addition of the inhibitor to the enzyme prior to addition of the substrate.

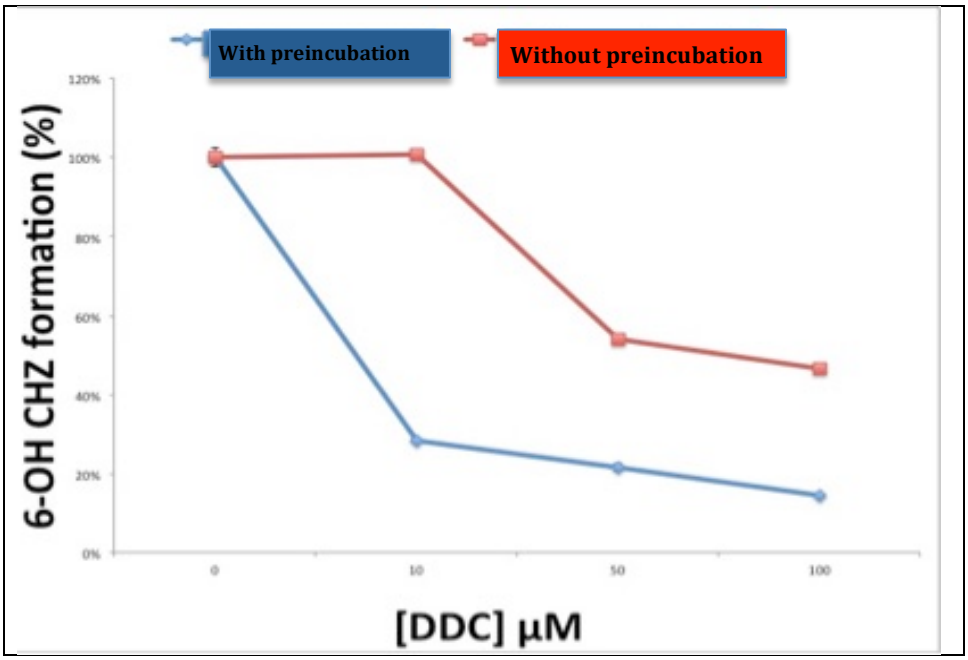


Figure 2.6.4.2 DDC preincubation versus non- preincubation methods
DDC, when preincubated with human liver microsomes, has increased inhibitory potency against 6-OH-CHZ formation. Formation of 6-OH-CHZ is expressed as a percent of the control formation rate when no DDC was present.

### 2.6.5 **CP inhibitory effect on CYP2E1**

Evaluation of a possible role of CYP2E1 in modifying sensitivity to CP requires studies to exclude a possible direct effect of CP on CYP2E1. This was investigated using human liver microsomal preparations. Liver microsomes were prepared from four different human liver tissue samples. The quantitative metabolic activity of CYP2E1 in liver samples was determined in vitro using CHZ as the index substrate, and DDC index inhibitor (following preincubation). Phosphate buffered saline (PBS Buffer) was prepared by dissolving 8g of NaCl, 0.2g of KCl, 1.44g of $Na_2HPO_4$, and 0.24g of $KH_2PO_4$ in 800 mL distilled water, with pH adjusted to 7.4 by HCL. The total volume was adjusted to 1L by adding distilled $H_2O$, and the buffer was then autoclaved. To prepare a 50 mM stock solution of CP, 300 mg of CP was dissolved in 20 mL of PBS. The CP master stock was wrapped with aluminum foil and kept in -20$^{o}$C. Four human liver microsomal preparations were provided from the Department's human liver tissue bank, and the total protein concentration measured as described previously. Each sample was prepared at a final concretion of 0.25 mg/mL. The three incubation conditions were: PBS as negative control; DDC 50 μM as positive control; and 50 μM CP. After completion of the incubation, the metabolic formation of 6-OH-CHZ from CHZ was determined as described above.

.

### 2.6.6 **The results**

Formation of 6-OH-CHZ from CHZ was not different between PBS and CP groups (see Figure 2.6.6.1). However, metabolic activity was significantly reduced by DDC. Therefore, a direct inhibitory effect of relevant concentrations of CP on CYP2E1 activity is excluded.

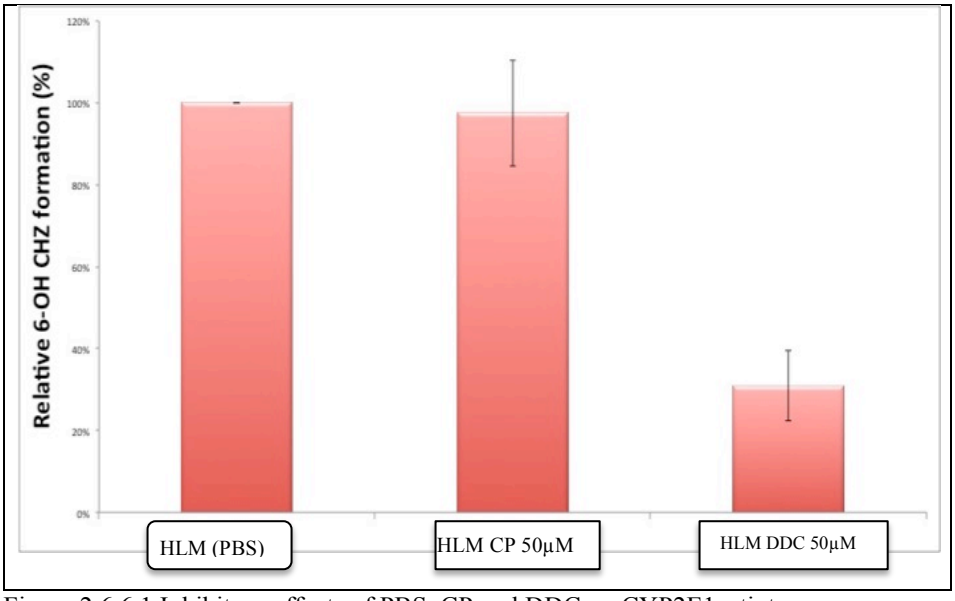


Figure 2.6.6.1 Inhibitory effects of PBS, CP and DDC on CYP2E1activty
Mean (±) SE relative rates of formation of 6-OH-CHZ. The three groups are PBS, CP 50µM and DDC 50µM. Values as the y-axis represent the peak height ratio of 6-OH-CHZ divided by the internal standard phenacetin.

### 2.6.7 **Study of CYP2E1 activity in Hep G2 cells**

To validate overexpression of microsomal CYP2E1 in Hep G2 cells transiently transfected with *CYP2E1* compared to scrambled plasmid or GFP transfection, metabolic activity was determined based on metabolism of CHZ. Samples were prepared using the intact cell method (see section 2.6.2). Metabolic activity was evaluated with CHZ (500 µM) incubated for 24 hours

in cell-full growth medium (negative control), in preparations of cells transfected with scrambled plasmids, and in cells transfected with *CYP2E1*.

### 2.6.7.1 The results

Small peaks consistent with 6-OH-CHZ appeared in both the incubation of cell free medium as well as incubation of scrambled transfected cells. Theses peaks were presumed to be explained by spontaneous oxidation of CHZ. In the cells transfected with *CYP2E1*, metabolic activity increased by 9-fold compared with the other 2 groups (see Figure 2.6.7.1).

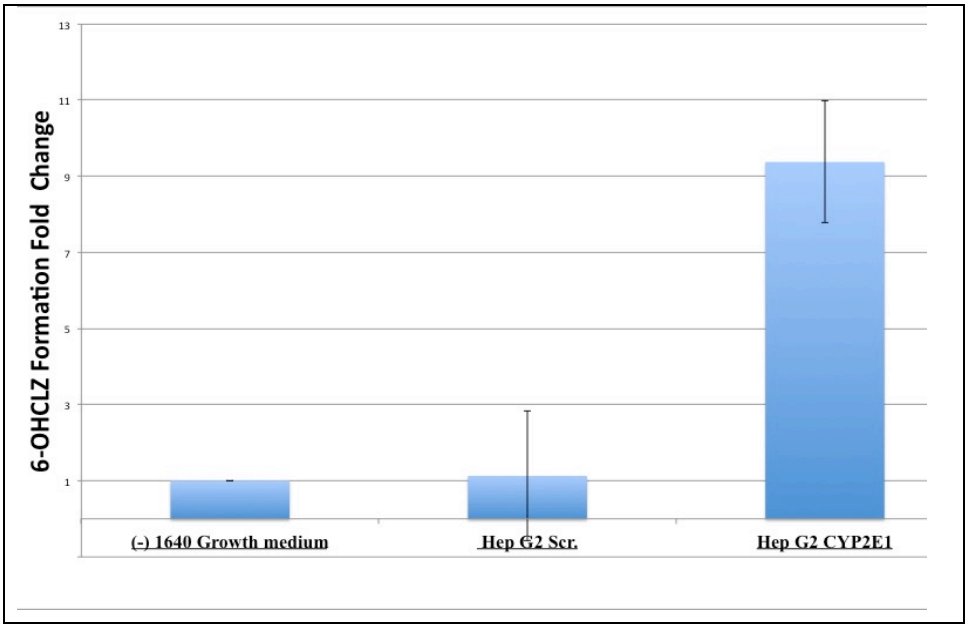


Figure 2.6.7.1 Metabolic activity of HepG2 (intact cell method)
Mean (±) SE CYP2E1 relative rates of formation of 6-OH-CHZ from CHZ when 500 µM CHZ was incubated for 24 hours with full growth medium alone, with scrambled-plasmid-transfected Hep G2 cells, and with *CYP2E1*-transfected Hep G2 cells (both transiently transfected).

## 2.6.8 Study of CYP2E1 activity in extrahepatic A2780/R and MOR/R cancer cells

### 2.6.8.1 Intact cell method

A2780/R cell lines with stable transiently transfected *CYP2E1* plasmid, and MOR/R cell lines with transiently transfected *CYP2E1* plasmid, were established as previously described. CYP2E1 metabolic activity was determined after incubation of cells with 500 μM CHZ for 24 hours. Hep G2 cells transfected with *CYP2E1* plasmid were used as positive control as in Section 2.6.7. Full growth medium was used as negative control.

### 2.6.8.2 The results

In Figure 2.6.8.1, incubation of CHZ with growth medium alone, and A2780/R and MOR/R cells transfected with *S*rc. plasmid as negative controls, yielded small 6-OH-CHZ peaks, consistent with spontaneous oxidation. 6-OH-CHZ production by CYP2E1 transfected A2780/R or MOR/R cells was not distinguishable from the negative controls. However, 6-OH-CHZ formation by Hep G2 cells transfected with *CYP2E1* plasmid exceeded the other groups.

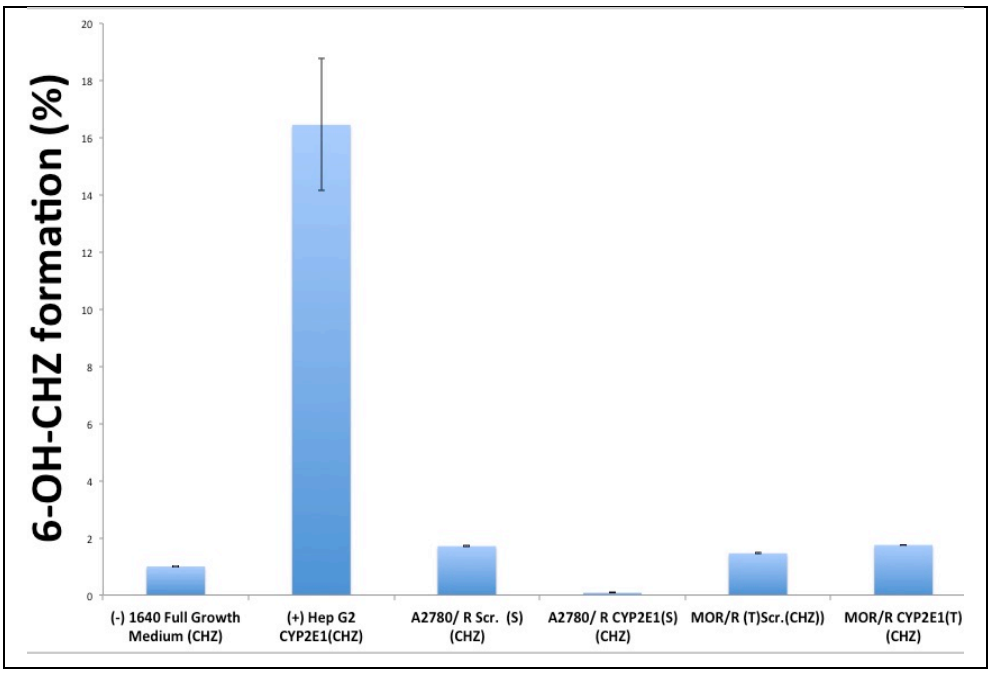


Figure 2.6.8.1 Metabolic activity of A2780/R and MOR/R (intact cell method) Mean (±) SE relative rates of formation of 6-OH-CHZ from CHZ when 500 µM CHZ was incubated for 24 hours with full growth medium alone, Hep G2 cells transfected with *CYP2E1* (transiently as positive control), A2780/R stably transfected with *CYP2E1* and stably transfected with A2780 Scr., and MOR/R cells transiently transfected with *CYP2E1* and Scr. plasmids.

### 2.6.8.3 Lysate method

Cell homogenates were prepared from A2780/R and MOR/R cells transfected with *CYP2E1* as in Section 2.6.2, and positive controls prepared from human liver microsomes using a final protein concentration of 0.25 mg/mL, and incubated in 25 µM CHZ for 20 minutes.

6-OH-CHZ was not formed by cell homogenates, indicating no evidence of CYP2E1 metabolic enzyme activity. The human liver microsomal preparation control showed a significant increase in 6-OH-CHZ formation.

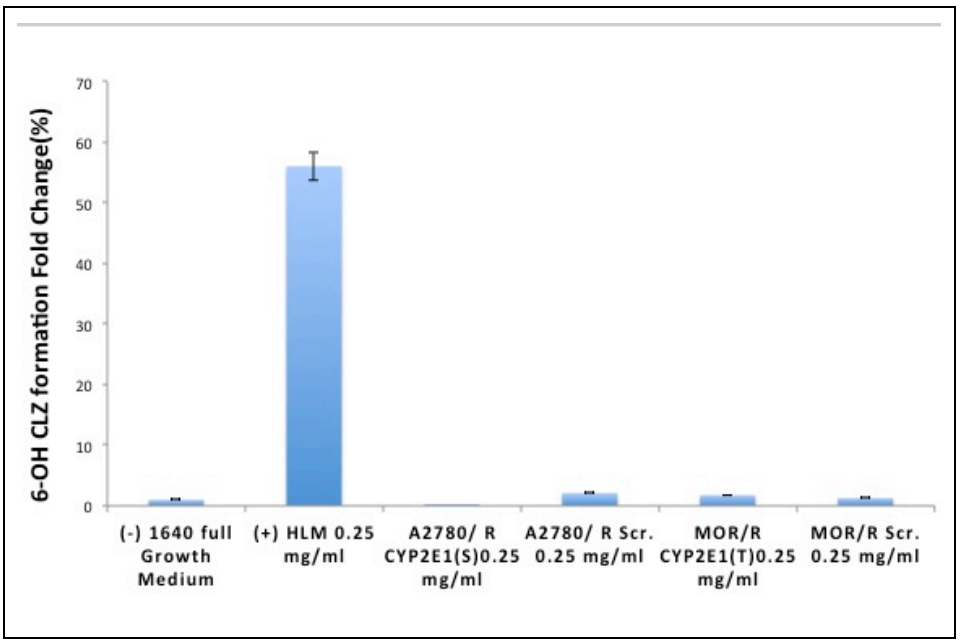


Figure 2.6.8.2 CYP2E1 Metabolic activity of A2780/R and MOR/R cells (Lysate method)
Mean (±) SE relative rates of formation of 6-OH-CHZ from CHZ when 25 µM CHZ was incubated for 20 min. with full growth medium alone, human liver microsomes (HLM), A2780/R stably transfected with *CYP2E1*, and stably transfected with A2780 Scr., and MOR/R cells transiently transfected with *CYP2E1* and Scr. plasmids. Lysate concentrations were 0.25 mg/mL.

### 2.6.8.4 Study of CYP2E1 activity in extrahepatic cells with addition of b5 and POR

Cyt b5 and POR and their roles as electron donors for monooxygenase reactions have been discussed previously. One possible cause of inactivity despite overexpression of *CYP2E1* mRNA in both A2780/R and MOR/R cells is a deficiency in electron-transport systems. Homogenates of A2780/R and MOR/R were prepared for metabolic activity evaluation as previously explained, with two positive controls. The first was human liver microsomes; the second positive control was recombinant CYP2E1 that lacked an electron transport system and was reconstituted with Cyt-b5 and POR. The

reconstitution was done based on the previous study protocol, in which the relative amounts of Cyt b5, POR, and CYP2E1 were adjusted to optimize metabolic activity. Human liver microsomes consistently showed formation of 6-OH-CHZ from CHZ. However, the recombinant CYP2E1 and the other cell lysates failed to produce metabolic activity,  Therefore we were not able to draw conclusions regarding the role of Cytb5 or POR in the lack of observed CYP2E1 metabolic activity.

.

## 2.7 Flow Cytometer (FACS)

### 2.7.1 **Fundamentals of FACS**

The schematic operation concept of the FACS system is shown in Figure 2.7.1.1. Cells are illuminated as they flow by a laser beam, which impinges on the structures and organelles inside the cells. These are projected out of the cell and form front- and side-scattered beams which can be analyzed to allow inferences regarding the shape, size, structure, and physical properties of the cells. The front beam provides a corresponding shape, and the side-scattered beams can be analyzed in relation to the particles and organelles (164). FACS has a wide range of applications, including ROS generation analysis, evaluation of viability, and cell sorting.

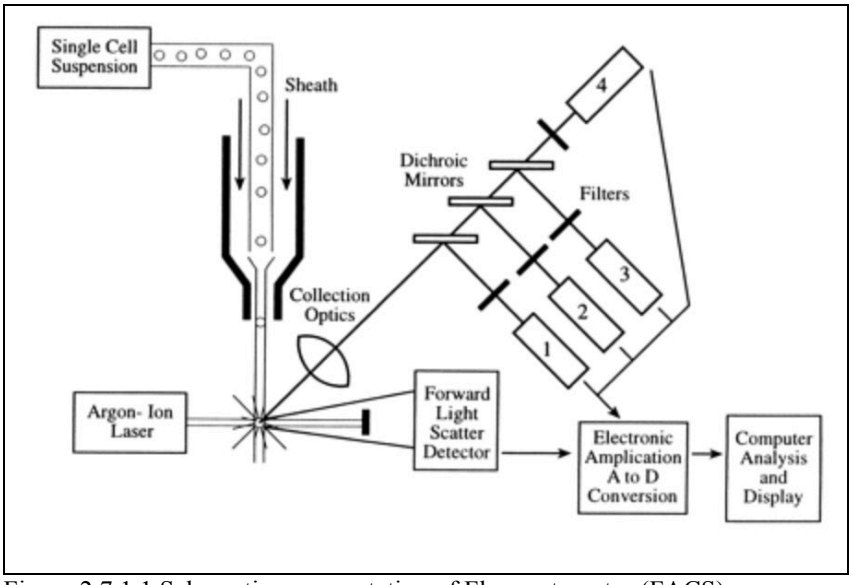


Figure 2.7.1.1 Schematic representation of Flow cytometry (FACS)
This picture was adapted from (162).

## 2.7.2 ROS measurement using the ($H_2$DCF-DA) flow cytometer

### 2.7.2.1 Introduction

2′-7′-Dichlorodihydrofluorescein diacetate (DCFH-DA) is a widely used marker to measure ROS. The redox state within cells will shift if there is excessive free radical formation. DCFH-DA is a non-fluorescent compound that is cell-permeable. Therefore, when DCFH-DA penetrates the cell membrane into the cell, it is converted by intracellular esterases into DCFH, which is a cell membrane-impermeable product. The later product is also non-fluorescent, and accumulates inside the cells. DCFH is then oxidized by ROS and yields the highly fluorescent product DCF (see Figure 2.7.2.1). Accumulation of DCF in cells may be measured by an increase in fluorescence at 530 nm when the sample is excited at 485 nm. Emission fluorescence at 530 nm is measured using a flow cytometer, and is assumed to be proportional to the concentration of hydrogen peroxide in the cells. DCF, the oxidized fluorescent product of $DCFH_2$, is membrane-permeable and can leak out of cells over time. Detecting slow hydrogen peroxide production over time can be difficult. This technique is a straightforward, inexpensive, and highly sensitive to changes in the redox state of a cell, and can be used to follow changes in ROS over time (165).

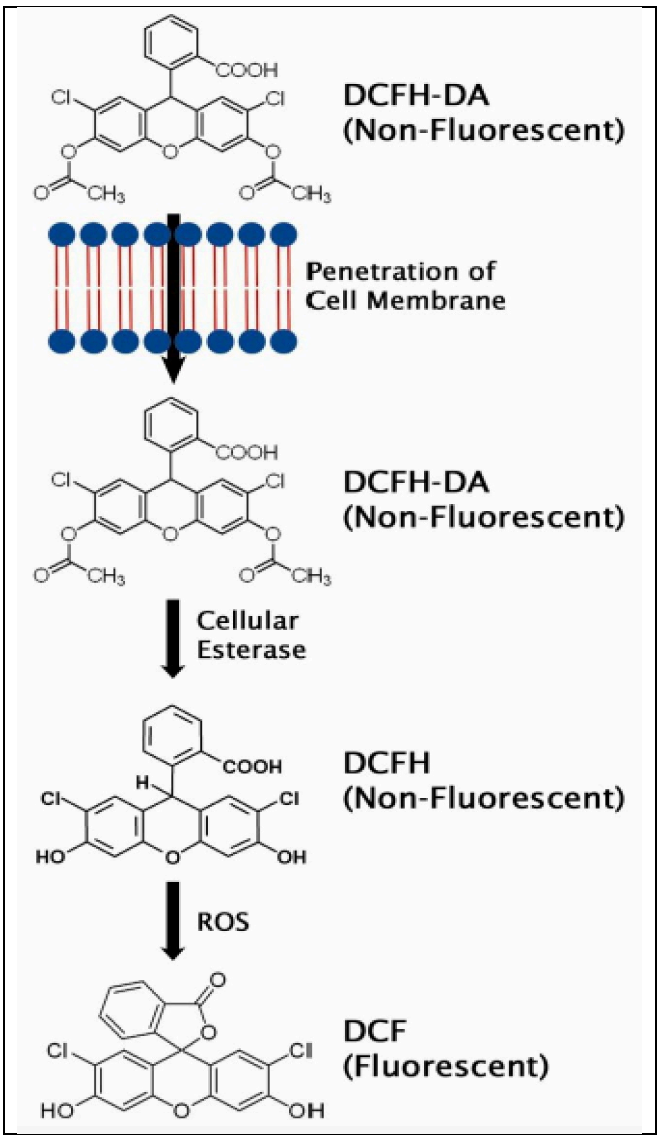

Figure 2.7.2.1 Schematic representation of DCF Assay
This was adapted from Cell Biolabs, Inc.

#### 2.7.2.2 ROS assay protocol

Each cell line intended for evaluation with the ROS assay was prepared under four different conditions. Approximately$10^6$ cells were seeded on four 35mm plates. The conditions were: the negative control that was not exposed to DCFDA; the negative control that was exposed to DCFDA; a positive control using a ROS inducer (TBHP) to validate the ROS assay; and cells exposed to CP to evaluate ROS generation (Figure 2.7.2.2).

DCFDA - cellular ROS Detection Assay Kits (ab113851) from Abcam® were used to measure relative ROS. Three of the four plates were treated with DCFDA, 25 µM, for 18 minutes. The fourth plate was treated with DMSO only as a negative no-DCFDA control. The cells were then washed three times with PBS. The four conditions were prepared as follows: condition one—negative, no DCFDA, incubated with 2% FBS in PBS; condition two -- negative, with DCFDA, incubated with 2% FBS in PBS; condition three -- positive control with DCFDA, treated with 50 µM TBHP; condition four -- CP with DCFDA, incubated with 50µM CP. All plates were wrapped with aluminum foil to prevent direct light exposure, and left in an incubator at $37^o$ C and 5% $CO_2$ for 2 h. After 2 h the cells were washed once with PBS, harvested as described before, and then centrifuged and resuspended with PBS. The cells were then placed in FACS tubes and left in ice for transfer to the FACS instrument. Using a Becton Dickinson FACS Calibur 4 Color Flow Cytometer, each tube was placed in the instrument.

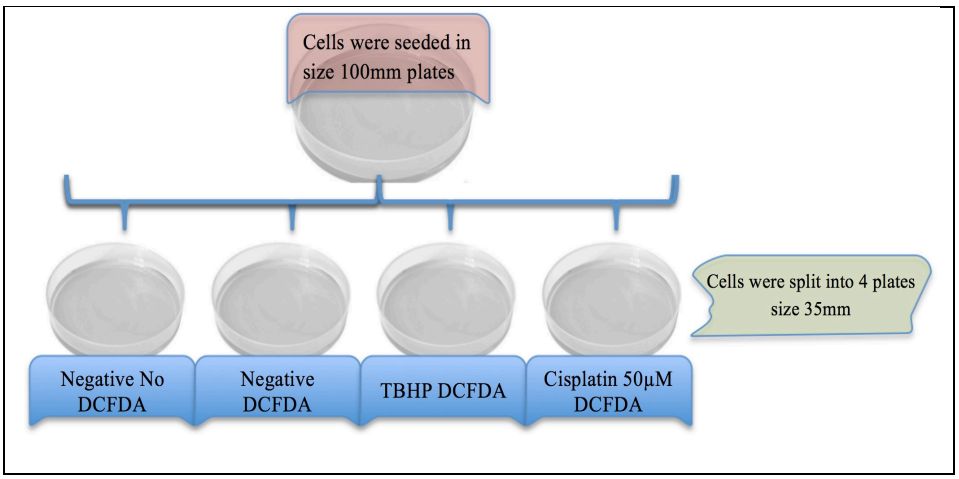


Figure 2.7.2.2 Cell preparation step for ROS assay
The cells were seeded in 100 mm plates on day 1. On day 3 the cells were harvested and seeded onto 4 plates for ROS relative measurement by FACS.

### 2.7.2.3 FACS data analyses

In Figure 2.7.2.3, (a), the Y-axis represents the side-scattered beams and the X-axis represents the front-scattered beams, both of which are the result of laser-beam deflection by the cells. SSC-H represents the complexity of the cells (such as organelles and cell-surface granularity), while FSCB represents the size of the cell. The healthy-shaped population is gated as R1 in the figure. In (b), fluorochrome FL3-H is used in the Y-axis for propidium iodide (PI), while FL1-H is used for fluorescent oxidized DCF. The PI is used to distinguish unhealthy dying cells from healthier cells. Thus the positive PI indicates the cells that failed to extrude PI, while the negative PI represents the healthier, not-dying cells that actively extrude the PI. The populations of these healthier cells were gated as R5, as seen in (b). Then, using FLI-H fluorochrome on the Y-axis, the population of cells expressing fluorescent oxidized DCF is gated as R6, as shown in (c). The R6 gating will count the events that represent a healthy living cell expressing fluorescent DCF, where

each event is represented as a red dot in the graph. The average number of events was calculated.

.

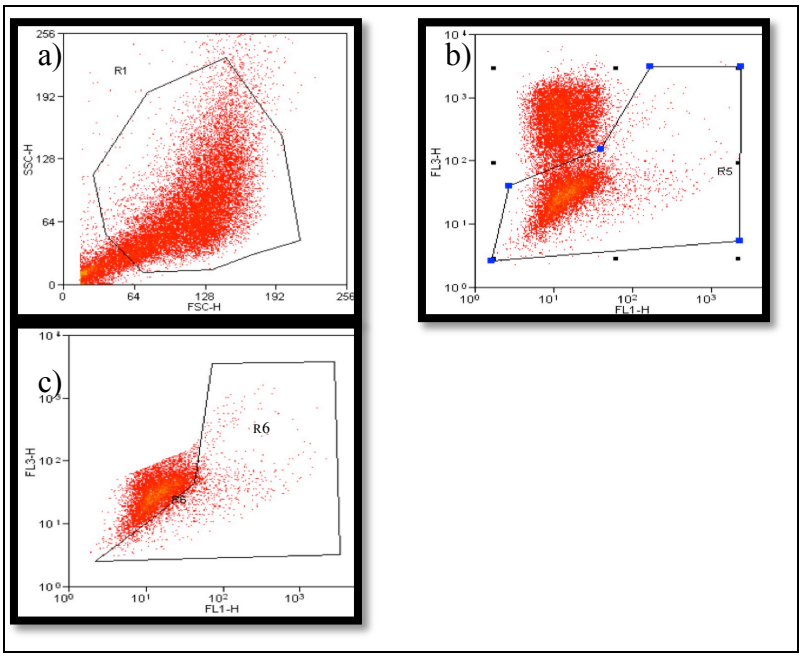


Figure 2.7.2.3 Flow cytometer-gating strategy for ROS assay (a) R1 is gating the events that most likely exclude debris and cellular components that are not represented with regular size and shapes relative to normal cells. (b) The R1 gate in (a) is represented in b), where the cells can be filtered into living and non- living cells. (c) The R5 gate in b) is represented in c) where R6 gate are the healthy living cells that exhibit DCF fluorescence.

### 2.7.3 **Results of ROS assay for CYP2E1-overexpressed Hep G2 cells**

Hep G2 cells were transfected with *CYP2E1* and Scr. as previously explained. Each cell group was then seeded in four 35 mm plates as described above.

The FACS reading results were calculated by counting the events, represented by the red dots in Figure 2.7.3.1, that indicate the number of DCF fluorescent cells gated in R6 for both cell groups in (a) and (b). Figure 2.7.3.1 shows a comparison between the Hep G2 Scr. as control and Hep G2 CYP2E1 after 50 µM CP treatment for 3 hours.

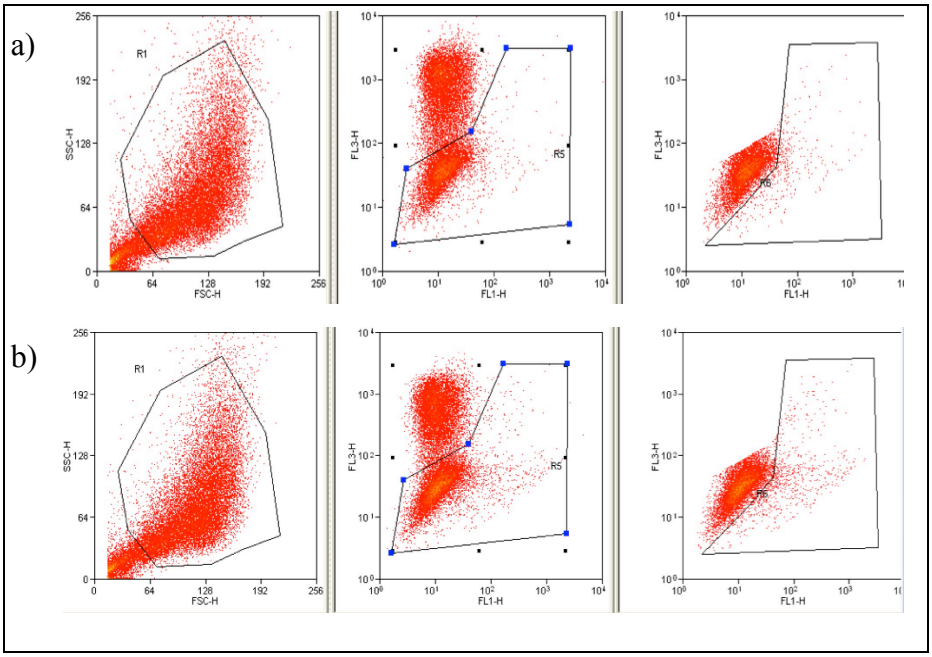


Figure 2.7.3.1 Hep G2 CYP2E1 versus Hep G2 Scr. flow cytometry
In (a) Hep G2 Scr. exposed to 50 µM CP, compared with (b) Hep G2 transfected with *CYP2E1*, and exposed to 50 µM CP.

The number of fluorescent oxidized DCF cell events divided by the total number of cell events were determined for each group of cells, Hep G2 CYP2E1 and Scr, for the two conditions of TBHP (positive control) and CP 50 μM,. These were normalized by dividing them by the corresponding negative control values.

In the descriptive statistical analysis, an unpaired t-test between the groups was used to analyze CP 50 μM normalized reading values compared to control. With a two-tailed P value of 0.0370; this is statistically significant, (Table 2.7.3-1) and (Figure 2.7.3.2).

As shown in Figure 2.7.3.2, ROS generation in the positive controls was significantly increased compared to the negative DMSO controls for both Hep G2 CYP2E1 and Hep G2 Scr. transfected cells.

The findings indicate that cells expressing CYP2E1 will significantly increase ROS generation compared to control scr.-transfected Hep G2 cells.

| Group | Hep G2 CYP2E1 | Hep G2 Control |
|---|---|---|
| Mean | 2.5 | 1.37 |
| SD | 0.28 | 0.14 |
| SEM | 0.20 | 0.10 |
| N | 2 | 2 |

Table 2.7.3-1 Data summary for Hep G2 ROS formation

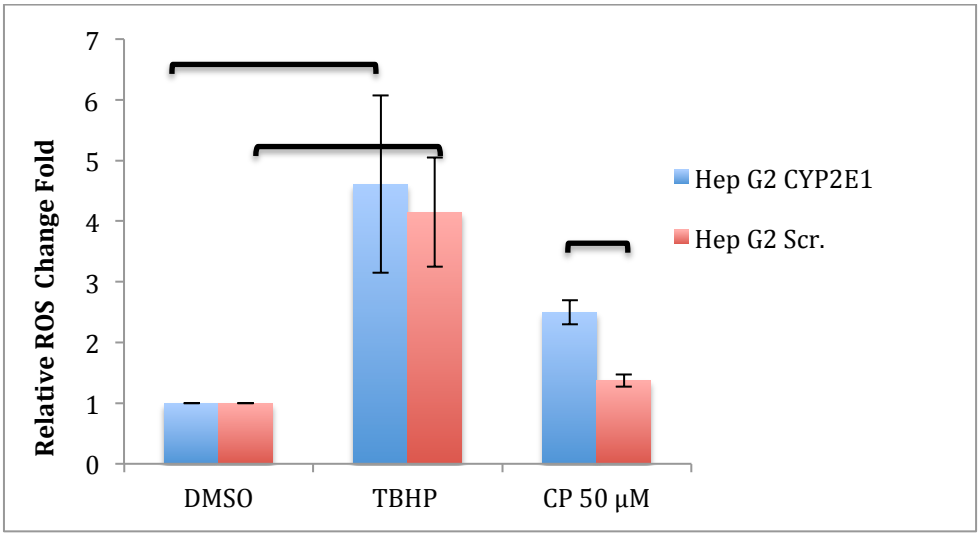


Figure 2.7.3.2: Relative ROS formation for Hep G2 *CYP2E1* transfected cells and Scr. transfected cells
Both the Hep G2 CYP2E1 cells and control cells showed significant increases in mean (±) SE relative ROS formation with exposure to the ROS inducer TBHP. With exposure to 50 µM CP, significant differences were observed between *CYP2E1* and Scr. transfected cells.

## 2.8 MTT assay

### 2.8.1 MTT introduction

The fundamental experiment in CYP2E1 enzyme effects on CP cancer resistant cells is the assessment of cell viability. Available methods of testing cell viability range from a straightforward trypan blue dye-exclusion assay to more complex assays of individual cells using RAMAN microscopy (166). Approaches to studying the cytotoxicity of the cells can be divided into: those used to evaluate the metabolic activity of the cell, and those used to evaluate DNA synthesis. Metabolic assays cannot distinguish between cells that are actively dividing and those that are not. We choose the MTT assay though consideration of cost, speed, availability of facilities, sensitivity, and accuracy. MTT assays don't have maximal sensitivity, but nonetheless are used extensively (167, 168). MTT assays may be particularly useful for testing and evaluating CP and newer anti-cancer agents in vitro (169). Their low cost and easy use are advantages over many other cytotoxicity assays. In one study the overall accuracy of the MTT assay clinical terms was 83% (170). Inconsistencies in previous studies have been attributed to variations in pH due to changes in the medium (171). In our MTT study we used the same media consistently.

### 2.8.2 **MTT mechanism of action**

The yellow dye 3-(4,5-dimethythiazol-2-yl)-2,5-diphenyl tetrazolium bromide (MTT) is reduced by mitochondrial succinate dehydrogenase to produce formazan. The MTT passes into the mitochondria within the living cells where the reduction takes place. The reduced compound is insoluble and dark blue in color. Organic solvents such as DMSO will dissolve formazan. The dark blue solubilized formazan is measured spectrophotometrically. MTT reduction occurs only in metabolically active cells; therefore, the level of activity reflects the viability of the cells.

### 2.8.3 **MTT assay method**

When a particular cell line was plated for MTT assay, the cells were detached from the plates after 24 h and seeded in white, 96-well, flat-bottom plates, as described previously. The seeded number of cells was optimized to 15 x $10^3$ cells/well. The following day, the cells were treated based on the experimental plan. Fresh MTT solution was prepared as follows: MTT is dissolved in sterile PBS (5 mg/mL in PBS) then filtered using 0.45 micro from MF-Millipore filters and kept in the dark by wrapping the tube with aluminum foil. On the $5^{th}$ day, all growth medium was aspirated from each well, after which 200 µL of MTT solution was added using a multichannel pipette. The plate was then left in the dark in the incubator at 5% $CO_2$ and -37$^oC$ for 4 hours.

After 4 hours, the contents of each well were aspirated, then 200 µL DMSO was added to dissolve any generated formazan compound. The plate was left in the incubator for 30 minutes, after which it was read using a Tecan Microplate reader Spectra Fluor plus with a 590 nm filter. To ensure a homogenous mixture in each well, the plate was shaken for 60 seconds before reading.

## 2.8.4 **MTT standardization**

Three strategies were used to standardize the MTT assay: first, by optimizing the method of seeding the cells onto the plate; second, by validating CP toxicity in sensitive and resistant cell lines; third, by checking the reproducibility and consistency of the assay.

### 2.8.4.1 Optimizing the cell-seeding method

To determine the appropriate seeding density of A2780 and MOR cells for the MTT assay, the cells were seeded onto 96-well, flat-bottom white plates. In triplicate fashion, no cells were seeded into the first three wells, and then 5 x $10^3$, 10 x $10^3$, 15 x $10^3$, and 20 x $10^3$ cells were seeded, respectively. After three days, MTT solution was added, then the derived formazan was solubilized by 150-200 µL DMSO. The absorbance (OD) was read in an ELISA plate Reader at 570 nm. OD was found to be linearly related to cell seeding density, as shown in (Figure 2.8.4.1 and Figure 2.8.4.2)

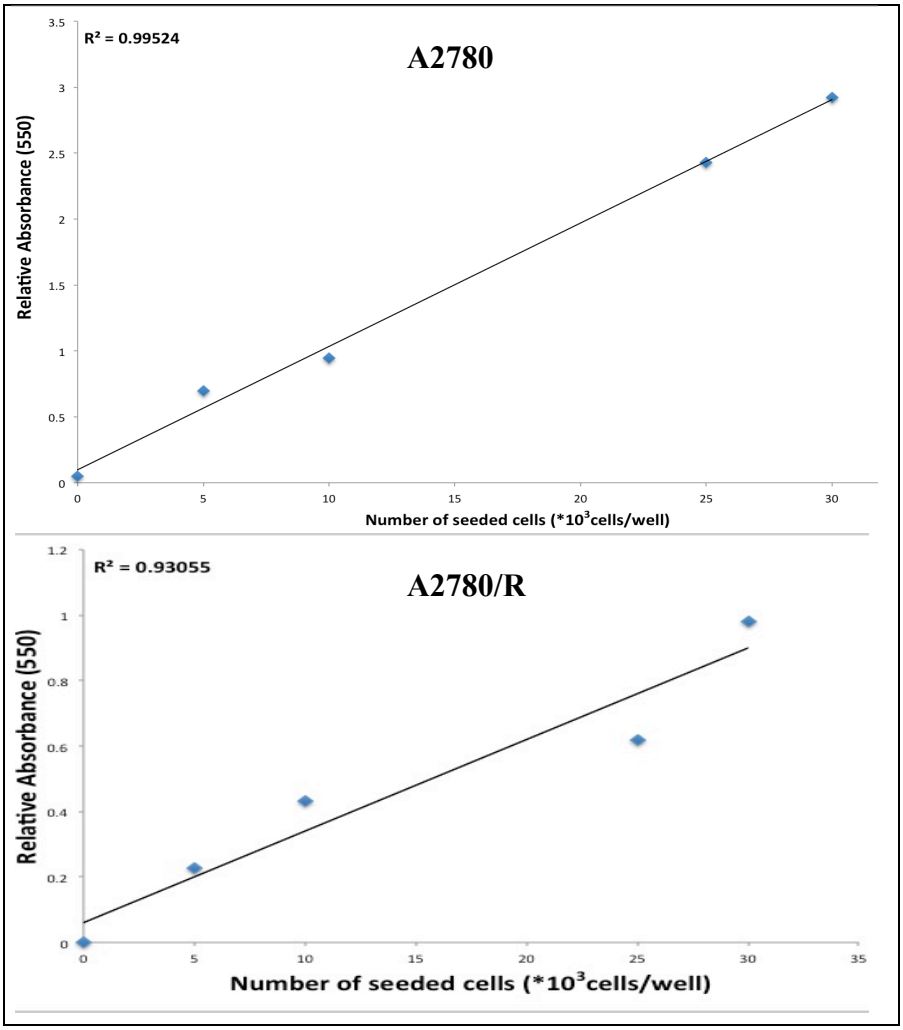


Figure 2.8.4.1 A2780 and A2780/R seeding density MTT assay
A2780 and A2780/R cells seeded in 96 well plates with different cell numbers, and left in the incubator to grow. The y-axis represents the optical density reading at 550 nm.

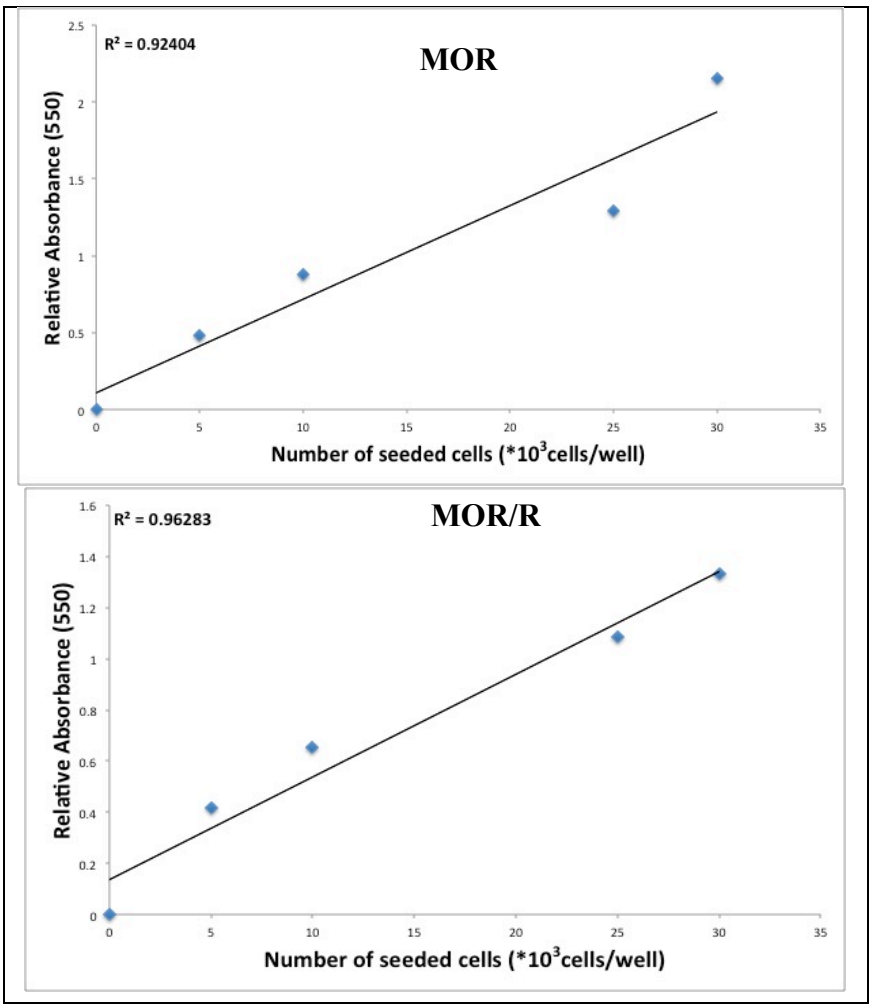


Figure 2.8.4.2 MOR and MOR/R seeding density MTT assay
MOR and MOR/R cells seeded in 96 well plates with different cell numbers, and left in the incubator to grow. The y-axis represents the optical density reading at 550nm.

### 2.8.4.2 MTT reproducibility

The second level of MTT assay optimization was a plan to assure reproducibility of any MTT assay experiment. All experimental points were done in triplicate.

In each experiment, the cells prepared for MTT assay were cultivated to reach at least 2.6 X $10^7$. Cells were thawed and seeded in 10 cm plates. At 70-80% confluence the cells were then passed onto two 10 cm, then after reaching 70-80% confluence were then passed onto four 10 cm plates. When the total cell number reached the required target, they were collectively seeded onto size T 150 plates, with a surface area of 150 $cm^2$, and number of cells seeded at 2.0 X $10^7$. After reaching 70-80% confluence, the cells were harvested and seeded onto eight 10 cm plates. For the actual experiment, each set of two plates consisted of cells transfected with *GFP*, scrambled, and *CYP2E1* plasmids respectively (see Figure 2.8.4.3).

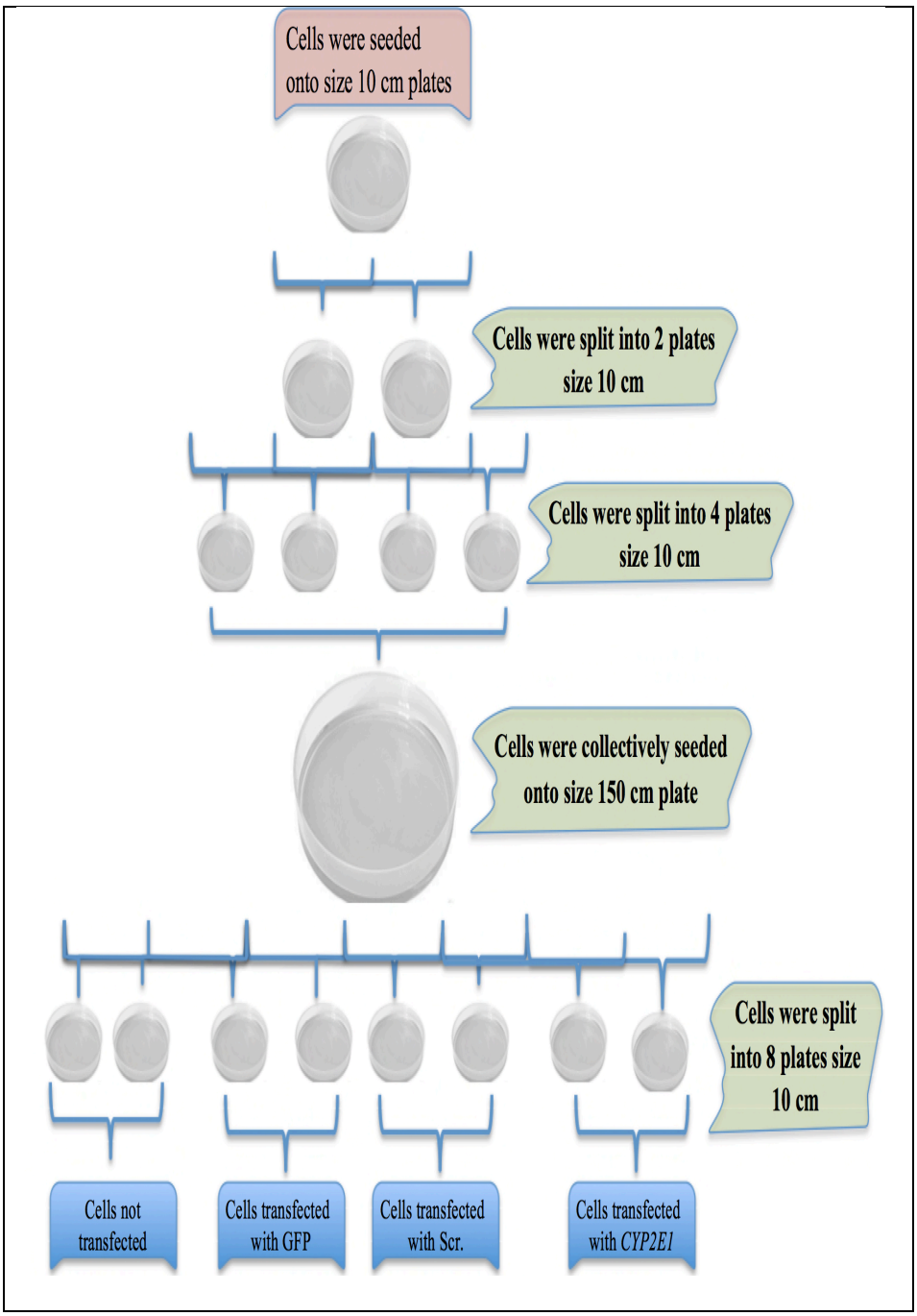


Figure 2.8.4.3 Illustration for cell growth and seeding plan for transfection process

### 2.8.4.3 Validation of CP toxicity in sensitive and resistant cell lines

The MTT viability assay validated CP sensitivity (toxicity) in cell lines identified as sensitive and resistant to CP. A2780 cells (CP sensitive) were compared to A2780/R (CP resistant), and MOR cells were compared to MOR-R cells. The cells were seeded at $20x10^3$ for A2780/A2780/R, and $15x10^3$ for MOR/MOR/R cell lines. After 24 h, the cells were exposed to different concentrations of CP, which was prepared in full growth medium. On the third day, the cell medium was renewed with the same CP concentration. The total incubation time was 5 days.

#### 2.8.4.3.1 The results

Figure 2.8.4.4 shows the OD values (Y-axis) in relation to CP concentration (X-axis) for 3 sets of A2780 cells, both sensitive and resistant. Note the significant differences in CP toxicity between the sensitive and resistant cell lines at 14, 7 and 3 μM CP concentrations. Figure 2.8.4.5 shows the same data but with OD values normalized as a percentage of the CP=0 control values.

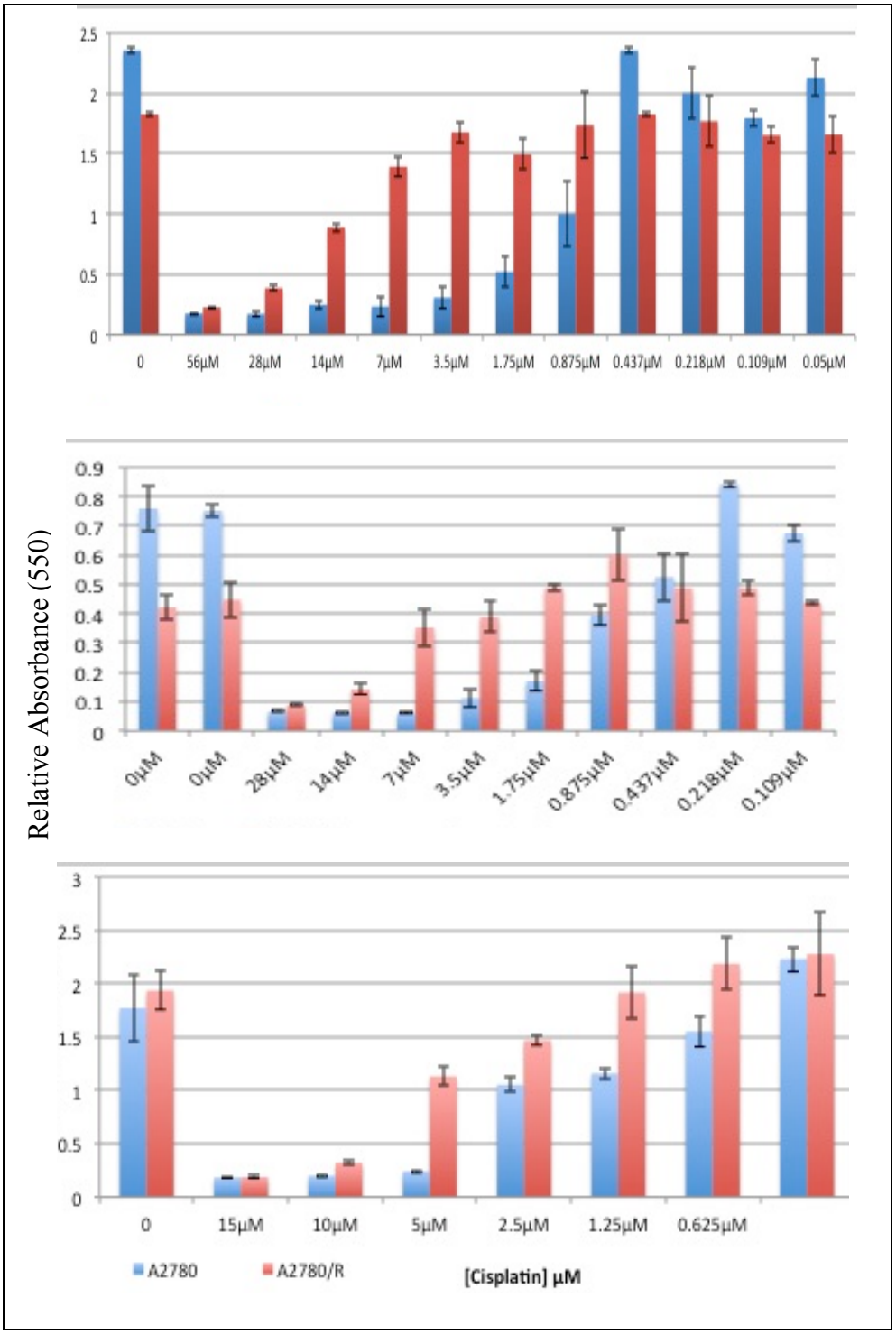


Figure 2.8.4.4 MTT assay for A2780 and A2780/R cells
Mean (±)SD O.D. values for A2780 and A2780/R cells in the MTT assay .The cells were exposed to different concentrations of CP, n=3at each point.

.

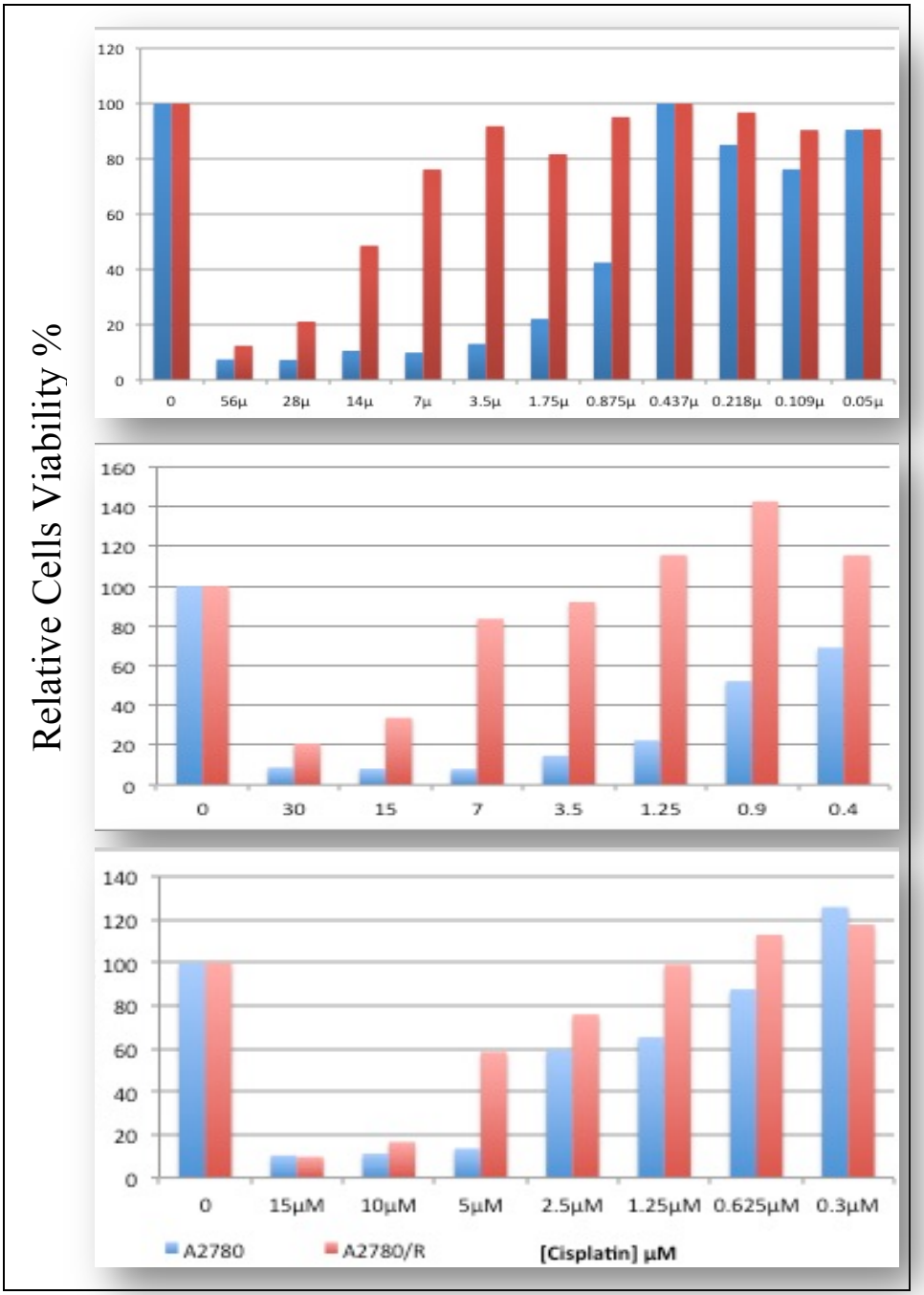


Figure 2.8.4.5 A2780 and A2780/R MTT assay showing normalized data
The data in the previous figure were normalized to yield relative cell viability (%); Each OD reading value was divided by the OD value of the untreated control cells, and then multiplied by100. There were significant differences between A2780 and A2780-R cells at multiple CP points.

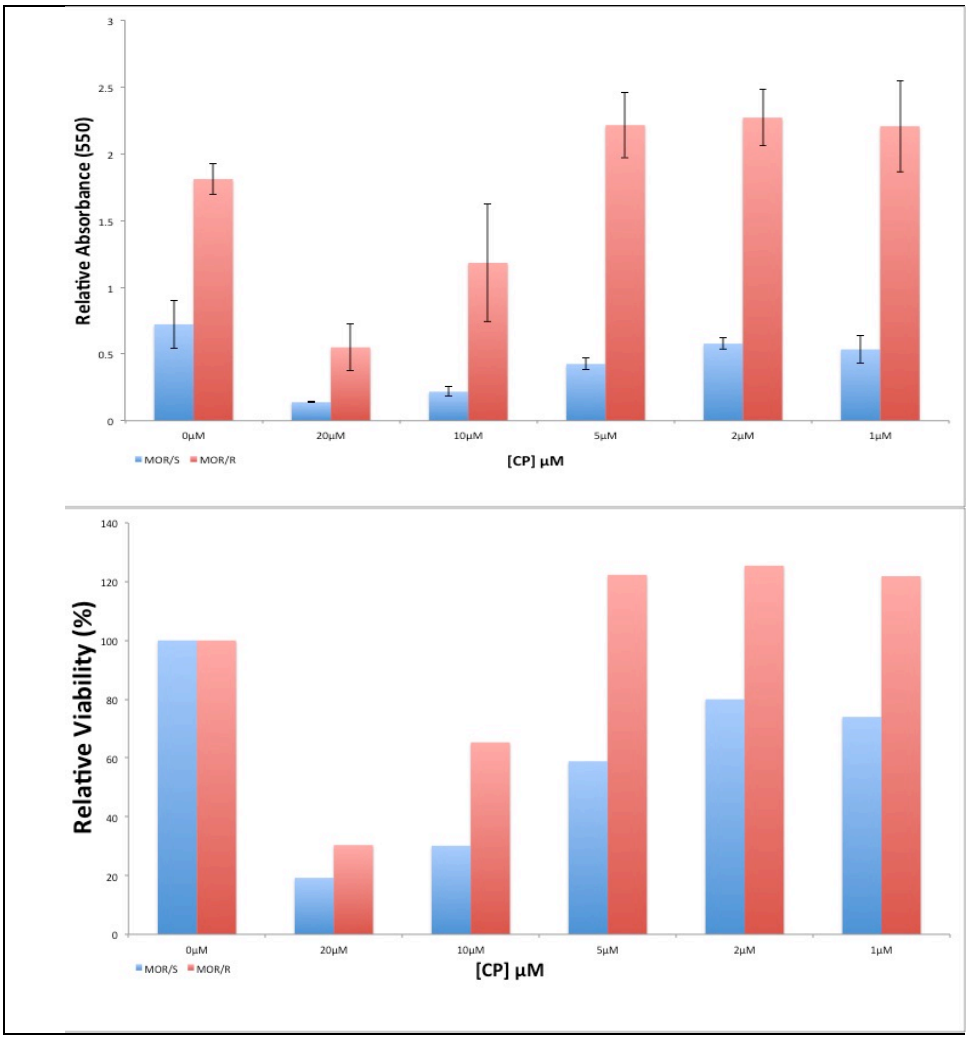


Figure 2.8.4.6 MOR and MOR/R MTT assay
Mean (±)SD O.D. values for MOR and MOR/R cells in the MTT assay .The cells were exposed to different concentrations of CP. In b), the data were normalized to yield relative cell viability (%);. each OD reading value was divided by the OD value of the untreated control cells, then multiplied by 100. There were significant differences between MOR and MOR/R cells at multiple CP points.

## 2.8.5 CP $IC_{50}$ for A2780 and A2780/R cells

The 50% cytotoxicity concentration ($IC_{50}$) of CP for the sensitive and resistant cell lines was determined by nonlinear regression using Sigma Plot software (172). The equation $R = 100\left(1 - \frac{E_{max}[CP]^b}{[CP]^b + IC^b}\right)$ was fitted to data points consisting of [CP] (the concentration of CP) and R ( the % cell viability normalized to CP=0 control). The iterated variables were: $E_{max}$ (the maximum degree of cytotoxicity); IC, the CP concentration giving an R value of 50% of (100-$E_{max}$); and b, an exponent. The $IC_{50}$ value for CP was determined from IC as follows: $IC50 = IC/(2E_{max} - 1)^{1/b}$

### 2.8.5.1 The results

Figure 2.8.5.1 shows the CP $IC_{50}$ for A2780 cells. As anticipated, $IC_{50}$.values are substantially lower in CP sensitive cells compared to resistant cells. There was also a dependence of $IC_{50}$ values on the conditions under which the cells were handled and treated, incubation time, and number of passages. Although these factors changed the absolute $IC_{50}$ values, the differences between sensitive and resistant cells were maintained.

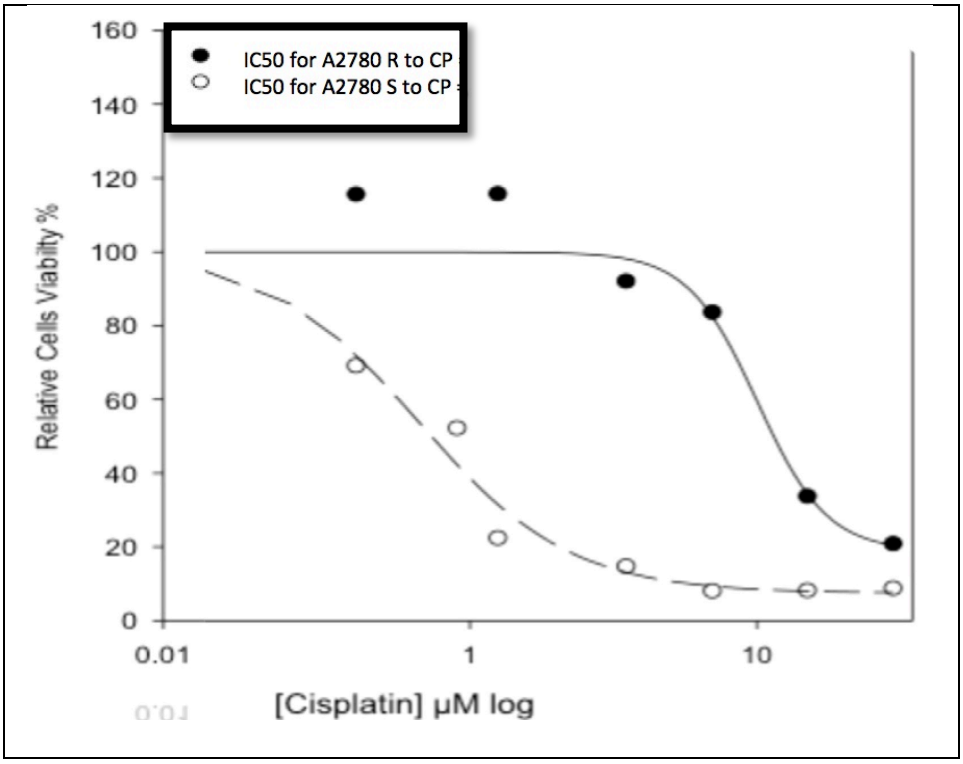


Figure 2.8.5.1 $IC_{50}$ for A2780 and A2780/R
Nonlinear regression showing values of CP $IC_{50}$ for A2780/ CP- resistant = 11.4 µM and for A2780/ CP-sensitive = 0.73 µM.

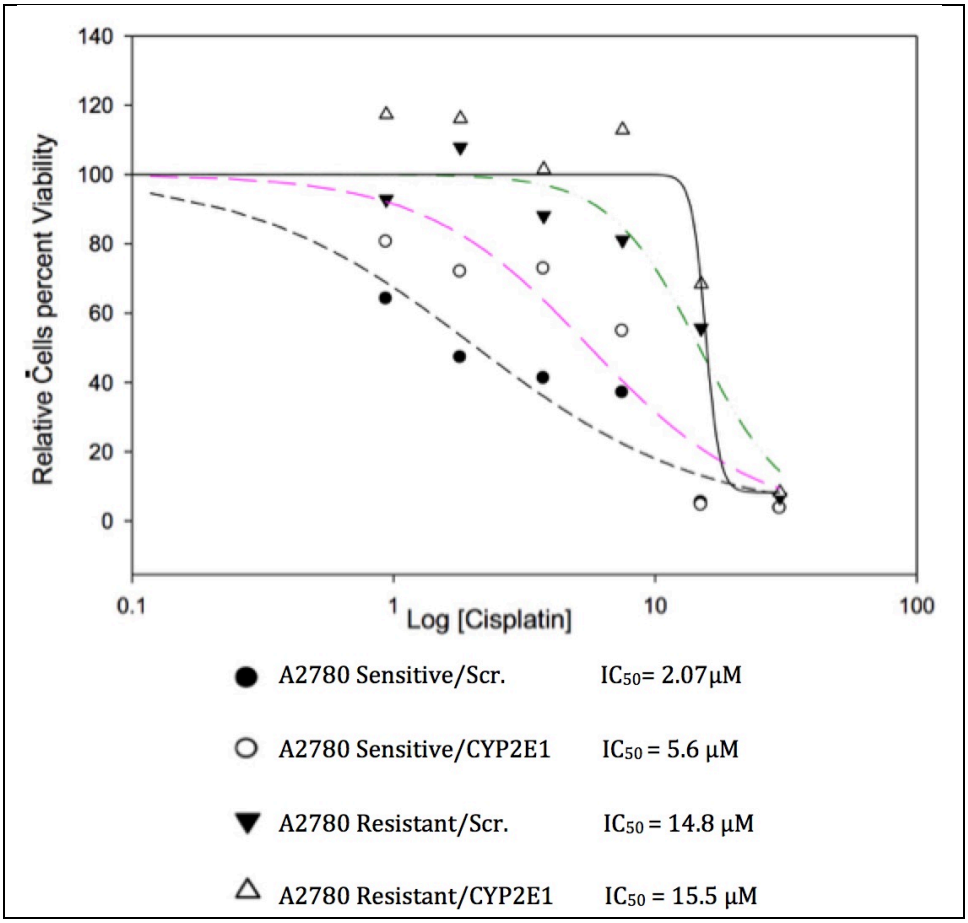


Figure 2.8.5.2 $IC_{50}$ for A2780 and A2780/R cells stably transfected with *CYP2E1*.

Nonlinear regression showing values of CP $IC_{50}$ for A2780/ CP- sensitive stably transfected with *Scrambled* and *CYP2E1* plasmids The $IC_{50}$ value for the CYP2E1 sensitive A2780 showed higher values in transfected cells with *CYP2E1*when compared to its counterpart negative control (scrambled transfected cells), which is indicative of no sensitization effect compared to the sensitive A2780 cells. The same applied to A2780 CP resistant cells when transfected with scrambled and *CYP2E1* plasmids. The $IC_{50}$ values for both are nearly identical.

## 2.8.6 **DDC cytotoxic effect on Hep G2 cells**

A study was done to exclude a possible effect of DDC, the CYP2E1 index inhibitor, on the viability of Hep G2 cells. The cells were seeded in 96-well plates and exposed on the following day to different concentrations of DDC ( Figure 2.8.6.1). The MTT assay was used to evaluate cell viability after 5 days of incubation.

### 2.8.6.1 The results

High concentrations of DDC (100 or 500 μM), impaired cell viability ($p < 0.05$), while no significant change was observed at a DDC concentration of 50 μM when compared to the negative control (DDC = 0). This suggests that DDC concentrations <50 μM are unlikely to impair cell viability. However, since there was no evidence that CYP2E1 expression was related to CP sensitivity phenotype (section 2.8.7), further studies of DDC were not undertaken.

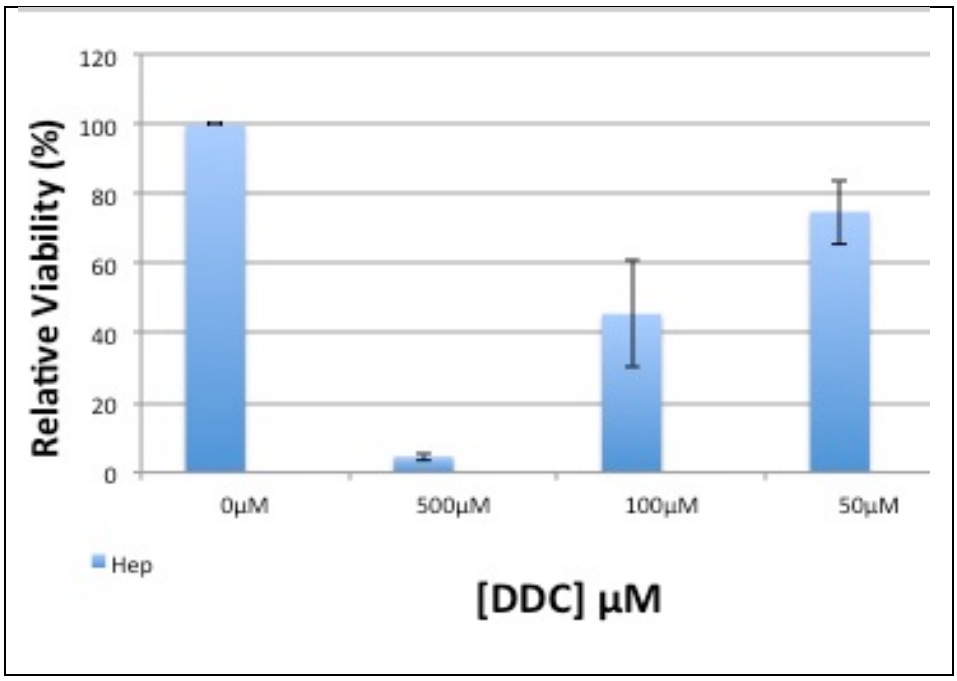


Figure 2.8.6.1 DDC cytotoxic effect on Hep G2 cells
Mean (±)SD relative viability of Hep G2 cells exposed to DDC concentrations of 500, 100, and 50 µM. There was no significant difference between the mean relative viability at 50 µM DDC compared to the control group (DDC = 0).

## 2.8.7 CP toxicity in HEP G2 CYP2E1 cells

Hep G2 cells were transfected with *CYP2E1*, GFP and nonsense *CYP2E1* (Scr) cDNA as described previously (Section 2.3). Studies were conducted using 4 groups of Hep G2 cells. The negative control cells were exposed only to transfection reagent without plasmid. The upper half of each plate was seeded with the negative control. The other cell groups were transfected with *CYP2E1*, GFP, and Scr. cDNA, then seeded onto 96 well plates in duplicate fashion. The following day the cells were exposed to a range of CP concentrations (0, 80, 40, 20, 10, 5, 2.5, 1.25, 0.65, 0.325, 0.162, 0.081 µM) for 5 days. On the third day, the full growth media with the same CP concentrations were refreshed. Treatment with CP continued for 5 days. In

each experiment, 8 plates were used. The MTT assay was conducted on all plates as explained in Section 2.8.

### 2.8.7.1 The results

Based on ANOVA, the only statistically significant differences among treatments occurred at a concentration of 5 µM. At all other concentration points the differences among treatments were not significant (Figure 2.8.7.1). Descriptive statistics for the relative viability (%) of each group at concentrations of 5 µM are shown in Table 2.8.7-1. Table 2.8.7-2 shows the outcome of ANOVA for 5 µM concentration points. Differences among treatments produced significance, with p=0.05. If anything, the three transfected groups had greater viability than the controls cells, and there were no apparent differences in viability values among the three transfected cell groups.

**Descriptive Statistics for Relative Viability (%) by treatment at [CP] of 5µM**

Concentration_5

| | N | Mean | Std. Deviation | Std. Error | 95% Confidence Interval for Mean | |
|---|---|---|---|---|---|---|
| | | | | | Lower Bound | Upper Bound |
| Hep G2 | 14 | 38.0477 | 22.12808 | 5.91398 | 25.2714 | 50.8241 |
| Hep G2 CYP2E1 | 8 | 57.1946 | 20.43064 | 7.22332 | 40.1142 | 74.2751 |
| Hep G2 Scr. | 8 | 58.3138 | 17.74650 | 6.27433 | 43.4774 | 73.1503 |
| Hep G2 GFP | 8 | 54.4505 | 12.33079 | 4.35959 | 44.1417 | 64.7593 |
| Total | 38 | 49.7984 | 20.58616 | 3.33952 | 43.0319 | 56.5649 |

Table 2.8.7-1 Relative viability (%) with treatment at [CP} 5µM

| ANOVA among treatments μM NTS AT [CP] of 5 μM | | | | | |
|---|---|---|---|---|---|
| [CP] 5 μM | Sum of Squares | df | Mean Square | F | Sig. |
| Between Groups | 3123.968 | 3 | 1041.323 | 2.820 | .054 |
| Within Groups | 12556.259 | 34 | 369.302 | | |
| Total | 15680.227 | 37 | | | |

Table 2.8.7-2 ANOVA among treatments at [CP] of 5 μ M

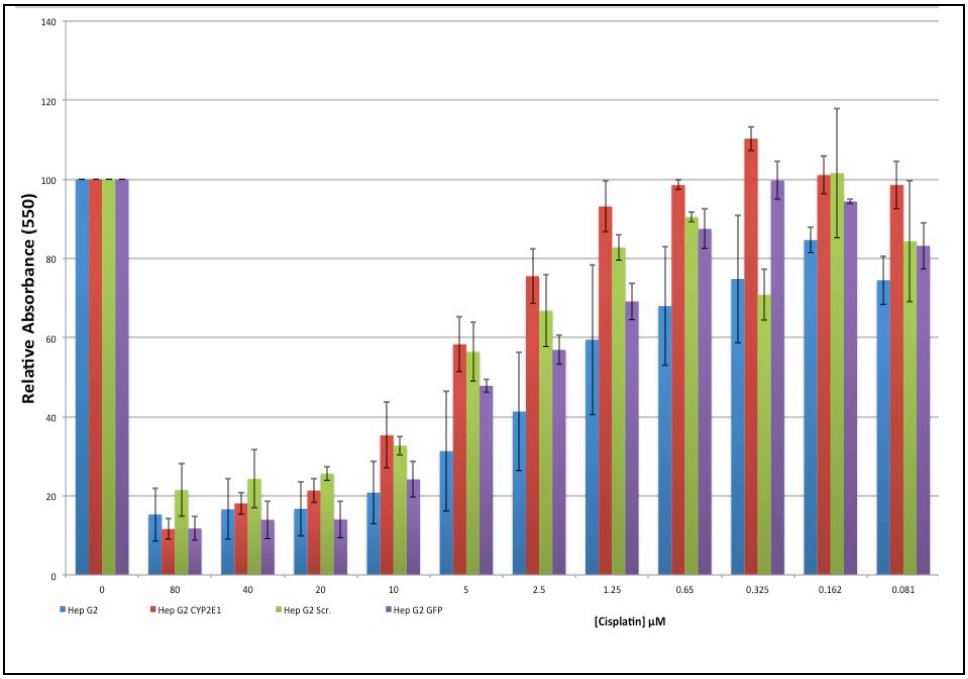


Figure 2.8.7.1 Viability assay for HepG2 cells treated with CP
Hep G2 cells transfected with *CYP2E1*, *GFP*, and Scr. treated with different concentrations of CP (0, 80, 40, 20, 10, 5, 2.5, 1.25, 0.65, 0.325, 0.162, 0.081 μM) for five days.

# 3 Discussion

CP is a widely used chemotherapeutic agent that can affect many types of cancer (173). However, two factors hinder its use: its side effects, and resistance development. Various approaches are available to overcome chemotherapy resistance and maximize the clinical benefit of cytotoxic agents, such as CP (174).

When resistance to CP develops, its therapeutic index will narrow, thereby reducing its clinical value(175). CP's principal mechanism of inducing cytotoxicity is by interfering with DNA replication. However, CP can destroy cancer cells through other mechanisms as well. Exploiting these parallel mechanisms might improve CP's cytotoxicity and widen its therapeutic index.

Interactions between CP and cellular components, such as microsomal CYP2E1, might be the basis for an increase in cellular ROS formation (176). ROS maintains a number of cellular functions, but also has a role in the development of oxidative stress, which may have adverse consequences (177). Microsomal CYP2E1 enzyme has been reported to play a role in two of CP's significant dose-dependent side effects: nephrotoxicity and hepatotoxicity (88, 178). The destruction of hepatocytes and nephrocytes is linked to an increase in ROS generation upon CP interacting with CYP2E1 (82). Microsomal CYP2E1 is predominantly expressed in hepatocytes, but has also been found in extrahepatic cells (179). CYP2E1's metabolic activity is clearly important for xenobiotic biotransformation, but its extrahepatic biological effects have not been fully established.

Increased *CYP2E1* mRNA expression has been reported in extrahepatic cancer tissue, as has increased CYP2E1 activity in some other diseases, such as diabetes (180, 181). However, the link to cancer development may involve an increase in ROS levels that induces oxidative stress. CYP2E1 is the most active ROS generator among CYP450 isoforms; in turn, ROS may have adverse cellular effects in both cancerous and noncancerous hepatic and extrahepatic cells (182). Therefore, excessive ROS generation in cancer cells resistant to CP might sensitize these cells. A principal objective of this work was to determine the role of microsomal CYP2E1 in generating ROS upon CP treatment. Specifically, we evaluated whether hepatic and extrahepatic cancer cells that are resistant to CP can be sensitized through microsomal CYP2E1 overexpression and ROS generation.

Two extrahepatic lines—A2780/R and MOR/R—and the hepatic cell line Hep G2 were transfected with microsomal *CYP2E1*. The qPCR results showed a significant increase in *CYP2E1* mRNA in all transfected cells, relative to the corresponding controls. A Western blot test did not confirm protein formation in the transfected extrahepatic cell lines, but in the Hep G2 transfected with *CYP2E1*, the cells showed a possible increase. Evidence of metabolic activity attributed to *CYP2E1*-transfected cells was the most important aspect of this study. This evidence was found using an in vitro metabolic model, with CHZ used as the index substrate to reflect CYP2E1 metabolic activity. We detected no 6-OH-CHZ formation from CHZ in either for the A2780 and A2780/R lines (stably transfected with *CYP2E1*) or the

MOR/R lines (transiently transfected with *CYP2E1*); however, 6-OH-CHZ was formed from CHZ in the Hep G2 cells transiently transfected with *CYP2E1*. This suggests a possible deficiency in the extrahepatic cells' CYP2E1 electron transport system, and/or a possible proteolytic system within the cells that inactivates newly formed CYP2E1 (183).

To determine *CYP2E1* transfection's phenotypic effect on CP cytotoxicity in Hep G2 cells, it was necessary to exclude CP's direct inhibitory effect on microsomal CYP2E1 activity. Therefore, we tested human liver microsomal preparations from four human liver samples to determine the rate of 6-OH-CHZ formation from CHZ due to exposure to 50 μM CP. This CP concentration is higher than clinically applicable but still did not significantly inhibit 6-0H-CHZ formation. We also established that DDC, a CYP2E1 inhibitor, did not affect Hep G2 cells' viability by itself at concentrations less than 50 μM. Finally, we verified that DDC acted as a time-dependent (mechanism-based or irreversible) CYP2E1 inhibitor.

To evaluate the effect of *CYP2E1* transfection when CP induces ROS in Hep G2 cells, we used FACS flow cytometry to measure the fluorescence generated upon ROS interacting with DFCL. When transiently transfected with *CYP2E1*, CP-exposed Hep G2 cells showed increased ROS fluorescence values relative to those of the controls. This suggested that, upon CP treatment, CYP2E1 transformation leads to ROS generation.

Finally, we tested whether Hep G2 cells, when transiently transfected with microsomal *CYP2E1* cDNA, became more sensitive to CP toxicity, based

on the MTT assay methodology. Exposing the *CYP2E1*-transfected and control Hep G2 cells to CP concentrations as high as 80 μM resulted in no evidence of altered CP sensitivity. The explanation for this is not established. There could be a compensatory upregulation of other antioxidant systems, such as those involving glutathione (GSH) or thioredoxin (Trx), which regulate intracellular ROS levels. Cancer cells may also be adapted to survive at high ROS levels, use less TrxR, and upregulate other antioxidant systems in the GSH system. Another possible mechanism is a metabolic shift in which the cell transfected with *CYP2E1* develops or increases its dependence on the anaerobic utilization of glycolysis and, as a consequence, increases the antioxidant system via NADPH.

Our findings support what has been reported in the literature, as the CYP2E1 biotransformation process yielded ROS. However, the MTT assay used in our study revealed no evidence of ROS affecting CP sensitivity when the cells were exposed to different CP concentrations for 5 days. This contradicts some studies suggesting CYP2E1 as a contributor to CP sensitivity. Some specific features of our studies may explain the differences. First, we used transient transfection for Hep G2; this suggests a possible reduction in ROS generation upon CP treatment, as compared to Cederbaum's study (88), which used a stably transfected cell line. Second, in our study's MTT protocol, the Hep G2 cells were exposed to different concentrations of CP ranging from 0–80 μM for 5 days. The concentrations of CP were based on our dose-response studies, which aimed to determine CP's $IC_{50}$, in the context of clinical

plasma concentrations. In Cederbaum's study, the MTT assay concentrations used were between 250 and 500 μM for 24 hours. This suggests that the incubation time might have impacted the results, as it has been reported that longer CP exposure yields different toxicity patterns (184). It may be that 5 days of exposure to CP allowed sufficient time for the cells to overcome any potential harmful effects of the generated ROS. Moreover, the high CP doses (250–500 μM) used in Cederbaum's study might have generated sufficient ROS to damage cells.

The literature also indicates that CP's nephrotoxic effect is reversed when a CYP2E1 inhibitor is used. Given that CYP2E1 is involved in nephrotoxicity, we might expect a greater incidence of hepatotoxicity than of nephrotoxicity during clinical CP use because liver cells contain more CYP2E1 than extrahepatic cells. However, clinical and laboratory studies have suggested the opposite(185). If CYP2E1 was a significant factor in cell damage upon CP exposure, hepatocytes might have greater capacity than other cell types to overcome CYP2E1's harmful effects.

Lastly, our data do not confirm what Cederbaum's study suggested regarding the effect of mitochondrial CYP2E1 in sensitizing Hep G2 cells. Much evidence in the literature indicates that mitochondrial targets have important roles in CP's toxic effect on cells; for example, CP toxicity is associated with cellular mitochondrial density(186). This might explain how mitochondrial *CYP2E1* transfection into Hep G2 cells produced sensitization even without biotransformation activity.

Finally, some studies have shown increased CYP2E1 activity in some conditions like diabetes (180, 187), which might suggest that nephrotoxicity is expected to increase upon treatment with CP; however, animal studies have reported that diabetes has a protective role against CP nephrotoxicity (188). This might imply that CYP2E1's potential effects on CP might be modified by other conditions and factors. In any case, our CP dose-response curve study on Hep G2 cells transfected with *CYP2E1* did not validate a link between CYP2E1 expression activity and altered sensitivity to CP exposure.

# 4 Conclusions and Questions for future studies

## 4.1 Conclusions

- The extrahepatic cell lines (A2780/MOR) lack the cellular machinery needed to produce detectable, metabolically active microsomal CYP2E1, with or without transfection.
- Augmented CYP2E1 metabolic activity and ROS activity following *CYP2E1* transfection did not alter CP sensitivity in Hep G2 cells.
- A role for CYP2E1 in CP sensitivity or resistance was not verified based on CP exposure response studies.

## 4.2 Questions for future studies

- CYP2E1-transfected Hep G2 cells did show phenotypic changes evident as increased CYP2E1 metabolic activity and increased ROS production. However, there was no change in sensitivity to CP toxicity. Studies are needed to elucidate the mechanism of this noncongruence. These studies could focus on adaptive processes that are recruited by CYP2E1-transfected Hep G2 cells to overcome the consequences of ROS generation.
- The studies evaluating the role of Cyt-b5 and oxidoreductase in A2780 and MOR cells' metabolic activity were not conclusive. These factors need more extensive evaluation in controlled systems, since they may contribute to the lack of enhanced CYP2E1 activity despite large increases in mRNA. Also to be evaluated is the possible role of proteolytic systems that would degrade newly-formed CYP2E1 enzyme.
- Ethanol is known to be an inducer of CYP2E1 expression and activity in human cellular systems. Further studies could be aimed at applying this property of ethanol as a chemical approach to enhancing expression/activity in hepatic and extrahepatic cells, and the possible consequences in terms of cell viability and CP sensitivity.

## References


1. Yancik R. Ovarian cancer. Age contrasts in incidence, histology, disease stage at diagnosis, and mortality. Cancer. 1993;71(2 Suppl):517-23. PubMed PMID: 8420671.
2. Lortet-Tieulent J, Soerjomataram I, Ferlay J, Rutherford M, Weiderpass E, Bray F. International trends in lung cancer incidence by histological subtype: adenocarcinoma stabilizing in men but still increasing in women. Lung cancer. 2014;84(1):13-22. doi: 10.1016/j.lungcan.2014.01.009. PubMed PMID: 24524818.
3. Chiriac CF. [The incidence of adenocarcinoma among lung cancers is increasing]. Pneumologia. 2003;52(3-4):177-80. PubMed PMID: 18210729.
4. Yu MW, Gladek-Yarborough A, Chiamprasert S, Santella RM, Liaw YF, Chen CJ. Cytochrome P450 2E1 and glutathione S-transferase M1 polymorphisms and susceptibility to hepatocellular carcinoma. Gastroenterology. 1995;109(4):1266-73. PubMed PMID: 7557094.
5. Sanyal AJ, Yoon SK, Lencioni R. The etiology of hepatocellular carcinoma and consequences for treatment. Oncologist. 2010;15 Suppl 4:14-22. doi: 10.1634/theoncologist.2010-S4-14. PubMed PMID: 21115577.
6. Yin Y, Tainsky MA, Bischoff FZ, Strong LC, Wahl GM. Wild-type p53 restores cell cycle control and inhibits gene amplification in cells with mutant p53 alleles. Cell. 1992;70(6):937-48. PubMed PMID: 1525830.
7. Hibi K, Trink B, Patturajan M, Westra WH, Caballero OL, Hill DE, Ratovitski EA, Jen J, Sidransky D. AIS is an oncogene amplified in squamous cell carcinoma. Proc Natl Acad Sci U S A. 2000;97(10):5462-7. Epub 2000/05/11. doi: 97/10/5462 [pii]. PubMed PMID: 10805802; PMCID: 25851.
8. Torre LA, Bray F, Siegel RL, Ferlay J, Lortet-Tieulent J, Jemal A. Global cancer statistics, 2012. CA Cancer J Clin. 2015;65(2):87-108. doi: 10.3322/caac.21262. PubMed PMID: 25651787.
9. A.C.S. Cancer facts and figures: American Cancer Society 2009. Available from: http://www.cancer.org/downloads/STT/500809web.pdf.
10. Performance of general hospitals in delivering adjuvant chemotherapy to breast cancer patients. G.I.V.I.O. (Interdisciplinary Group for Cancer Care Evaluation), Italy. Tumori. 1988;74(4):377-86. PubMed PMID: 3055576.
11. Cotter TG, Glynn JM, Echeverri F, Green DR. The induction of apoptosis by chemotherapeutic agents occurs in all phases of the cell cycle. Anticancer research. 1992;12(3):773-9. PubMed PMID: 1622137.
12. Thorsteinsson M, Soletormos G, Jess P. Low number of detectable circulating tumor cells in non-metastatic colon cancer. Anticancer research. 2011;31(2):613-7. PubMed PMID: 21378346.
13. Brown PO, Palmer C. The preclinical natural history of serous ovarian cancer: defining the target for early detection. PLoS Med. 2009;6(7):e1000114. doi: 10.1371/journal.pmed.1000114. PubMed PMID: 19636370; PMCID: 2711307.

14. Gottesman MM, Fojo T, Bates SE. Multidrug resistance in cancer: role of ATP-dependent transporters. Nat Rev Cancer. 2002;2(1):48-58. doi: 10.1038/nrc706. PubMed PMID: 11902585.
15. Bozic I, Reiter JG, Allen B, Antal T, Chatterjee K, Shah P, Moon YS, Yaqubie A, Kelly N, Le DT, Lipson EJ, Chapman PB, Diaz LA, Jr., Vogelstein B, Nowak MA. Evolutionary dynamics of cancer in response to targeted combination therapy. Elife. 2013;2:e00747. doi: 10.7554/eLife.00747. PubMed PMID: 23805382; PMCID: 3691570.
16. Marin JJ, Romero MR, Blazquez AG, Herraez E, Keck E, Briz O. Importance and limitations of chemotherapy among the available treatments for gastrointestinal tumours. Anticancer Agents Med Chem. 2009;9(2):162-84. PubMed PMID: 19199863.
17. Krohner KM, Spitak AF. Cancer nursing education in the community hospital: principles and practice. Oncol Nurs Forum. 1992;19(5):783-6. PubMed PMID: 1608842.
18. DiMasi JA, Grabowski HG. Economics of new oncology drug development. J Clin Oncol. 2007;25(2):209-16. doi: 10.1200/JCO.2006.09.0803. PubMed PMID: 17210942.
19. Siddiqui M, Rajkumar SV. The high cost of cancer drugs and what we can do about it. Mayo Clin Proc. 2012;87(10):935-43. doi: 10.1016/j.mayocp.2012.07.007. PubMed PMID: 23036669; PMCID: 3538397.
20. Martoni A, Cacciari N, Angelelli B, Zamagni C, Pannuti F. Chemotherapy of advanced ovarian cancer. Front Biosci. 1997;2:g20-6. PubMed PMID: 9159262.
21. Gore ME, Fryatt I, Wiltshaw E, Dawson T, Robinson BA, Calvert AH. Cisplatin/carboplatin cross-resistance in ovarian cancer. Br J Cancer. 1989;60(5):767-9. PubMed PMID: 2803953; PMCID: 2247292.
22. Eustace P. History and development of cisplatin in the management of malignant disease. Cancer nursing. 1980;3(5):373-8. Epub 1980/10/01. PubMed PMID: 6902674.
23. Andersson A, Fagerberg J, Lewensohn R, Ehrsson H. Pharmacokinetics of cisplatin and its monohydrated complex in humans. J Pharm Sci. 1996;85(8):824-7. doi: 10.1021/js960037a. PubMed PMID: 8863271.
24. Kidani Y. [Development of antitumor platinum complexes]. Gan To Kagaku Ryoho. 1983;10(12):2442-52. PubMed PMID: 6360050.
25. Check W. How do things stand with cisplatin? JAMA. 1978;240(23):2521-5. PubMed PMID: 712945.
26. Eastman A. The formation, isolation and characterization of DNA adducts produced by anticancer platinum complexes. Pharmacol Ther. 1987;34(2):155-66. PubMed PMID: 3317449.
27. Baik MH, Friesner RA, Lippard SJ. Theoretical study of cisplatin binding to purine bases: why does cisplatin prefer guanine over adenine? J Am Chem Soc. 2003;125(46):14082-92. doi: 10.1021/ja036960d. PubMed PMID: 14611245.

28. Huang JC, Zamble DB, Reardon JT, Lippard SJ, Sancar A. HMG-domain proteins specifically inhibit the repair of the major DNA adduct of the anticancer drug cisplatin by human excision nuclease. Proc Natl Acad Sci U S A. 1994;91(22):10394-8. Epub 1994/10/25. PubMed PMID: 7937961; PMCID: 45026.
29. Park S, Yoon SP, Kim J. Cisplatin induces primary necrosis through poly(ADP-ribose) polymerase 1 activation in kidney proximal tubular cells. Anat Cell Biol. 2015;48(1):66-74. doi: 10.5115/acb.2015.48.1.66. PubMed PMID: 25806124; PMCID: 4371183.
30. Ames BN. Dietary carcinogens and anticarcinogens. Oxygen radicals and degenerative diseases. Science. 1983;221(4617):1256-64. Epub 1983/09/23. PubMed PMID: 6351251.
31. Fruehauf JP, Meyskens FL, Jr. Reactive oxygen species: a breath of life or death? Clin Cancer Res. 2007;13(3):789-94. Epub 2007/02/10. doi: 10.1158/1078-0432.CCR-06-2082. PubMed PMID: 17289868.
32. Berndtsson M, Hagg M, Panaretakis T, Havelka AM, Shoshan MC, Linder S. Acute apoptosis by cisplatin requires induction of reactive oxygen species but is not associated with damage to nuclear DNA. Int J Cancer. 2007;120(1):175-80. Epub 2006/10/18. doi: 10.1002/ijc.22132. PubMed PMID: 17044026.
33. Todd RC, Lovejoy KS, Lippard SJ. Understanding the effect of carbonate ion on cisplatin binding to DNA. J Am Chem Soc. 2007;129(20):6370-1. doi: 10.1021/ja071143p. PubMed PMID: 17465550; PMCID: 2494524.
34. Narins RG, Carley M, Bloom EJ, Harrison DS. The nephrotoxicity of chemotherapeutic agents. Semin Nephrol. 1990;10(6):556-64. Epub 1990/11/01. PubMed PMID: 2255813.
35. Chen JT, Tatsuki Y, Hirai Y, Hasumi K. [Increase in CDDP therapeutic index by lower concentration and longer infusion time--home chemotherapy for ovarian cancer]. Gan To Kagaku Ryoho. 1993;20(2):265-70. PubMed PMID: 8434965.
36. Hung A, Crane C, Delclos M, Ballo M, Ajani J, Lin E, Feig B, Skibber J, Janjan N. Cisplatin-based combined modality therapy for anal carcinoma: a wider therapeutic index. Cancer. 2003;97(5):1195-202. doi: 10.1002/cncr.11161. PubMed PMID: 12599225.
37. Vuong T, Kopek N, Ducruet T, Portelance L, Faria S, Bahoric B, Devic S. Conformal therapy improves the therapeutic index of patients with anal canal cancer treated with combined chemotherapy and external beam radiotherapy. Int J Radiat Oncol Biol Phys. 2007;67(5):1394-400. doi: 10.1016/j.ijrobp.2006.11.038. PubMed PMID: 17276620.
38. Tyagi AK, Agarwal C, Chan DC, Agarwal R. Synergistic anti-cancer effects of silibinin with conventional cytotoxic agents doxorubicin, cisplatin and carboplatin against human breast carcinoma MCF-7 and MDA-MB468 cells. Oncol Rep. 2004;11(2):493-9. PubMed PMID: 14719089.

39. Kitazono-Saitoh M, Takiguchi Y, Kitazono S, Ashinuma H, Kitamura A, Tada Y, Kurosu K, Sakaida E, Sekine I, Tanabe N, Tagawa M, Tatsumi K. Interaction and cross-resistance of cisplatin and pemetrexed in malignant pleural mesothelioma cell lines. Oncol Rep. 2012;28(1):33-40. doi: 10.3892/or.2012.1799. PubMed PMID: 22562354.
40. Dimanche-Boitrel MT, Garrido C, Chauffert B. Kinetic resistance to anticancer agents. Cytotechnology. 1993;12(1-3):347-56. PubMed PMID: 7764456.
41. Durand RE, Vanderbyl SL. Tumor resistance to therapy: a genetic or kinetic problem? Cancer Commun. 1989;1(5):277-83. PubMed PMID: 2702035.
42. Goldie JH, Coldman AJ. A mathematic model for relating the drug sensitivity of tumors to their spontaneous mutation rate. Cancer Treat Rep. 1979;63(11-12):1727-33. PubMed PMID: 526911.
43. Stewart DJ. Mechanisms of resistance to cisplatin and carboplatin. Crit Rev Oncol Hematol. 2007;63(1):12-31. Epub 2007/03/06. doi: 10.1016/j.critrevonc.2007.02.001. PubMed PMID: 17336087.
44. Brozovic A, Ambriovic-Ristov A, Osmak M. The relationship between cisplatin-induced reactive oxygen species, glutathione, and BCL-2 and resistance to cisplatin. Crit Rev Toxicol. 2010;40(4):347-59. Epub 2010/02/19. doi: 10.3109/10408441003601836. PubMed PMID: 20163198.
45. Godwin AK, Meister A, O'Dwyer PJ, Huang CS, Hamilton TC, Anderson ME. High resistance to cisplatin in human ovarian cancer cell lines is associated with marked increase of glutathione synthesis. Proc Natl Acad Sci U S A. 1992;89(7):3070-4. Epub 1992/04/01. PubMed PMID: 1348364; PMCID: 48805.
46. Koppenol WH, Bounds PL, Dang CV. Otto Warburg's contributions to current concepts of cancer metabolism. Nat Rev Cancer. 2011;11(5):325-37. doi: 10.1038/nrc3038. PubMed PMID: 21508971.
47. Wallace DC. Mitochondria and cancer: Warburg addressed. Cold Spring Harb Symp Quant Biol. 2005;70:363-74. doi: 10.1101/sqb.2005.70.035. PubMed PMID: 16869773.
48. Anastasiou D, Poulogiannis G, Asara JM, Boxer MB, Jiang JK, Shen M, Bellinger G, Sasaki AT, Locasale JW, Auld DS, Thomas CJ, Vander Heiden MG, Cantley LC. Inhibition of pyruvate kinase M2 by reactive oxygen species contributes to cellular antioxidant responses. Science. 2011;334(6060):1278-83. doi: 10.1126/science.1211485. PubMed PMID: 22052977; PMCID: 3471535.
49. Droge W. Free radicals in the physiological control of cell function. Physiol Rev. 2002;82(1):47-95. doi: 10.1152/physrev.00018.2001. PubMed PMID: 11773609.
50. Commoner B, Townsend J, Pake GE. Free radicals in biological materials. Nature. 1954;174(4432):689-91. PubMed PMID: 13213980.
51. Mittal CK, Murad F. Activation of guanylate cyclase by superoxide dismutase and hydroxyl radical: a physiological regulator of guanosine 3',5'-

monophosphate formation. Proc Natl Acad Sci U S A. 1977;74(10):4360-4. PubMed PMID: 22077; PMCID: 431941.
52. Kehrer JP. The Haber-Weiss reaction and mechanisms of toxicity. Toxicology. 2000;149(1):43-50. PubMed PMID: 10963860.
53. Kohlstadt I. Scientific evidence for musculoskeletal, bariatric, and sports nutrition. Boca Raton: CRC/Taylor & Francis; 2006. xx, 621 p. p.
54. Schwab M. Encyclopedia of cancer. 3rd ed. Heidelberg ; New York: Springer; 2011.
55. Kosower NS, Kosower EM. The glutathione status of cells. Int Rev Cytol. 1978;54:109-60. Epub 1978/01/01. PubMed PMID: 42630.
56. Hayes JD, Pulford DJ. The glutathione S-transferase supergene family: regulation of GST and the contribution of the isoenzymes to cancer chemoprotection and drug resistance. Crit Rev Biochem Mol Biol. 1995;30(6):445-600. Epub 1995/01/01. doi: 10.3109/10409239509083491. PubMed PMID: 8770536.
57. Dickinson DA, Forman HJ. Cellular glutathione and thiols metabolism. Biochem Pharmacol. 2002;64(5-6):1019-26. Epub 2002/09/06. PubMed PMID: 12213601.
58. Awasthi YC. Toxicology of glutathione transferases. Boca Raton, Fla. ; London: Taylor & Francis; 2006. 375 p., [8] p. of plates p.
59. Beckett GJ, Hayes JD. Glutathione S-transferases: biomedical applications. Advances in clinical chemistry. 1993;30:281-380. Epub 1993/01/01. PubMed PMID: 8237562.
60. Saydam N, Kirb A, Demir O, Hazan E, Oto O, Saydam O, Guner G. Determination of glutathione, glutathione reductase, glutathione peroxidase and glutathione S-transferase levels in human lung cancer tissues. Cancer Lett. 1997;119(1):13-9. Epub 2008/04/01. PubMed PMID: 18372516.
61. Tanaka T, Yokomizo A, Uchiumi T, Furukawa M, Wada M, Kuwano M. The close association of pi-class glutathione S-transferase with drug sensitivity to alkylating agents and cisplatin in human cancer cells. Int J Oncol. 1997;10(5):1009-14. Epub 1997/05/01. PubMed PMID: 21533477.
62. Townsend DM, Tew KD. The role of glutathione-S-transferase in anti-cancer drug resistance. Oncogene. 2003;22(47):7369-75. Epub 2003/10/25. doi: 10.1038/sj.onc.1206940. PubMed PMID: 14576844.
63. Galli F, Piroddi M, Annetti C, Aisa C, Floridi E, Floridi A. Oxidative stress and reactive oxygen species. Contrib Nephrol. 2005;149:240-60. doi: 10.1159/000085686. PubMed PMID: 15876848.
64. Gordon N. Apoptosis (programmed cell death) and other reasons for elimination of neurons and axons. Brain Dev. 1995;17(1):73-7. PubMed PMID: 7762769.
65. Zakeri Z, Bursch W, Tenniswood M, Lockshin RA. Cell death: programmed, apoptosis, necrosis, or other? Cell Death Differ. 1995;2(2):87-96. PubMed PMID: 17180070.

66. Muppidi J, Porter M, Siegel RM. Measurement of apoptosis and other forms of cell death. Curr Protoc Immunol. 2004;Chapter 3:Unit 3 17. doi: 10.1002/0471142735.im0317s59. PubMed PMID: 18432928.
67. Lee RM, Choi H, Shin JS, Kim K, Yoo KH. Distinguishing between apoptosis and necrosis using a capacitance sensor. Biosens Bioelectron. 2009;24(8):2586-91. doi: 10.1016/j.bios.2009.01.028. PubMed PMID: 19233636.
68. Shindo R, Kakehashi H, Okumura K, Kumagai Y, Nakano H. Critical contribution of oxidative stress to TNFalpha-induced necroptosis downstream of RIPK1 activation. Biochem Biophys Res Commun. 2013;436(2):212-6. doi: 10.1016/j.bbrc.2013.05.075. PubMed PMID: 23727581.
69. Choi K, Kim J, Kim GW, Choi C. Oxidative stress-induced necrotic cell death via mitochondira-dependent burst of reactive oxygen species. Curr Neurovasc Res. 2009;6(4):213-22. PubMed PMID: 19807658.
70. Kannan K, Jain SK. Oxidative stress and apoptosis. Pathophysiology. 2000;7(3):153-63. PubMed PMID: 10996508.
71. Lin X, Zheng W, Liu J, Zhang Y, Qin H, Wu H, Xue B, Lu Y, Shen P. Oxidative stress in malignant melanoma enhances tumor necrosis factor-alpha secretion of tumor-associated macrophages that promote cancer cell invasion. Antioxid Redox Signal. 2013;19(12):1337-55. doi: 10.1089/ars.2012.4617. PubMed PMID: 23373752.
72. Masuda H, Tanaka T, Takahama U. Cisplatin generates superoxide anion by interaction with DNA in a cell-free system. Biochem Biophys Res Commun. 1994;203(2):1175-80. doi: 10.1006/bbrc.1994.2306. PubMed PMID: 8093036.
73. Choie DD, Longnecker DS, del Campo AA. Acute and chronic cisplatin nephropathy in rats. Laboratory investigation; a journal of technical methods and pathology. 1981;44(5):397-402. Epub 1981/05/01. PubMed PMID: 7194946.
74. Meijer S, Sleijfer DT, Mulder NH, Donker AJ. Cisplatin-induced nephrotoxicity. Neth J Med. 1982;25(8):262-9. Epub 1982/01/01. PubMed PMID: 6755283.
75. Goldstein RS, Mayor GH. Minireview. The nephrotoxicity of cisplatin. Life Sci. 1983;32(7):685-90. Epub 1983/02/14. PubMed PMID: 6338333.
76. Safirstein R, Winston J, Goldstein M, Moel D, Dikman S, Guttenplan J. Cisplatin nephrotoxicity. Am J Kidney Dis. 1986;8(5):356-67. Epub 1986/11/01. PubMed PMID: 3538859.
77. Safirstein R, Wiston J. Cisplatin nephrotoxicity. J Uoeh. 1987;9 Suppl:216-22. Epub 1987/03/20. PubMed PMID: 3299604.
78. Daugaard G, Abildgaard U. Cisplatin nephrotoxicity. A review. Cancer Chemother Pharmacol. 1989;25(1):1-9. Epub 1989/01/01. PubMed PMID: 2686850.
79. Fillastre JP, Raguenez-Viotte G. Cisplatin nephrotoxicity. Toxicol Lett. 1989;46(1-3):163-75. Epub 1989/03/01. PubMed PMID: 2650023.

80. Pabla N, Dong Z. Cisplatin nephrotoxicity: mechanisms and renoprotective strategies. Kidney Int. 2008;73(9):994-1007. Epub 2008/02/15. doi: 10.1038/sj.ki.5002786. PubMed PMID: 18272962.
81. Daugaard G. Cisplatin nephrotoxicity: experimental and clinical studies. Dan Med Bull. 1990;37(1):1-12. Epub 1990/02/01. PubMed PMID: 2178884.
82. Weiner MW, Jacobs C. Mechanism of cisplatin nephrotoxicity. Fed Proc. 1983;42(13):2974-8. Epub 1983/10/01. PubMed PMID: 6684595.
83. Bompart G. Cisplatin-induced changes in cytochrome P-450, lipid peroxidation and drug-metabolizing enzyme activities in rat kidney cortex. Toxicol Lett. 1989;48(2):193-9. Epub 1989/08/01. PubMed PMID: 2772925.
84. Townsend DM, Tew KD, He L, King JB, Hanigan MH. Role of glutathione S-transferase Pi in cisplatin-induced nephrotoxicity. Biomed Pharmacother. 2009;63(2):79-85. Epub 2008/09/30. doi: 10.1016/j.biopha.2008.08.004. PubMed PMID: 18819770; PMCID: 2667699.
85. Townsend DM, Hanigan MH. Inhibition of gamma-glutamyl transpeptidase or cysteine S-conjugate beta-lyase activity blocks the nephrotoxicity of cisplatin in mice. J Pharmacol Exp Ther. 2002;300(1):142-8. Epub 2001/12/26. PubMed PMID: 11752109.
86. Liu H, Baliga R. Cytochrome P450 2E1 null mice provide novel protection against cisplatin-induced nephrotoxicity and apoptosis. Kidney Int. 2003;63(5):1687-96. doi: 10.1046/j.1523-1755.2003.00908.x. PubMed PMID: 12675844.
87. Domitrovic R, Cvijanovic O, Pernjak-Pugel E, Skoda M, Mikelic L, Crncevic-Orlic Z. Berberine exerts nephroprotective effect against cisplatin-induced kidney damage through inhibition of oxidative/nitrosative stress, inflammation, autophagy and apoptosis. Food Chem Toxicol. 2013;62:397-406. doi: 10.1016/j.fct.2013.09.003. PubMed PMID: 24025684.
88. Lu Y, Cederbaum AI. Cisplatin-induced hepatotoxicity is enhanced by elevated expression of cytochrome P450 2E1. Toxicol Sci. 2006;89(2):515-23. doi: 10.1093/toxsci/kfj031. PubMed PMID: 16251482.
89. Hassan I, Chibber S, Naseem I. Ameliorative effect of riboflavin on the cisplatin induced nephrotoxicity and hepatotoxicity under photoillumination. Food Chem Toxicol. 2010;48(8-9):2052-8. doi: 10.1016/j.fct.2010.05.004. PubMed PMID: 20457210.
90. Berndtsson M, Hagg M, Panaretakis T, Havelka AM, Shoshan MC, Linder S. Acute apoptosis by cisplatin requires induction of reactive oxygen species but is not associated with damage to nuclear DNA. Int J Cancer. 2007;120(1):175-80. doi: 10.1002/ijc.22132. PubMed PMID: 17044026.
91. Danielson PB. The cytochrome P450 superfamily: biochemistry, evolution and drug metabolism in humans. Curr Drug Metab. 2002;3(6):561-97. PubMed PMID: 12369887.
92. Lynch T, Price A. The effect of cytochrome P450 metabolism on drug response, interactions, and adverse effects. Am Fam Physician. 2007;76(3):391-6. PubMed PMID: 17708140.

93. Bernhardt R. Cytochrome P450: structure, function, and generation of reactive oxygen species. Rev Physiol Biochem Pharmacol. 1996;127:137-221. PubMed PMID: 8533008.
94. Guengerich FP. Cytochrome p450 and chemical toxicology. Chem Res Toxicol. 2008;21(1):70-83. doi: 10.1021/tx700079z. PubMed PMID: 18052394.
95. Nelson DR, Kamataki T, Waxman DJ, Guengerich FP, Estabrook RW, Feyereisen R, Gonzalez FJ, Coon MJ, Gunsalus IC, Gotoh O, et al. The P450 superfamily: update on new sequences, gene mapping, accession numbers, early trivial names of enzymes, and nomenclature. DNA Cell Biol. 1993;12(1):1-51. PubMed PMID: 7678494.
96. Nelson DR, Koymans L, Kamataki T, Stegeman JJ, Feyereisen R, Waxman DJ, Waterman MR, Gotoh O, Coon MJ, Estabrook RW, Gunsalus IC, Nebert DW. P450 superfamily: update on new sequences, gene mapping, accession numbers and nomenclature. Pharmacogenetics. 1996;6(1):1-42. PubMed PMID: 8845856.
97. Hata M, Hirano Y, Hoshino T, Tsuda M. Monooxygenation mechanism by cytochrome p-450. J Am Chem Soc. 2001;123(26):6410-6. PubMed PMID: 11427068.
98. Williams PA, Cosme J, Sridhar V, Johnson EF, McRee DE. Mammalian microsomal cytochrome P450 monooxygenase: structural adaptations for membrane binding and functional diversity. Mol Cell. 2000;5(1):121-31. PubMed PMID: 10678174.
99. Omura T, Ito A. Biosynthesis and intracellular sorting of mitochondrial forms of cytochrome P450. Methods Enzymol. 1991;206:75-81. PubMed PMID: 1784250.
100. White SH, Ladokhin AS, Jayasinghe S, Hristova K. How membranes shape protein structure. J Biol Chem. 2001;276(35):32395-8. doi: 10.1074/jbc.R100008200. PubMed PMID: 11432876.
101. Andersen OS, Koeppe RE, 2nd. Bilayer thickness and membrane protein function: an energetic perspective. Annu Rev Biophys Biomol Struct. 2007;36:107-30. doi: 10.1146/annurev.biophys.36.040306.132643. PubMed PMID: 17263662.
102. Berka K, Hendrychova T, Anzenbacher P, Otyepka M. Membrane position of ibuprofen agrees with suggested access path entrance to cytochrome P450 2C9 active site. J Phys Chem A. 2011;115(41):11248-55. doi: 10.1021/jp204488j. PubMed PMID: 21744854; PMCID: 3257864.
103. Hannemann F, Bichet A, Ewen KM, Bernhardt R. Cytochrome P450 systems--biological variations of electron transport chains. Biochim Biophys Acta. 2007;1770(3):330-44. doi: 10.1016/j.bbagen.2006.07.017. PubMed PMID: 16978787.
104. Grinberg AV, Hannemann F, Schiffler B, Muller J, Heinemann U, Bernhardt R. Adrenodoxin: structure, stability, and electron transfer properties. Proteins. 2000;40(4):590-612. PubMed PMID: 10899784.

105. Ewen KM, Ringle M, Bernhardt R. Adrenodoxin--a versatile ferredoxin. IUBMB Life. 2012;64(6):506-12. doi: 10.1002/iub.1029. PubMed PMID: 22556163.
106. Dong MS, Yamazaki H, Guo Z, Guengerich FP. Recombinant human cytochrome P450 1A2 and an N-terminal-truncated form: construction, purification, aggregation properties, and interactions with flavodoxin, ferredoxin, and NADPH-cytochrome P450 reductase. Arch Biochem Biophys. 1996;327(1):11-9. doi: 10.1006/abbi.1996.0086. PubMed PMID: 8615680.
107. Hubbard PA, Shen AL, Paschke R, Kasper CB, Kim JJ. NADPH-cytochrome P450 oxidoreductase. Structural basis for hydride and electron transfer. J Biol Chem. 2001;276(31):29163-70. doi: 10.1074/jbc.M101731200. PubMed PMID: 11371558.
108. Iyanagi T, Xia C, Kim JJ. NADPH-cytochrome P450 oxidoreductase: prototypic member of the diflavin reductase family. Arch Biochem Biophys. 2012;528(1):72-89. doi: 10.1016/j.abb.2012.09.002. PubMed PMID: 22982532; PMCID: 3606592.
109. Rao NA, Felton SP, Huennekens FM, Mackler B. Flavin mononucleotide: the coenzyme of reduced diphosphopyridine nucleotide dehydrogenase. J Biol Chem. 1963;238:449-55. PubMed PMID: 13973054.
110. Gruenke LD, Konopka K, Cadieu M, Waskell L. The stoichiometry of the cytochrome P-450-catalyzed metabolism of methoxyflurane and benzphetamine in the presence and absence of cytochrome b5. J Biol Chem. 1995;270(42):24707-18. PubMed PMID: 7559586.
111. Schenkman JB, Jansson I. The many roles of cytochrome b5. Pharmacol Ther. 2003;97(2):139-52. PubMed PMID: 12559387.
112. Kim SK, Park HJ, Seok H, Jeon HS, Lee TW, Lee SH, Moon JY, Ihm CG, Kim TH, Kim YH, Kang SW, Park SJ, Jeong KH, Chung JH. Association studies of cytochrome P450, family 2, subfamily E, polypeptide 1 (CYP2E1) gene polymorphisms with acute rejection in kidney transplantation recipients. Clin Transplant. 2014;28(6):707-12. doi: 10.1111/ctr.12369. PubMed PMID: 24654912.
113. Morimoto M, Hagbjork AL, Nanji AA, Ingelman-Sundberg M, Lindros KO, Fu PC, Albano E, French SW. Role of cytochrome P4502E1 in alcoholic liver disease pathogenesis. Alcohol. 1993;10(6):459-64. PubMed PMID: 8123200.
114. Cederbaum AI. CYP2E1--biochemical and toxicological aspects and role in alcohol-induced liver injury. Mt Sinai J Med. 2006;73(4):657-72. PubMed PMID: 16878272.
115. Koivisto T, Mishin VM, Mak KM, Cohen PA, Lieber CS. Induction of cytochrome P-4502E1 by ethanol in rat Kupffer cells. Alcohol Clin Exp Res. 1996;20(2):207-12. Epub 1996/04/01. PubMed PMID: 8730209.
116. Shimizu M, Lasker JM, Tsutsumi M, Lieber CS. Immunohistochemical localization of ethanol-inducible P450IIE1 in the rat alimentary tract. Gastroenterology. 1990;99(4):1044-53. Epub 1990/10/01. PubMed PMID: 2203661.

117. Ioannides C. Cytochromes P450 : role in the metabolism and toxicity of drugs and other xenobiotics. Cambridge: RSC Pub.; 2008. xviii, 521 p. p.
118. Ferguson CS, Miksys S, Palmour RM, Tyndale RF. Ethanol self-administration and nicotine treatment induce brain levels of CYP2B6 and CYP2E1 in African green monkeys. Neuropharmacology. 2013;72:74-81. doi: 10.1016/j.neuropharm.2013.04.022. PubMed PMID: 23639433.
119. Carroccio A, Wu D, Cederbaum AI. Ethanol increases content and activity of human cytochrome P4502E1 in a transduced HepG2 cell line. Biochem Biophys Res Commun. 1994;203(1):727-33. Epub 1994/08/30. PubMed PMID: 8074729.
120. Kanno S, Matsukawa E, Miura A, Shouji A, Asou K, Ishikawa M. Diethyldithiocarbamate-induced cytotoxicity and apoptosis in leukemia cell lines. Biol Pharm Bull. 2003;26(7):964-8. PubMed PMID: 12843619.
121. Hadizadeh S, Najafzadeh N, Mazani M, Amani M, Mansouri-Torshizi H, Niapour A. Cytotoxic Effects of Newly Synthesized Palladium(II) Complexes of Diethyldithiocarbamate on Gastrointestinal Cancer Cell Lines. Biochem Res Int. 2014;2014:813457. doi: 10.1155/2014/813457. PubMed PMID: 25147738; PMCID: 4131412.
122. Yang MX, Cederbaum AI. Role of the proteasome complex in degradation of human CYP2E1 in transfected HepG2 cells. Biochem Biophys Res Commun. 1996;226(3):711-6. doi: 10.1006/bbrc.1996.1418. PubMed PMID: 8831679.
123. Yang MX, Cederbaum AI. Characterization of cytochrome P4502E1 turnover in transfected HepG2 cells expressing human CYP2E1. Arch Biochem Biophys. 1997;341(1):25-33. doi: 10.1006/abbi.1997.9907. PubMed PMID: 9143349.
124. Bardag-Gorce F, French BA, Nan L, Song H, Nguyen SK, Yong H, Dede J, French SW. CYP2E1 induced by ethanol causes oxidative stress, proteasome inhibition and cytokeratin aggresome (Mallory body-like) formation. Exp Mol Pathol. 2006;81(3):191-201. doi: 10.1016/j.yexmp.2006.07.007. PubMed PMID: 17034788.
125. Carroccio A, Wu D, Cederbaum AI. Ethanol increases content and activity of human cytochrome P4502E1 in a transduced HepG2 cell line. Biochem Biophys Res Commun. 1994;203(1):727-33. PubMed PMID: 8074729.
126. Rosenberg B, VanCamp L, Trosko JE, Mansour VH. Platinum compounds: a new class of potent antitumour agents. Nature. 1969;222(5191):385-6. PubMed PMID: 5782119.
127. Black DJ, Livingston RB. Antineoplastic drugs in 1990. A review (Part I). Drugs. 1990;39(4):489-501. PubMed PMID: 2190792.
128. Ando Y, Shimizu T, Nakamura K, Mushiroda T, Nakagawa T, Kodama T, Kamataki T. Potent and non-specific inhibition of cytochrome P450 by JM216, a new oral platinum agent. British journal of cancer. 1998;78(9):1170-4. PubMed PMID: 9820175; PMCID: 2062991.

129. Masek V, Starha P, Harvanova M, Michalova M, Milde D, Travnicek Z, Anzenbacherova E. Interaction of selected platinum(II) complexes containing roscovitine-based CDK inhibitors as ligands with human liver microsomal cytochrome P450. Biomedical papers of the Medical Faculty of the University Palacky, Olomouc, Czechoslovakia. 2014. doi: 10.5507/bp.2014.031. PubMed PMID: 25004912.
130. Masek V, Anzenbacherova E, Machova M, Brabec V, Anzenbacher P. Interaction of antitumor platinum complexes with human liver microsomal cytochromes P450. Anti-cancer drugs. 2009;20(5):305-11. PubMed PMID: 19378397.
131. Baliga R, Zhang Z, Baliga M, Ueda N, Shah SV. Role of cytochrome P-450 as a source of catalytic iron in cisplatin-induced nephrotoxicity. Kidney Int. 1998;54(5):1562-9. Epub 1998/12/09. doi: 10.1046/j.1523-1755.1998.00161.x. PubMed PMID: 9844132.
132. Liu H, Baliga M, Baliga R. Effect of cytochrome P450 2E1 inhibitors on cisplatin-induced cytotoxicity to renal proximal tubular epithelial cells. Anticancer Res. 2002;22(2A):863-8. Epub 2002/05/17. PubMed PMID: 12014663.
133. Liu H, Baliga R. Cytochrome P450 2E1 null mice provide novel protection against cisplatin-induced nephrotoxicity and apoptosis. Kidney Int. 2003;63(5):1687-96. Epub 2003/04/05. doi: 10.1046/j.1523-1755.2003.00908.x. PubMed PMID: 12675844.
134. Lu Y, Cederbaum AI. Cisplatin-induced hepatotoxicity is enhanced by elevated expression of cytochrome P450 2E1. Toxicol Sci. 2006;89(2):515-23. Epub 2005/10/28. doi: 10.1093/toxsci/kfj031. PubMed PMID: 16251482.
135. Lu Y, Cederbaum A. The mode of cisplatin-induced cell death in CYP2E1-overexpressing HepG2 cells: modulation by ERK, ROS, glutathione, and thioredoxin. Free Radic Biol Med. 2007;43(7):1061-75. doi: 10.1016/j.freeradbiomed.2007.06.021. PubMed PMID: 17761302; PMCID: 1995748.
136. Bai J, Cederbaum AI. Overexpression of CYP2E1 in mitochondria sensitizes HepG2 cells to the toxicity caused by depletion of glutathione. J Biol Chem. 2006;281(8):5128-36. Epub 2005/12/29. doi: 10.1074/jbc.M510484200. PubMed PMID: 16380384.
137. Yan QG, Shi JG, Zhang F, Zhao QT, Pang XW, Chen R, Hu PZ, Li QL, Wang Z, Huang GS. Overexpression of CYP2E1 enhances sensitivity of hepG2 cells to fas-mediated cytotoxicity. Cancer Biol Ther. 2008;7(8):1280-7. Epub 2008/05/24. PubMed PMID: 18497573.
138. Balusikova K, Kovar J. Alcohol dehydrogenase and cytochrome P450 2E1 can be induced by long-term exposure to ethanol in cultured liver HEP-G2 cells. In vitro cellular & developmental biology Animal. 2013;49(8):619-25. doi: 10.1007/s11626-013-9636-y. PubMed PMID: 23824954.
139. Jimenez-Lopez JM, Carrasco MP, Segovia JL, Marco C. Resistance of HepG2 cells against the adverse effects of ethanol related to neutral lipid and

phospholipid metabolism. Biochem Pharmacol. 2002;63(8):1485-90. PubMed PMID: 11996890.
140. Li J, Liu TH, You H, Xu YQ, Wang C. [Stimulation of human hepatic stellate cells by cytochrome P4502E1-mediated oxidative stress]. Zhonghua gan zang bing za zhi = Zhonghua ganzangbing zazhi = Chinese journal of hepatology. 2010;18(8):576-80. doi: 10.3760/cma.j.issn.1007-3418.2010.08.007. PubMed PMID: 20825710.
141. Armoni M, Harel C, Ramdas M, Karnieli E. CYP2E1 impairs GLUT4 gene expression and function: NRF2 as a possible mediator. Hormone and metabolic research = Hormon- und Stoffwechselforschung = Hormones et metabolisme. 2014;46(7):477-83. doi: 10.1055/s-0033-1363990. PubMed PMID: 24500986.
142. Barmada S, Kienle E, Koop DR. Rabbit P450 2E1 expressed in CHO-K1 cells has a short half-life. Biochem Biophys Res Commun. 1995;206(2):601-7. doi: 10.1006/bbrc.1995.1085. PubMed PMID: 7826377.
143. Zhang W, Lu D, Dong W, Zhang L, Zhang X, Quan X, Ma C, Lian H, Zhang L. Expression of CYP2E1 increases oxidative stress and induces apoptosis of cardiomyocytes in transgenic mice. The FEBS journal. 2011;278(9):1484-92. doi: 10.1111/j.1742-4658.2011.08063.x. PubMed PMID: 21352494.
144. Bai J, Cederbaum AI. Overexpression of CYP2E1 in mitochondria sensitizes HepG2 cells to the toxicity caused by depletion of glutathione. J Biol Chem. 2006;281(8):5128-36. doi: 10.1074/jbc.M510484200. PubMed PMID: 16380384.
145. Lederberg J. Plasmid (1952-1997). Plasmid. 1998;39(1):1-9. doi: 10.1006/plas.1997.1320. PubMed PMID: 9473441.
146. Sambrook J, Fritsch EF, Maniatis T. Molecular cloning : a laboratory manual. 2nd ed. Cold Spring Harbor, N.Y.: Cold Spring Harbor Laboratory Press; 1989.
147. McKay GA, Wright GD. Kinetic mechanism of aminoglycoside phosphotransferase type IIIa. Evidence for a Theorell-Chance mechanism. The Journal of biological chemistry. 1995;270(42):24686-92. PubMed PMID: 7559583.
148. Southern EM. Detection of specific sequences among DNA fragments separated by gel electrophoresis. Journal of molecular biology. 1975;98(3):503-17. PubMed PMID: 1195397.
149. Alwine JC, Kemp DJ, Stark GR. Method for detection of specific RNAs in agarose gels by transfer to diazobenzyloxymethyl-paper and hybridization with DNA probes. Proceedings of the National Academy of Sciences of the United States of America. 1977;74(12):5350-4. PubMed PMID: 414220; PMCID: 431715.
150. Mullis K, Faloona F, Scharf S, Saiki R, Horn G, Erlich H. Specific enzymatic amplification of DNA in vitro: the polymerase chain reaction. 1986. Biotechnology. 1992;24:17-27. PubMed PMID: 1422010.

151. Muro-Cacho CA. In situ PCR. Overview of procedures and applications. Frontiers in bioscience : a journal and virtual library. 1997;2:c15-29. PubMed PMID: 9281304.
152. Janssens N, Janicot M, Perera T, Bakker A. Housekeeping genes as internal standards in cancer research. Molecular diagnosis : a journal devoted to the understanding of human disease through the clinical application of molecular biology. 2004;8(2):107-13. PubMed PMID: 15527325.
153. Barber RD, Harmer DW, Coleman RA, Clark BJ. GAPDH as a housekeeping gene: analysis of GAPDH mRNA expression in a panel of 72 human tissues. Physiological genomics. 2005;21(3):389-95. doi: 10.1152/physiolgenomics.00025.2005. PubMed PMID: 15769908.
154. Livak KJ, Schmittgen TD. Analysis of relative gene expression data using real-time quantitative PCR and the 2(-Delta Delta C(T)) Method. Methods. 2001;25(4):402-8. doi: 10.1006/meth.2001.1262. PubMed PMID: 11846609.
155. Gorr TA, Vogel J. Western blotting revisited: Critical perusal of underappreciated technical issues. Proteomics Clin Appl. 2015. doi: 10.1002/prca.201400118. PubMed PMID: 25597284.
156. Venkatakrishnan K, Greenblatt DJ, von Moltke LL, Schmider J, Harmatz JS, Shader RI. Five distinct human cytochromes mediate amitriptyline N-demethylation in vitro: dominance of CYP 2C19 and 3A4. J Clin Pharmacol. 1998;38(2):112-21. PubMed PMID: 9549641.
157. Volak LP, Ghirmai S, Cashman JR, Court MH. Curcuminoids inhibit multiple human cytochromes P450, UDP-glucuronosyltransferase, and sulfotransferase enzymes, whereas piperine is a relatively selective CYP3A4 inhibitor. Drug Metab Dispos. 2008;36(8):1594-605. doi: 10.1124/dmd.108.020552. PubMed PMID: 18480186; PMCID: 2574793.
158. Peter R, Bocker R, Beaune PH, Iwasaki M, Guengerich FP, Yang CS. Hydroxylation of chlorzoxazone as a specific probe for human liver cytochrome P-450IIE1. Chemical research in toxicology. 1990;3(6):566-73. PubMed PMID: 2103328.
159. Zerilli A, Lucas D, Berthou F, Bardou LG, Menez JF. Determination of cytochrome P450 2E1 activity in microsomes by thin-layer chromatography using [2-14C]chlorzoxazone. J Chromatogr B Biomed Appl. 1996;677(1):156-60. PubMed PMID: 8925089.
160. Lucas D, Berthou F, Girre C, Poitrenaud F, Menez JF. High-performance liquid chromatographic determination of chlorzoxazone and 6-hydroxychlorzoxazone in serum: a tool for indirect evaluation of cytochrome P4502E1 activity in humans. J Chromatogr. 1993;622(1):79-86. PubMed PMID: 8120116.
161. Stott I, Murthy A, Robinson A, Thomas NW, Fry JR. Low-dose diethyldithiocarbamate attenuates the hepatotoxicity of 1,3-dichloro-2-propanol and selectively inhibits CYP2E1 activity in the rat. Human & experimental toxicology. 1997;16(5):262-6. PubMed PMID: 9192205.

162. Brown M, Wittwer C. Flow cytometry: principles and clinical applications in hematology. Clin Chem. 2000;46(8 Pt 2):1221-9. PubMed PMID: 10926916.
163. Silverman RB. Mechanism-based enzyme inactivators. Methods in enzymology. 1995;249:240-83. PubMed PMID: 7791614.
164. Givan AL. Flow cytometry: an introduction. Methods Mol Biol. 2004;263:1-32. doi: 10.1385/1-59259-773-4:001. PubMed PMID: 14976358.
165. Eruslanov E, Kusmartsev S. Identification of ROS using oxidized DCFDA and flow-cytometry. Methods Mol Biol. 2010;594:57-72. doi: 10.1007/978-1-60761-411-1_4. PubMed PMID: 20072909.
166. Stoddart MJ. Cell viability assays: introduction. Methods in molecular biology. 2011;740:1-6. doi: 10.1007/978-1-61779-108-6_1. PubMed PMID: 21468961.
167. Liu Y, Peterson DA, Kimura H, Schubert D. FOR MECHANES,. Journal of neurochemistry. 1997;69(2):581-93. PubMed PMID: 9231715.
168. van Meerloo J, Kaspers GJ, Cloos J. Cell sensitivity assays: the MTT assay. Methods in molecular biology. 2011;731:237-45. doi: 10.1007/978-1-61779-080-5_20. PubMed PMID: 21516412.
169. Carmichael J, Mitchell JB, DeGraff WG, Gamson J, Gazdar AF, Johnson BE, Glatstein E, Minna JD. Chemosensitivity testing of human lung cancer cell lines using the MTT assay. British journal of cancer. 1988;57(6):540-7. PubMed PMID: 2841961; PMCID: 2246465.
170. Suto A, Kubota T, Shimoyama Y, Ishibiki K, Abe O. MTT assay with reference to the clinical effect of chemotherapy. Journal of surgical oncology. 1989;42(1):28-32. PubMed PMID: 2770307.
171. Jabbar SA, Twentyman PR, Watson JV. The MTT assay underestimates the growth inhibitory effects of interferons. British journal of cancer. 1989;60(4):523-8. PubMed PMID: 2529890; PMCID: 2247113.
172. Greenblatt DJ, Zhao Y, Venkatakrishnan K, Duan SX, Harmatz JS, Parent SJ, Court MH, von Moltke LL. Mechanism of cytochrome P450-3A inhibition by ketoconazole. The Journal of pharmacy and pharmacology. 2011;63(2):214-21. doi: 10.1111/j.2042-7158.2010.01202.x. PubMed PMID: 21235585.
173. Boulikas T, Vougiouka M. Recent clinical trials using cisplatin, carboplatin and their combination chemotherapy drugs (review). Oncol Rep. 2004;11(3):559-95. PubMed PMID: 14767508.
174. Holohan C, Van Schaeybroeck S, Longley DB, Johnston PG. Cancer drug resistance: an evolving paradigm. Nat Rev Cancer. 2013;13(10):714-26. doi: 10.1038/nrc3599. PubMed PMID: 24060863.
175. Spencer CM, Faulds D. Paclitaxel. A review of its pharmacodynamic and pharmacokinetic properties and therapeutic potential in the treatment of cancer. Drugs. 1994;48(5):794-847. PubMed PMID: 7530632.
176. Pourahmad J, Hosseini MJ, Eskandari MR, Shekarabi SM, Daraei B. Mitochondrial/lysosomal toxic cross-talk plays a key role in cisplatin

nephrotoxicity. Xenobiotica. 2010;40(11):763-71. doi: 10.3109/00498254.2010.512093. PubMed PMID: 20809784.
177. Popovics P, Schally AV, Szalontay L, Block NL, Rick FG. Targeted cytotoxic analog of luteinizing hormone-releasing hormone (LHRH), AEZS-108 (AN-152), inhibits the growth of DU-145 human castration-resistant prostate cancer in vivo and in vitro through elevating p21 and ROS levels. Oncotarget. 2014;5(12):4567-78. PubMed PMID: 24994120; PMCID: 4147346.
178. Domitrovic R, Cvijanovic O, Susnic V, Katalinic N. Renoprotective mechanisms of chlorogenic acid in cisplatin-induced kidney injury. Toxicology. 2014;324:98-107. doi: 10.1016/j.tox.2014.07.004. PubMed PMID: 25043994.
179. Hasler JA. Pharmacogenetics of cytochromes P450. Mol Aspects Med. 1999;20(1-2):12-24, 5-137. PubMed PMID: 10575648.
180. Wang Z, Hall SD, Maya JF, Li L, Asghar A, Gorski JC. Diabetes mellitus increases the in vivo activity of cytochrome P450 2E1 in humans. Br J Clin Pharmacol. 2003;55(1):77-85. PubMed PMID: 12534643; PMCID: 1884181.
181. Molina-Ortiz D, Camacho-Carranza R, Gonzalez-Zamora JF, Shalkow-Kalincovstein J, Cardenas-Cardos R, Nosti-Palacios R, Vences-Mejia A. Differential expression of cytochrome P450 enzymes in normal and tumor tissues from childhood rhabdomyosarcoma. PLoS One. 2014;9(4):e93261. doi: 10.1371/journal.pone.0093261. PubMed PMID: 24699256; PMCID: 3974704.
182. Leung T, Rajendran R, Singh S, Garva R, Krstic-Demonacos M, Demonacos C. Cytochrome P450 2E1 (CYP2E1) regulates the response to oxidative stress and migration of breast cancer cells. Breast Cancer Res. 2013;15(6):R107. doi: 10.1186/bcr3574. PubMed PMID: 24207099; PMCID: 3979157.
183. Joshi M, Tyndale RF. Induction and recovery time course of rat brain CYP2E1 after nicotine treatment. Drug Metab Dispos. 2006;34(4):647-52. doi: 10.1124/dmd.105.008029. PubMed PMID: 16434548.
184. Troger V, Fischel JL, Formento P, Gioanni J, Milano G. Effects of prolonged exposure to cisplatin on cytotoxicity and intracellular drug concentration. Eur J Cancer. 1992;28(1):82-6. PubMed PMID: 1567698.
185. Liu J, Liu Y, Habeebu SS, Klaassen CD. Metallothionein (MT)-null mice are sensitive to cisplatin-induced hepatotoxicity. Toxicol Appl Pharmacol. 1998;149(1):24-31. doi: 10.1006/taap.1997.8325. PubMed PMID: 9512723.
186. Qian W, Nishikawa M, Haque AM, Hirose M, Mashimo M, Sato E, Inoue M. Mitochondrial density determines the cellular sensitivity to cisplatin-induced cell death. Am J Physiol Cell Physiol. 2005;289(6):C1466-75. doi: 10.1152/ajpcell.00265.2005. PubMed PMID: 16107504.
187. Raza H, Prabu SK, Robin MA, Avadhani NG. Elevated mitochondrial cytochrome P450 2E1 and glutathione S-transferase A4-4 in streptozotocin-

induced diabetic rats: tissue-specific variations and roles in oxidative stress. Diabetes. 2004;53(1):185-94. PubMed PMID: 14693714.
188. Scott LA, Madan E, Valentovic MA. Attenuation of cisplatin nephrotoxicity by streptozotocin-induced diabetes. Fundam Appl Toxicol. 1989;12(3):530-9. PubMed PMID: 2731667.